Sediment Pulses in a Gravel-Bed Flume with Alternate Bars

PAR

Blaise Étienne Marceau DHONT

acceptée sur proposition du jury:

Prof. A. Schleiss, président du jury
Prof. C. Ancey, directeur de thèse
Dr A. Recking, rapporteur
Dr M. Jodeau, rapporteuse
Prof. P. Molnar, rapporteur

Remerciements

Je tiens avant tout à remercier Christophe Ancey, mon directeur de thèse, pour m'avoir fait confiance et avoir rendu cette aventure possible, ainsi que les membres de mon jury pour leurs commentaires constructifs. Mes remerciements vont également vers Bob, le couteau suisse du laboratoire sans qui ce travail expérimental n'aurait pas vu le jour, et Barbara pour sa bienveillance toute fribourgeoise au cours de ces quatre années. Je remercie également Panpam, bricoleur hors pair et compagnon de café, qui s'est toujours montré disponible face aux caprices de la halle hydraulique.

Merci à Joris, compagnon de la première année, pour m'avoir mis sur les rails, ainsi qu'à François dont j'ai repris les travaux et qui a toujours été ouvert à la discussion. Mes années de thésard n'auraient pas été les mêmes sans l'arrivée de Daniel et Gauthier dans le laboratoire, ainsi que sans l'équipe du LMS : Dimitrios, Etienne et Alessandro. Merci à vous pour les innombrables aventures vécues ensemble. Aux derniers arrivés au LHE, Tomás, Ivan et Zhenzhu, je souhaite le meilleur pour la suite.

Enfin, mes remerciements ne sauraient être complets sans aller également vers Paul-Sam, Edouard, Bastian, Romain, Sylvain, Jules, Domi, Thomas, Stéphanie, Charlotte, Arde, Pierre-Steph et Pauline qui ont contribués à cette belle époque Lausannoise, ainsi que vers tous ceux m'ayant accompagné dans mes aventures diverses de ces dernières années et qui se reconnaîtront ici.

Au moment d'écrire ces lignes, mes pensées vont finalement vers ma famille, soutien de toujours.

Lausanne, le 10 Novembre 2017   B. D.

Abstract

The proper understanding of gravel-bed river dynamics is a crucial issue for the effective protection against related natural hazards, design of hydraulic structures, and preservation of their high ecological value in mountain regions. However, despite more than one century of research in the field, most available models fail to accurately predict bedload transport rates in such alluvial rivers because of the complex relationships between the flow, channel morphology, and sediment transport. It is now recognized that spatio-temporal variability is an inherent property of bedload transport in gravel-bed rivers which results in its pulsating character even under steady flow conditions.

This experimental study aims to better understand the physical mechanisms involved in sediment transport in gravel-bed channels characterized by alternate bars. More specifically, it is concerned with the origins of the pulsating nature of bedload transport under steady external conditions in relation to bed macro-forms. Experiments were conducted over long time periods, in the order of hundreds of hours, in order to investigate transport rate fluctuations over a wide spectrum of time scales and if any dynamic equilibrium state was reached.

Three experiments were altogether performed, each characterized by a different sediment feed rate, in a 16-m long and 60-cm wide tilting flume using moderately-sorted gravel. The bedload transport rates were continuously recorded at the flume outlet during the runs using vertical impact plates. Additionally, the bed and water elevations were measured every ten minutes using ultrasonic probes and a laser-sheet imaging technique both mounted on an automated moving cart.

The joint analysis of the topographical and bedload transport measurements demonstrated that sediment waves migrated in a step like motion from pool to pool inducing most recorded pulses. They were thus identified as the primary mode of sediment transport in the alternate bar system. Additionally, these migrating low-relief bedforms were found to cause occasional bar failures which generated particularly large pulses.

At the largest fluctuation time scale (about 10 h), bedload pulses were associated with quasi-periodic variations in the global bed volume. This observation suggests that the sediment storage capacity of the bed, for a given bed configuration and external conditions, may govern and set an upper limit to the system fluctuations.

Abstract

The comparison between the experiments showed that the bed responded to the increase in sediment supply by increasing its average slope and/or evolving toward a more braided configuration. In addition, this adjustment of the bed transport capacity was found to be associated with a smoothing of the bedload transport pulsating regime resulting in shorter and more frequent pulses of lower magnitude.

In conclusion, this study shed new light on bedload transport in gravel-bed rivers by documenting several of its aspects under controlled conditions. More specifically, it bears experimental evidence of the presence of sediment waves in alternate bar systems, and show how the dynamics of these two types of bedform drive sediment transport and control bedload macro-pulse characteristics in gravel-bed channels.

Key words: gravel-bed rivers, sediment transport, bedload pulses, alternate bars, sediment waves

Résumé

La bonne compréhension de la dynamique des rivières à lit de gravier est essentielle pour la protection efficace contre les risques naturels qui leur sont associés, le dimensionnement des ouvrages hydrauliques et la préservation de leur forte valeur écologique dans les régions de montagne. Cependant, malgré plus d'un siècle de recherche dans le domaine, les modèles de transport solide dans de tels systèmes alluviaux sont peu précis en raison de la complexité des interactions entre l'écoulement, la morphologie du lit et le transport sédimentaire. Le transport par charriage est ainsi reconnu comme un processus de nature intermittente caractérisé par des pulses sédimentaires, et ce même en régime permanent.

Cette étude expérimentale vise à mieux comprendre les processus physiques associés au transport sédimentaire dans les rivières à lit de gravier en présence de bancs alternés. Plus précisément, elle s'intéresse à la relation entre les macro-structures du lit et les pulses sédimentaires en régime permanent. Par ailleurs, les expériences ont été conduites sur de longues périodes, jusqu'à 560 h, afin d'étudier les fluctuations du débit solide sur différentes échelles de temps ainsi que la façon dont l'équilibre dynamique du lit s'établit.

Au total, trois expériences chacune caractérisée par un débit solide en entrée différent ont été effectuées dans un canal de 16 m de long et 60 cm de large sur un lit de gravier à granulométrie moyennement resserrée. Pendant chacune d'elles, le débit solide a été mesuré en continu en sortie de canal à l'aide d'accéléromètres. De plus, la hauteur d'eau et la topographie ont été mesurées toutes les dix minutes à l'aide de sondes ultrasoniques et d'une nappe laser montées sur un charriot roulant.

L'analyse des mesures de topographie et de débit solide montre que des vagues sédimentaires migrant de manière intermittente de mouille en mouille sont à l'origine de la majorité des pulses sédimentaires et constituent le principal mode de transport des sédiments. De plus, ces macro-structures du lit peuvent induire occasionnellement la mobilisation des bancs alternés et leur migration vers l'aval.

Pour les longues échelles temporelles, les pulses sédimentaires sont associés aux fluctuations quasi-périodiques du volume total du lit. Cette corrélation semble indiquer que la capacité de stockage du lit, pour une configuration et des conditions aux limites données, limite les fluctuations dans le système.

Résumé

Il apparaît également que l'augmentation du débit solide en entrée induit une élévation de la pente et/ou une évolution vers une configuration plus tressée du lit. Cet ajustement de la capacité de transport est de plus associé à un régime de pulses caractérisé par des fluctuations plus fréquentes, plus courtes et de plus faibles amplitudes.

En conclusion, cette étude apporte un nouvel éclairage sur le transport solide dans les rivières à lit de gravier. Plus précisément, elle atteste de la présence de vagues sédimentaires dans les systèmes de bancs alternés, et montre comment la dynamique de ces deux types de macro-structure commande les pulses de débit solide.

Mots clefs : rivières à lit de gravier, transport par charriage, pulses sédimentaires, bancs alternés, vagues sédimentaires

Contents

Contents

Contents

List of Figures

List of Tables

1 Introduction

Rivers in mountain regions provide essential resources, such as water and energy, for human settlement. However, with the economic and urban development of mountain valleys (Wohl, 2010), the risks arising from the unsteady nature of rivers (Church and Ferguson, 2015) have increased dramatically. As a consequence, the proper understanding of river dynamics is today a crucial issue for the protection against natural hazards (Arnaud-Fassetta et al., 2009), the design of hydraulic structures (Carson and Griffiths, 1987; Radecki-Pawlik et al., 2017), and the preservation of the high ecological value of river habitats (Wohl, 2006).

In mountain valleys and forelands, rivers flow on coarse alluvial substrata and are thus classified as *gravel-bed rivers* (Church, 2010). In such river systems, the flow and the channel morphology interact through feedback mechanisms governed by sediment transport (Church, 2006). Gravel-bed river dynamics are therefore a complex problem (Church, 2010) which, despite more than one century of scientific work into sediment transport (Fabre, 1797; Carson and Griffiths, 1987; Gomez, 1991), has not yet been fully solved (Gomez and Church, 1989; Barry, 2004; Wohl, 2014; Church and Ferguson, 2015).

In the following section, a brief review of the major bedload transport equations is given for the purpose of presenting some of the physical processes involved in sediment transport and illustrating the complexity of the issue in mountain streams. We then comment further on key concepts related to gravel-bed rivers which we refer to throughout the study, including: grain sorting, bedform dynamics, bedload pulses, and dynamic equilibrium. This review aims to provide an overview of the current knowledge in the field and to highlight the major shortcomings which are addressed in this work. For a more comprehensive state-of-the-art review, we refer the reader to the literature cited hereafter.

This introductory chapter ends with the presentation of the objectives of the study which aims to better understand the physical processes involved in sediment transport in gravel-bed channels. More specifically, we are interested in the origins of the pulsating nature of bedload transport (Gomez et al., 1989; Singh et al., 2009), which hinders the development of accurate prediction models (Bravo-Espinosa et al., 2003; Recking et al., 2012), in river systems with alternate bars. The approach employed is experimental and our flume experiments are in

the continuation of the previous laboratory studies concerned with sediment transport rate fluctuations and bedform dynamics under steady external conditions (e.g., Iseya and Ikeda, 1987; Kuhnle and Southard, 1988; Gomez et al., 1989; Recking et al., 2009; Singh et al., 2009) with the originality of being particularly long.

1.1 Bedload transport

Sediment transport in gravel-bed rivers essentially occurs in the form of bedload (Church, 2010) which depicts the movement of bed material in close contact with the bed trough sliding, rolling and saltation motion (Graf and Altinakar, 2000). This mode of transport is therefore fundamentally different from suspended load and wash load which involve finer particles (e.g., fine sand and silt) that are rarely or never in contact with the bed. Two critical characteristics of bedload transport emerge from this difference: it is intermittent (Gomez et al., 1989) and shapes the channel morphology (Church, 2006).

A considerable number of scientific studies have investigated bedload transport, and most of the current theories find their roots in the literature produced during the first part of the 20th century. Based on experimental studies carried out in laboratory flumes, such as the pioneer work conducted by Gilbert (1914), many empirical and semi-empirical equations were developed with the aim of predicting the bedload transport rate (BTR) in fluvial systems. Gomez and Church (1989) distinguish four main approaches based upon the bed shear stress (du Boys, 1879), the stream discharge (Schoklitsch, 1934), the stream power (Bagnold, 1980), and the stochastic description of particle motion (Einstein, 1950).

One of the first bedload transport formulae was proposed by du Boys (1879) who described bedload transport as the progression of sliding grain layers. His theory states that the BTR depends on the fluid shear stress applied to the bed in excess of the critical shear stress required to initiate particle motion. Many bedload transport equations arose from refinements of this early concept (Chanson, 2004), the most notorious being perhaps the one proposed by Meyer-Peter and Müller (1948). However, a major challenge of this approach is the determination of the critical shear stress which has motivated some authors to use alternate incipient motion criteria related, for instance, to flow velocity or flow rate (Schoklitsch, 1950).

Shields (1936) conducted an extensive work on the determination of the critical shear stress and proposed to describe the stability of a bed particle as the ratio between the destabilizing forces (due to the stream flow) and the stabilizing forces (due to the buoyant particle weight). In this way, the Shields number is defined as

$$\tau^\star = \frac{\tau}{(\rho_s - \rho)gD} \tag{1.1}$$

with τ the bed shear stress, ρ_s the sediment density, ρ the fluid density, g the acceleration due to gravity, and D the grain diameter. Note that $\tau = \rho g h S_w$ with h the flow depth and S_w the water-surface slope in steady uniform flows, and that D is generally indexed by the median diameter d_{50} when the grain size distribution is non-uniform (Church, 2010). The

Shields number is therefore a dimensionless representation of the bed shear stress and can be seen as a measure of the competence of the stream flow to mobilize sediment (Church, 2010). Based on a series of experimental runs with well-sorted sediment mixtures, Shields (1936) established that the critical value of $\tau^\star$ to initiate bedload transport under turbulent flow conditions was about 0.06. However, because bed material in mountain streams is usually poorly-sorted, most studies report lower critical values (Church, 2006).

A major contribution in predicting BTRs in steep-gradient streams was brought by Meyer-Peter and Müller (1948). They proposed an empirical formula, sometimes referred to as the Swiss formula, based on extensive laboratory experiments (Meyer-Peter, 1949, 1951) and the data collected by Gilbert (1914) for coarse material. Their equation relies on excess shear stress, following du Boys' intuition, and relates BTR to flow rate, flow depth, bed gradient and particle size. It encountered a large success, especially for wide channels and coarse material, and is still widely used in hydraulic engineering although thresholded equations are a matter of discussion (Barry, 2004; Recking, 2010).

Bagnold (1956, 1966) proposed a different approach to model bedload transport based on the observation that particles in movement form a thick suspension of a grain-fluid mixture. His theory essentially relies on the equilibrium in the momentum transfer between the liquid and solid phases (Ancey et al., 2008) and seems to give satisfactory results for sufficiently high discharges and steady uniform or gently varying flows (Julien, 1998). However, one limit of this model is that the intermittent nature of bedload transport at low flow rates is ignored because of the mean-field approximation of the stream velocity which, among other, neglects the effects of turbulence (Ancey et al., 2008).

In contrast to Bagnold (1956), Einstein (1942, 1950) used a stochastic approach to account for the intermittency of particle transport. Assuming that the jump length of the moving particles is independent from the flow conditions and the transport rate, he proposed a formula that expresses an equilibrium condition between the particle entrainment and deposition rates. His approach suggests that bedload transport depends on the fluctuations of the stream velocity rather that on the mean value, and constitutes up to now the framework for the probabilistic description of bedload transport (Ancey et al., 2006; Furbish et al., 2012).

Bagnold's first theory about bedload transport (Bagnold, 1956) conducted him to propose later an analogy between a river and an engine in which stream power operates with a certain efficiency to carry sediment (Bagnold, 1980). He thus developed a formula which relates the BTR to the rate of energy expenditure in the channel. His formula is particularly suited for gravel-bed rivers since it considers a bimodal sediment mixture (Gomez and Church, 1989). In addition, only few parameters are required which is attractive as collecting extensive field measurements is challenging in mountain streams (Young, 1989). However, as Meyer-Peter and Müller (1948) formula, Bagnold's equation is thresholded and exhibits the same poor performance in predicting low BTRs.

The different theories summarized above give an overview of some of the various physical

processes involved in bedload transport and illustrate its complexity (Church, 2010). A detailed review of the cited equations, and of the concepts they refer to, can be found in the vast devoted literature (e.g., Graf, 1971; Yalin, 1972; Gomez, 1991). Despite their shortcomings, these early bedload transport formulae constitute nevertheless the basis of the substantial work initiated in the 1980s to address issues specific to mountain streams, including gravel-bed rivers.

For the purpose of illustrating the main issues addressed over the past decades, one can cite Smart and Jaeggi (1983) and Rickenmann (1990) who extended the work of Meyer-Peter and Müller (1948) to steep slope (up to 20%) and highly concentrated flows (i.e., debris flows), and Parker et al. (1982) who proposed to compute BTR by grain size classes to account for the selective transport of non-uniform sediment (Parker and Sutherland, 1990). In addition, the concept of critical shear stress was questioned by Recking (2010) who developed a non-thresholded equation for low transport rates (i.e., partially mobile grains) based on the comparison between BTR and flow resistance records originating from an extensive dataset of flume and field measurements (Recking et al., 2008). Finally, many authors addressed the issue of form roughness (increased flow resistance due to bed morphology) applying correction factors for roughness coefficients in bedload transport equations (Gomez and Church, 1989; Recking et al., 2013).

Despite the considerable efforts put to better predict bedload transport (of which a tiny part is cited above), available equations often overestimate BTRs by one or more orders of magnitude and their performance seems acceptable only under unlimited sediment supply conditions (D'Agostino and Lenzi, 1999; Rickenmann, 2001; Almedeij and Diplas, 2003; Bravo-Espinosa et al., 2003; Gomez, 2006; Rickenmann and Koschni, 2010; Comiti and Mao, 2012). For instance, D'Agostino and Lenzi (1999) studied the Rio Cordon in Italy and obtained reasonable BTR predictions only during extreme floods which mobilized all grain size classes (equal mobility state). Rickenmann (2001) confirmed the poor performance of bedload transport equations in mountain streams and pointed the low relative flow depth (which for instance affects flow resistance and turbulence effects), additional form roughness (e.g., due to channel morphology and bedforms), and sediment supply limitation (e.g., because of grain sorting effects) as the main causes.

1.2 Gravel-bed rivers

1.2.1 Self-formed channels

The challenge posed by bedload transport modelling in gravel-bed rivers relies to a large extent on their intrinsic nature: they are alluvial systems formed in sediment they have transported and deposited (Church, 2006). In other words, gravel-bed rivers are self-formed which means their morphology is a direct consequence of bedload transport. Gravel-bed river dynamics are therefore the result of the mutual interaction between the flow and the morphology through sediment transport (Church, 2010). This feedback loop is illustrated in figure 1.1.

The morphology of gravel-bed rivers on bed gradients below about 2% is mostly characterized

by riffle-pool-bar triplets (see figure 1.2) which result in alternate bar configurations (Church, 2006). However, the morphology of alluvial rivers is sensitive to sediment supply (Montgomery and Buffington, 1997; Venditti et al., 2012; Podolak and Wilcock, 2013) and, when the latter increases, the flow tends to be divided into a number of sub-channels around the bars yielding to a braided configuration (Church, 2010) generally associated with steeper bed slopes (Paola, 2001; Madej et al., 2009; Pryor et al., 2011). The transition from single thread to braided morphology, and the relation with parameters relatively easy to measure such as the slope, grain size, discharge, and width-to-depth ratio, has been the object of numerous studies (Leopold and Wolman, 1957; Parker, 1976; Ashmore, 1991; Schumm, 1985; Kleinhans and van den Berg, 2011). However the link between morphological changes and both sediment supply and transport in gravel-bed rivers, although obvious, is still an open question (Mueller and Pitlick, 2014; Church and Ferguson, 2015; Recking et al., 2016).
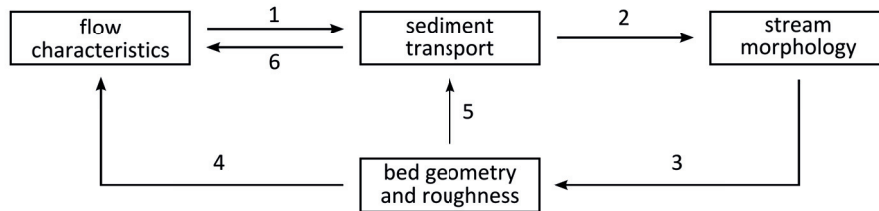
Figure 1.1: Interactions between the stream flow and morphology in gravel-bed rivers: (1) stream flow entrains sediment, (2) sediment transport induces bed erosion and sediment deposition, (3) morphological changes affect bed geometry and roughness which in turn (4) changes flow characteristics and thus (5) sediment transport, and (6) sediment transport can also affect flow characteristics; modified from Richard (1997).

Alternate bars in gravel-bed rivers can be "forced" by a persistent local perturbation of the flow or topography (e.g., channel curvature), or "free" if they arise spontaneously from the fundamental system instability (Seminara, 1998). In the latter case, the instability is formed by a small-scale perturbation of the flow over the erodible bed (Nelson, 1990) that grows in size to some finite wavelength (Ikeda, 1983; Nelson, 1990) and ultimately results in a periodic pattern (Lanzoni, 2000b). Both linear and weakly non-linear theory (Blondeaux and Seminara, 1985; Colombini et al., 1987; Schielen et al., 1993) have been developed and the issue of bar formation in alluvial channels can therefore be considered as fairly settled (Lanzoni, 2000b).

Forced bars in gravel-bed rivers are by definition stationary whereas free bars are generally reported to migrate in the downstream direction (Venditti et al., 2012; Crosato et al., 2012). A condition for non-migrating free bars to develop is, for instance, that the channel width-to-depth ratio is at the value of resonance (Blondeaux and Seminara, 1985; Seminara and Tubino, 1992). However, Crosato et al. (2011) observed non-migrating bars without any resonant condition or steady local perturbation and suggested that they are the expression of an intrinsic property of alluvial channels.
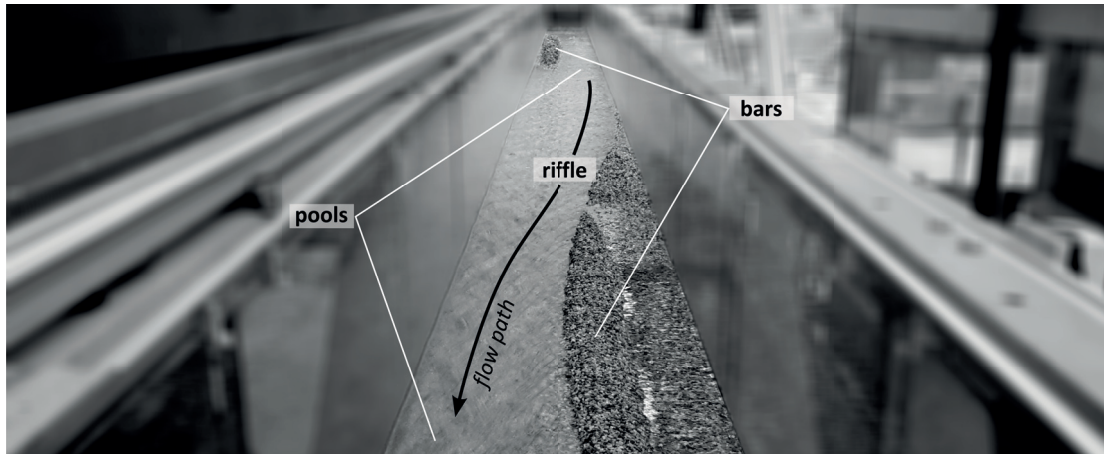
Figure 1.2: Illustration of alternate bars in a gravel-bed flume using an image taken during our experiments.

1.2.2 Grain sorting mechanisms

Gravel-bed rivers are characterized by poorly-sorted sediment and, as a result of the interaction between moving and static grains, their bed is self-organized (Church, 2010). Indeed, vertical sorting is often observed because finer grains are preferentially moved away. As a consequence, coarse grains form an armor layer at the bed surface covering finer material (Parker et al., 1982; Pitlick et al., 2008). armoring increases bed resistance to shear stress and thus limits its erosion (Harrison, 1950; Church et al., 1998; Church and Hassan, 2002). It is typically observed in the absence of large sediment inputs and when the shear stress is less than the critical value required to initiate the movement of all grain size classes (Gomez, 1994; Parker and Sutherland, 1990). However, during floods, the armor layer can be dismantled releasing large amounts of sediment. If all grain size classes are then mobilized, bedload transport is said to be in an equal mobility state (Parker et al., 1982). As a consequence, many studies described different transport states depending on the flow conditions (Recking et al., 2013), including a partial transport state where only fine grains are moving (Wilcock and Jaeggi, 1993).

armor layers are often spatially localized (longitudinal grain sorting) which results in sediment patches characterized by different grain sizes (Paola and Seal, 1995; Laronne et al., 2001; Vericat et al., 2008). Laronne et al. (2001) suggested that fine particle patches are the main source of sediment during ordinary floods, and that bedload is then transported from patch to patch. In addition, sediment patches were reported to migrate in the form of bedload sheets typically described as low-amplitude bedforms (Recking et al., 2009) with coarse migrating fronts and finer tails (Whiting et al., 1988), which can induce large BTR variations (Venditti et al., 2017). The formation of bed clusters composed of coarse particles has also been reported under low bedload transport conditions (Reid et al., 1992; Church et al., 1998; Strom et al., 2004). As armor layers, such structures increase the stability of the bed surface (Church et al., 1998) and can be dismantled when the flow rate increases, feeding thus bedload with sediment (Strom et al., 2004). Although there have been many insights into how these bed features form, the

knowledge about their inter-relation (if exists) is limited (Venditti et al., 2017).

1.2.3 States of bedload transport

Given the considerations above, three bedload transport phases are commonly distinguished in gravel-bed rivers (Ryan et al., 2002; Bathurst, 2007; Recking et al., 2013):

- Phase 1: below a certain critical flow rate, coarse particles on the bed surface are static and bedload consists of fine sediment originating from patches and further upstream.

- Phase 2: for larger flow rates, coarse particles are destabilized and transported over short distances (sliding and rolling motion). Sub-pavement sediment is released and feeds bedload.

- Phase 3: after a second critical flow rate, surface structures (i.e., armor layers) are entirely dismantled and coarse material moves over long distances (rolling and saltation motion). Bedload includes all grain size classes (equal mobility state).

Equal mobility is rarely observed in gravel-bed rivers (Andrews, 1983; Mueller et al., 2005; Parker et al., 2007) and, because of the grain sorting effects and migrating bedforms commented above, bedload transport rates can vary by several orders of magnitude even under steady flow conditions (Recking et al., 2016; Venditti et al., 2017). As a consequence, bedload transport in gravel-bed rivers is generally characterized by large fluctuations in both space and time (Ergenzinger, 1988; Recking et al., 2013).

1.3 Bedload transport rate fluctuations

The fluctuating nature of bedload transport in gravel-bed rivers (see figure 1.3) was first identified during the field measurement campaigns performed in the 1930s (Ehrenberger, 1931; Mühlofer, 1933; Nesper, 1937; Einstein, 1937) and later confirmed with the development of new measurement techniques (Emmett, 1975; Reid et al., 1985; Whiting et al., 1988; Cudden and Hoey, 2003). It became recognized that spatial and temporal variability was an inherent characteristic of bedload transport (Ergenzinger, 1988; Gomez et al., 1989; Singh et al., 2009), which initiated numerous experimental studies performed under steady flow and sediment feeding conditions (Hubbell, 1987; Iseya and Ikeda, 1987; Kuhnle and Southard, 1988; Gomez et al., 1989; Ashmore, 1991; Hoey, 1992; Frey et al., 2003; Recking et al., 2009; Singh et al., 2009; Ghilardi et al., 2014a).

These studies report large BTR fluctuations up to several times the mean value (Recking, 2006) in single thread (Kuhnle and Southard, 1988; Gomez et al., 1989; Recking et al., 2009; Singh et al., 2009) and braided (Ashmore, 1991; Hoey and Sutherland, 1991) channels with generally poorly-sorted sediment but sometimes also with well-sorted mixtures (Gomez et al., 1989). These bedload pulses (Reid et al., 1985), or bursts (Singh et al., 2009), were identified to originate from migrating bars (Miwa and Daido, 1995; Gomez et al., 1989, see figure 1.4) and low-relief bedforms such as sediment waves (Ashmore, 1991), bed waves (Hoey, 1992) and
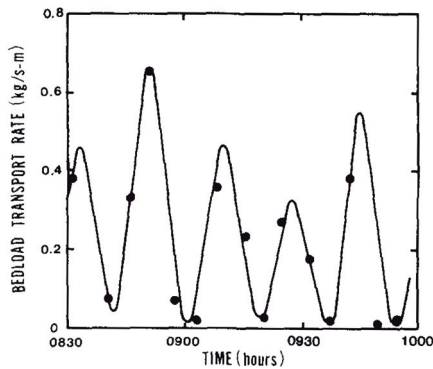
Figure 1.3: Temporal variations in the bedload tranport rates measured by Ehrenberger (1931) in River Danube (Vienna) on June 24th, 1931; reproduced from Gomez (1991). The time series is characterized by large fluctuations.
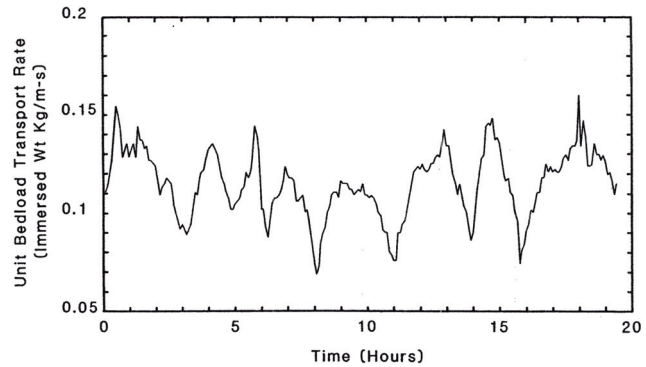
Figure 1.4: Temporal variations in the bedload tranport rates measured by Gomez et al. (1989) in a straight laboratory flume under steady flow conditions (ERC run); reproduced from Gomez et al. (1989). The bedload pulses in the time series are associated with the migration of alternating bars.

bedload sheets (Kuhnle and Southard, 1988; Recking et al., 2009). Note that many different phenomena have been described as sediment waves or derived expressions (e.g., bed waves, bed material waves, bedload sheets, sediment slugs and sediment pulses), as pointed by James (2010), and that this terminology is used in this work in reference to low-height bedforms of which migration induces local changes in bed elevation. Such migrating bars and sediment waves associated with bedload pulses are bed structures somehow related to grain sorting mechanisms (Iseya and Ikeda, 1987; Laronne and Duncan, 1992; Griffiths, 1993) and are classified as macro-forms in the sense that they scale with the flume width (Hoey, 1992).

This latter distinction highlights that BTR fluctuations can be observed over a wide range of temporal and spatial scales (Gomez et al., 1989; Singh et al., 2009; Heyman et al., 2013; Ma et al., 2014) from the movement of individual particles (Ancey et al., 2008, 2015) to global changes in river reach morphology (Hoey, 1992). An interesting characteristic of fluctuations related to macro-form migration is that they are often reported as periodic (Kuhnle and Southard, 1988; Gomez et al., 1989; Ashmore, 1991; Hoey, 1992; Ghilardi et al., 2014b) which suggests they are not only random realizations of stochastic processes (Cudden and Hoey, 2003), although the latter approach is appropriate to describe fluctuations at the particle scale (Ancey et al., 2008). Such fluctuations were observed for periods ranging from minutes to hours, sometimes overlapping which indicates that the related physical processes can occur simultaneously (Gomez et al., 1989; Recking, 2006).

The pulsating nature of bedload transport in gravel-bed rivers (Reid et al., 1985) pushed most authors to describe equilibrium in such systems as dynamic (Hoey, 1992) although this terminology remains a matter of discussion (Thorn and Welford, 1994; Nanson and Huang, 2016). Indeed, dynamic equilibrium is a convenient term to characterize the behavior of

alluvial channels under steady external conditions (typically constant flow and sediment feed rates) given the debate on river equilibrium (Bracken and Wainwright, 2006). It is generally used for two purposes: to depict the adjustment of the system mean parameters (e.g., a raise in the average bed slope) to a change in external conditions (e.g., an increase in the sediment feed rate), and to depict the oscillations of the system parameters (e.g., bed slope fluctuations) about mean values (e.g., the average bed slope). We use it for this latter purpose in the following unless stated otherwise.

The common procedure to ensure that dynamic equilibrium is achieved in experiments under steady external conditions is to wait long enough so that the average BTR meets the imposed sediment feed rate (mass-balance equilibrium) and the bed slope stabilizes (Iseya and Ikeda, 1987; Gomez et al., 1989; Frey et al., 2003; Recking et al., 2009). This method refers implicitly to Lane's balance (Lane, 1955) which states that equilibrium is achieved once the bed slope has adjusted to the imposed flow and sediment feed rates in such a way that the stream flow can transport the sediment of a given size at the rate necessary to achieve mass-balance equilibrium (Church, 2006). In other words, it means that the available stream power balances the work used for sediment transport (discharge×slope $\propto$ transport rate×grain size), as illustrated in figure 1.5. However, this approach is incomplete since, in addition to the slope, the channel transport capacity can also adjust through grain sorting mechanisms (e.g., armoring) and morphological changes (e.g., braiding) which both affect bed shear stress (Recking et al., 2013; Podolak and Wilcock, 2013). Because of the variability of these processes in alluvial channels (as discussed previously), Lane's balance in figure 1.5 keeps swinging which can be seen as an illustration of the dynamic equilibrium state (Nanson and Huang, 2016).
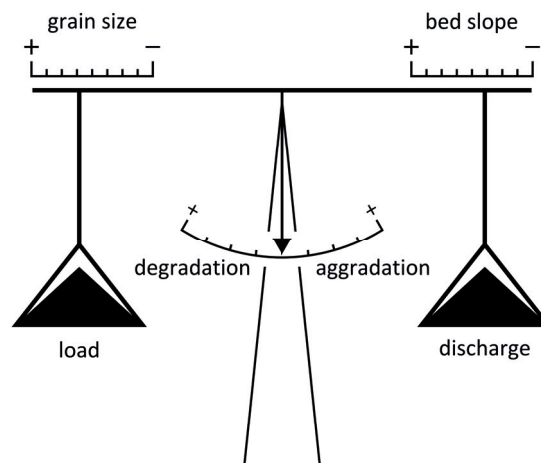
Figure 1.5: Illustration of the morphological equilibrium concept proposed by Lane (1955); modified from Recking et al. (2013).

Most experimentalists wait for dynamic equilibrium to be achieved since initial conditions are generally not representative of natural systems (e.g., a flat bed of a given slope). However the criteria used, for instance an average BTR close to its average value, are only indicative. Indeed, no universally accepted measurement of equilibrium in geomorphology (if exists) has been proposed (Nanson and Huang, 2016). Moreover the time to reach dynamic equilibrium can be long (Recking, 2006) compared to usual experiment durations (typically a few tens of hours).

These considerations highlight the need for long experiments when studying gravel-bed river morphodynamics. This necessity is emphasized by the time scales of the BTR fluctuations usually observed which can be up to several hours (see review in Kuhnle, 1996): the experiment durations must be much longer than the latter to capture the whole system dynamics. The great improvements in bedload and bed topography monitoring technologies over the last decades (Gomez et al., 1989; Rickenmann, 2017) made possible such requirements. For instance, (Lanzoni, 2000a) and (Crosato et al., 2011) have investigated bar formation and dynamics in alluvial channels over weeks. However, such long experiment durations remain marginal and techniques allowing the joint measurement at high-resolution of the bed topography and the BTR are still a fundamental need for researchers (Marr et al., 2010; Vesipa et al., 2017; Dhont et al., 2017).

1.4   Thesis objectives, organization and contribution

The pulsating nature of bedload transport in gravel-bed rivers discussed above is a challenging problem that hinders the development of accurate prediction models. Although migrating bedforms have been identified as one of the main causes responsible for large BTR fluctuations under steady flow and sediment feeding conditions, several issues demand further investigation, including: their parametrization, their dependence on sediment supply, the interaction between bed structures of different sizes, and the relation between the various bedform types and bedload transport (Church, 2010; Church and Ferguson, 2015; Venditti et al., 2017).

In this study, we address some aspects of these issues in the context of straight alluvial channels with alternate bars. Our approach is experimental and focuses on the origins of BTR fluctuations in a mobile-bed flume under steady external conditions. More specifically, we aim to identify the physical mechanisms related to bedload transport at the macro-scale and to assess their contribution to bedload pulses. The objectives of the study are therefore to:

- equip a laboratory flume with high-resolution monitoring tools for BTR and bed topography (addressed in Chapter 2);
- verify the pulsating nature of bedload transport in an alternate bar system under steady flow and sediment feeding conditions (addressed in Chapter 3);
- characterize bedload pulses in terms of magnitude, duration, frequency, associated time scale, and periodicity; and assess the effect of different sediment feed rates on their

characteristics (addressed in Chapter 3);

– identify and describe the mechanisms occurring in the bed involved in the transfer of sediment along the flume length (addressed in Chapter 4);

– relate these mechanisms to bedload pulses and assess their respective contributions to the pulsating nature of bedload transport (addressed in Chapter 5).

The document is organized in six chapters including this one. The experimental setup and procedure, along with the measuring tools used, are detailed in Chapter 2. In Chapter 3, the BTR fluctuations measured at the flume outlet are investigated with consideration of their time scales, the different feed rates tested, and the system equilibrium state. The evolution of the bed topography is analyzed in Chapter 4 with a particular interest on the bar-and-pool system dynamics. Chapter 5 links the results of the two previous chapters, and comments on the bed-related mechanisms generating bedload pulses. The results presented are discussed at the end of each chapter concerned in a dedicated section, and the conclusions of the study are finally drawn in Chapter 6 along with a general discussion of the major results obtained. Among the main contributions arising from this experimental investigation, the following are of particular interest:

– Impact plates and laser-sheet imaging are effective techniques allowing the collection of bedload transport and bed topography measurements at fine resolution and over long time periods in flume experiments.

– Sediment waves are the primary mode of bedload transport in quasi-stationary alternate bar systems. They migrate from pool to pool, in a step-like motion, generating local aggradation-degradation cycles in the bed and bedload pulses.

– Global variations in bed volume are correlated to large-scale bedload pulses. Their quasi-periodic character suggests the existence of a maximum storage capacity, associated with a given bed configuration and dependent on the experimental conditions, that governs the largest bedload transport rate fluctuations.

2 Methods

This study relies on the analysis of three flume experiments carried out under steady flow conditions over long durations (larger than 100 h). In this chapter, we first present the experimental setup and the procedure applied when conducting the experiments. Then, we detail the measurement methods employed of which data are analyzed in the following chapters. They comprise impact plates measuring the bedload transport rate (BTR) at the flume outlet, and a moving cart equipped with ultrasonic probes and a laser-sheet imaging technique dedicated to topographical measurements (bed scans).

2.1 Experimental setup

The experiments were carried out in a 17-m long (16-m usable) and 60-cm wide tilting flume with glass walls allowing lateral observations (see figure 2.1). The flume bed was about 31.5-cm thick and made of moderately-sorted natural gravel (according to the classification of Folk and Ward, 1957). The apparent density of the sediment mixture was 1490 kg/m^{-3}, its characteristic diameters were d_{30} = 5.2 mm, d_{50} = 6.0 mm, and d_{90} = 7.7 mm, and the mean diameter was 5.5 mm with a corresponding standard deviation of 1.2 mm.

The mobile bed was retained at the flume outlet by a porous plate of which aperture was controlled by two valves. This arrangement allowed to adjust the subsurface flow near the flume outlet in order to limit boundary effects such as flow resurgence (the valve aperture was set only once, prior to the experimental campaign). The upstream part of the flume was obstructed by a porous box filled with gravel which reduced the boundary effects due to the flow incoming from the tank located just upstream. During the experiments, the tank was filled at the desired rate by a pump connected the closed loop system recirculating water.

The sediment feeding system consisted of a hopper delivering sediment at the flume inlet by means of a conveyor belt. The sediment feed rate was controlled adjusting the speed of a rotating cylinder with slots which obstructed the hopper outlet. The sediment delivered by the conveyor belt was subsequently fed into the flume through a pin board that distributed the gravel along the width (the distribution had a Gaussian shape centered in the middle of the flume as illustrated in figure 2.2). The sediment flushed out from the flume was collected in a heavy-duty bag having a storage capacity larger than 500 kg. When the bag was filled, the
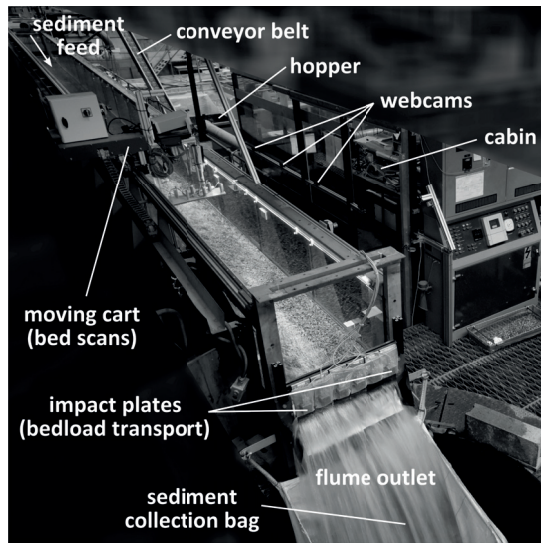
Figure 2.1: General view of the experimental facility.
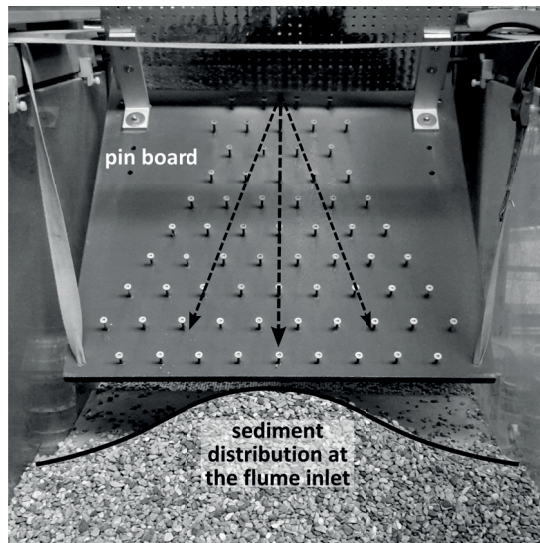
Figure 2.2: Sediment distribution at the flume inlet.

experiments were paused and the sediment collected was transferred to the hopper using a bridge crane.

2.2 Experimental procedure

Given the aim of investigating bedload transport in alternate bar systems, a series of preliminary runs were conducted to define the range of sediment feed rate, flow rate and slope values for which such bedforms develop in the bed. These tests were based on the criteria given in Yalin (1972, 1992) and limited, among other, by the flow rate the pump could deliver. In addition, the final experimental parameters were chosen so that the experimental setup was roughly representative of natural river systems at the 1:10 scale using the scaling relationships proposed in Ashworth et al. (1994). More precisely, the study was initially inspired by the "Plat de la Lé" reach of the Navisence River (Switzerland), characterized by 1–3% slopes and gravel bars, which was a case study investigated by our laboratory (Ancey et al., 2014). At the end of the preliminary runs, it appeared that discharges, feed rates and slopes in the order of respectively 15 l/s, 5 g/s and 1.6% resulted in the development of alternate bars and allowed an optimal use of the measurement tools.

Based on the above considerations, we conducted three experiments with different steady sediment feed rates (2.5, 5.0 and 7.5 g/s) and under the same steady flow conditions (15 l/s) in order to assess the effect of sediment supply on the system dynamics (see table 2.1). We varied the feed rate instead of the flow rate because the setting of the BTR monitoring devices at the flume outlet (i.e., the spacing between the impact plates and the flume outlet, see section 2.3.1) depended on discharge. In addition, we limited our experimental campaign to

Table 2.1: Parameters of the three experiments conducted under steady external conditions.

		Units	Exp. 1	Exp. 3	Exp. 2
sediment feed rate	$Q_{s,in}$	g/s	2.5	5.0	7.5
flow rate	Q_l	l/s	15	15	15
flume slope		%	1.6	1.6	1.7
total duration		h	264.3	574.3	126.1
number of runs			19	41	17
run duration		h	8–24	8–24	8
effective duration (with measurements) *		h	261.1	567.5	123.2
total weight of the sediment collected		kg	2497.4	9871.3	3134.6

* measurements made during the first 9 minutes and the last minute of each run, when the flow
  was unsteady, were ignored

three experiments because our priority was to perform very long experiments (up to ~600 h)
in order to ensure dynamic equilibrium conditions in the flume and the observation of all
potential types of BTR fluctuations at different time scales.

At the beginning of each experiment, the bed was flattened and the flume slope was set close
to the "equilibrium" bed slope measured during the preliminary tests conducted under similar
conditions. Indeed, we desired the bed thickness to remain roughly uniform along the flume
length once the experiments were started in order to minimize the effects due to varying
subsurface flow conditions. Note that the average stream velocity, estimated by the time
required for 2-cm polystyrene balls to travel along the entire flume length, was about 1 m/s at
the beginning of all three experiments when the bed was flat (the corresponding flow depths
were 3.5 ± 0.5 cm). In such conditions, the flow was observed to be turbulent and supercritical.

Each experiments consisted of a series of runs (see table 2.1) between which the discharge was
stopped and the measurements were interrupted. Indeed the hopper had a limited capacity
and needed to be refilled with the sediment collected at the flume outlet. During this process,
the sediment weight was recorded in order to compute the average BTR during the runs.

In all three experiments, the run duration was set to 8 h in order two carry out two experiments
per day (one during daytime and one during nighttime). However, in experiment 1 and 3, the
run duration was increased up to 24 h, from respectively run 12 and run 20, for time saving
purposes. Note that some runs were not completed because of occasional pump failures; and
that a particular attention was paid at the beginning of each run to gently increase the flow
rate in the flume in order to avoid as much as possible any perturbation of the bed.

During the runs, the bed and water elevations were measured every 10 min scanning the
bed with the moving cart (see section 2.3.2), and the BTR was monitored continuously at
the flume outlet using impact plates (see section 2.3.1). The acquisition of these different

measurements was synchronised and fully automated so that they were comparable with each other and no external intervention was required. Note that the measurements made during the first 9 minutes (necessary to reach the desired flow rate) and the last minute (when the discharge was stopped) of each run were ignored.

The evolution of the bed topography along with the corresponding BTR measurements can be visualized online for experiment 1, experiment 2, and experiment 3. In addition, during experiment 3, the evolution of the bed topography in the last part of the flume was filmed from the left side using six webcams. The movie is also available online (see Appendix A.1 for a complete list of online material).

Note that stream velocity measurements were performed before the end of the first 20 runs of experiment 3, over the last part of the flume, using a high-speed camera and seeding 1-cm polystyrene balls in the flume (i.e., using a Particle Tracking Velocimetry technique). These measurements were however not used in this study.

2.3 Instrumentation

2.3.1 Impact plates

The BTR was measured at the flume outlet using six impact plates mounted in-line as illustrated in figure 2.3. Each device consisted of an accelerometer housed in a water-proof aluminium box and a perforated steel plate, both fixed on an aluminium support plate (see Appendix A.2 for the accelerometer characteristics). They were placed vertically 5 cm away the flume outlet in such a way the grains flushed out from the flume hit the perforated grid once. In order to avoid the transmission of extraneous vibrations, each device was insulated from the support frame by a rubber sheet. Note that these sensors were originally developed in our laboratory by Mettra (2014).

The vibrations due to grain impacts were recorded continuously during the experiments logging the acceleration measured in the horizontal direction with a sampling frequency of 10 kHz. The acquisition was performed using a National Instrument® acquisition board and the Data Acquisition Toolbox™ in Matlab®. The signal of each accelerometer was then post-treated in order to compute the number of impulses (i.e., the number of oscillations above a threshold amplitude value) which is a robust proxy for the BTR (Rickenmann et al., 2014). In addition, the number of impulses (which increases with the size of the impacting grain) was found to be linearly correlated with the BTR in previous experiments (Dhont et al., 2017).

The post-treatment applied in this study included the following steps: (1) signal smoothing using a 1000 Hz low-pass filter, (2) detection of the impulses larger than 25 mV, and (3) computation of the number of impulses over 1-min time steps. During a calibration campaign conducted prior to the experiments, a calibration curve relating the number of impulses to the BTR was computed for each accelerometer (see Appendix A.3). Based on these relation-

ships, the average BTRs over 1 min were finally computed for each experiment.
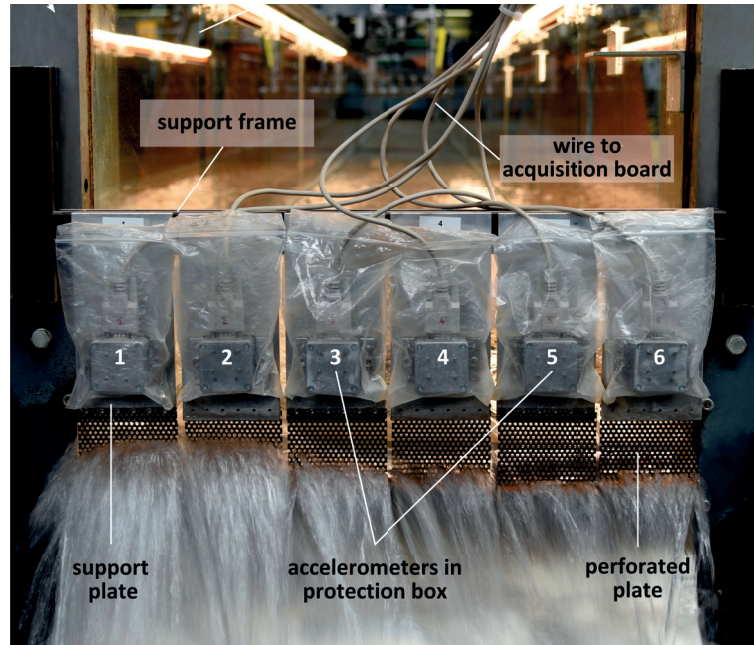
Figure 2.3: View of the impact plates measuring the bedload transport rate at the flume outlet.

In order to assess the measurement accuracy of the impact plates, we performed 164 runs, each lasting between 30 s and 5 min, during which the sediment were collected and weighted. We then compared the BTRs measured by the impact plates and the BTRs computed based on the weighing: the standard deviation of the residuals was found to be about 30% (the mean value being close to zero). The reliability of the impact plates was further assessed once the three experiments were completed comparing the accelerometer data with the sediment weights measured after each run (which lasted between 8 h and 24 h): the measurement accuracy regarding the total mass of sediment evacuated from the flume was found to be finer than 10% (for weights in the order of 100 kg).

2.3.2 Water and bed elevation measurements

The water and bed elevation measurements rely on two techniques both mounted on a moving cart scanning the bed over its entire length: a series of ultrasonic probe and a laser-sheet imaging system. Each scan lasted about 3 minutes and covered a 14 m×60 cm bed area starting 1 m away the flume outlet. Indeed, the first and the last meter of the bed could not be measured because of technical limitations. The bed scans were performed automatically every 10 min during the experimental runs, and the reference level for the elevation measurements was the bottom of the flume. An additional scan was also performed between each run, when the bed was dry.

2.3.2.1 Ultrasonic probes

The water elevation was measured using 8 ultrasonic probes fixed on a support plate and equally spaced in the cross-sectional direction, as illustrated in figure 2.4. Given the distance between the probes and the bed surface, each sensor measured the average water elevation underneath its location over a circular area of about 9 cm in diameter. During the scans, the data from the ultrasonic probes were acquired with a sampling frequency of 1000 Hz using a National Instrument® acquisition board and the Data Acquisition Toolbox™ in Matlab®. The raw data were subsequently resampled at 50 Hz and therefore consisted of 8 longitudinal profiles having about 5 measuring points per centimeter. Each profile was then smoothed using a Gaussian filter and converted into centimeters based on the calibration performed prior to the experiments (see coefficients in Appendix A.4). Finally the water elevation was interpolated over a 14 m×60 cm grid having respectively a 5 cm and 1 cm spatial resolution in the longitudinal and in the cross-sectional direction, as illustrated in figure 2.5.
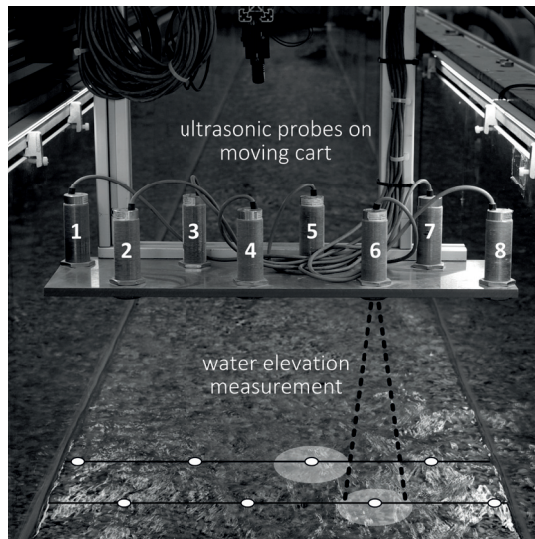
Figure 2.4: Measurement of the water elevation using height ultrasonic probes mounted on a moving cart.
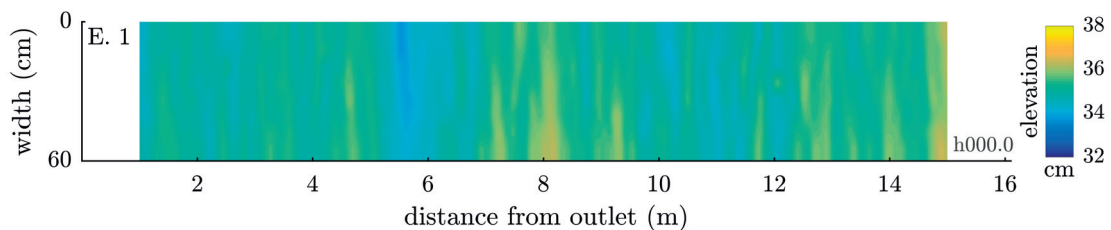
Figure 2.5: Water elevation with respect to the flume bottom measured using the ultrasonic probes at the beginning of experiment 1 and interpolated over a 14 m×60 cm grid. The first and the last meter of the flume were not measured because of technical limitations.

The calibration of each ultrasonic probes was performed measuring the elevation of six wooden boards successively piled up on the bed surface (in such a way elevation values between 25 and 39 cm were considered). The measurement accuracy of the probes was subsequently assessed using a similar procedure, and it was found to be finer than 2 mm. However, this accuracy is expected to be coarser when measuring the water elevation since the latter is a "rougher" surface.

2.3.2.2 Laser-sheet imaging technique

The bed elevation was measured using a laser-sheet imaging technique consisting of a color camera taking top-view images of a green laser sheet projected on the bed surface, as illustrated in figure 2.6(left). The laser was powerful enough (50 mW) for its projection on the bed, after passing through the water, to appear clearly in the images taken by the camera. As a consequence, this technique did not require the discharge to be stopped during the experiments. The camera and laser characteristics are detailed in Appendix A.5.

The camera and the laser were both fixed on the moving cart in such a way that their positions were aligned with the middle of the flume and their orientations (in the horizontal plan) corresponded with the cross-sectional direction. Moreover, the camera was pointing perpendicularly toward the bed surface and the laser sheet had a 28.1° angle to the vertical. Given these settings, the laser projection appeared on every image taken during the experiments regardless the variations in bed topography (i.e., it was always in the field of view of the camera).

The camera was set to take 6 frames-per-second which corresponded to roughly one image every two centimeters in the longitudinal direction (~900 images per bed scan). Each frame was then orthorectified (i.e., corrected for optical distortions from the sensor system) and post-treated using an image processing algorithm in order to compute the coordinates (in pixels) of the laser projection in the image. Based on these coordinates, the bed elevation along the cross-section corresponding to the laser projection was subsequently calculated using trigonometrical relationships detailed hereafter.

A two-dimensional representation of the laser-sheet imaging technique viewed from the side, ignoring the refraction effects at the air-water interface, is given in figure 2.6(right). Given the geometry of the schematic, one can derive that

$$\frac{x}{d} = \frac{z}{f} \quad \text{and} \quad \frac{x}{x_L} = \frac{z - z_L}{z_L} \tag{2.1}$$

which can be rewritten

$$z = \frac{f z_L x_L}{f x_L - d z_L} \quad \text{and} \quad x = \frac{d z_L x_L}{f x_L - d z_L} \tag{2.2}$$

with x the horizontal distance between the laser projection and the camera, d the distance corresponding to x on the camera sensor, z the height between the camera and the bed surface,
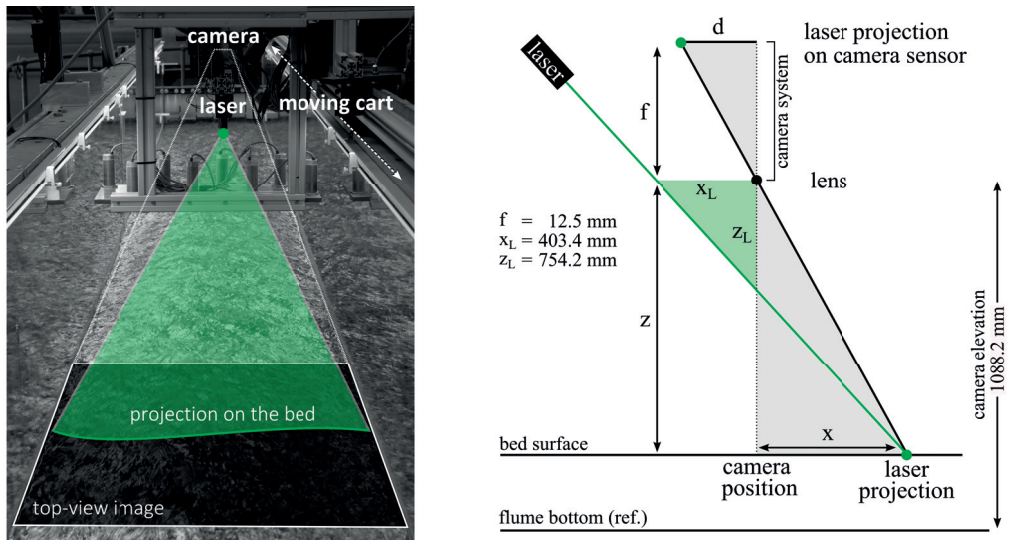
Figure 2.6: Front view (left image) and schematic representation viewed from the side (right image) of the laser-sheet imaging technique consisting of a camera and a laser mounted on a moving cart.

and f the focal length of the camera. The parameters x_L and z_L depict indirectly the angle of the laser and its position compared to the camera.

Based on equation 2.2, the bed elevation could be computed along the cross-section associated with each image since x and z were the only unknown variables. Indeed, f is a property of the camera, d depends on the coordinates of the laser projection in the image (computed previously) and on the sensor characteristics (size and resolution), and x_L and z_L were computed prior to the experiments based on the camera and laser positions.

The elevation data associated with each image were then referenced with respect to the flume based on the height between the camera and the flume bottom and the camera position corresponding to each image. Indeed, the latter was recorded during the bed scans using a proximity sensor counting the teeth of the cart rail. The bed elevation measurements were finally interpolated over the same 14 m×60 cm grid as the water elevation measurements for comparison purposes (see figure 2.7).
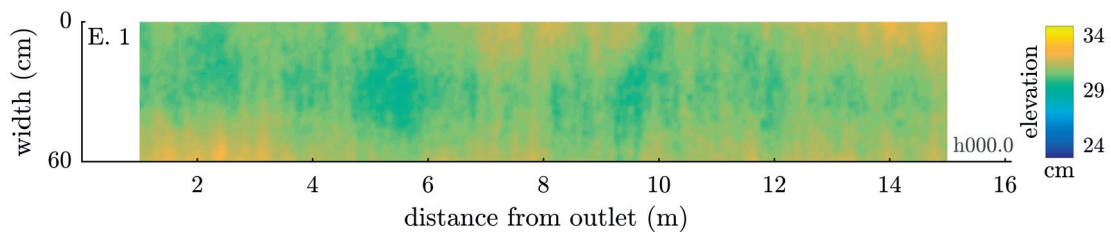
Figure 2.7: Bed elevation with respect to the flume bottom measured using the laser-sheet imaging technique at the beginning of experiment 1 and interpolated over a 14 m×60 cm grid.

In order to account for refraction effects, the following correction was applied to the the bed topography measurements:

$$z_b = z_w - 1.4(z_w - z_{b,raw}) \tag{2.3}$$

with z_b the bed elevation from the flume bottom corrected for refraction effects, $z_{b,raw}$ the bed elevation prior to correction, and z_w the water elevation from the flume bottom computed using the ultrasonic probes. This correction was derived based on the Snell–Descartes law applied to an air-water interface (see Appendix A.6 for derivation). Note that $z_w - z_{b,raw}$ is an estimation of the flow depth and that the factor 1.4 corresponds approximatively to the ratio between the water and air refractive indexes (≈ 1.33).

The invariant parameters in equations 2.2 (i.e., x_L, z_L and the camera elevation with respect to the flume bottom) were computed accurately prior to the experiments using the procedure described above in reverse (i.e., knowing z and x). For this purpose, we placed a board recovered with graph paper on the bed surface (under dry bed conditions) at a known elevation (in order to compute z and x accurately). Repeating the operation one time at a different elevation, we had enough parameters to compute the laser angle and to solve the equation system.

The measurement accuracy under dry conditions was then assessed measuring the height of the steps of a PVC staircase of known dimensions (15 mm step height) placed on the bed surface: it was found to be finer than 1 mm. In order to assess the measurement accuracy under wet conditions (i.e., with water flowing in the flume), we compared the bed topography measured at the end of each run (see table 2.1) under dry conditions and the same topography measured just before the discharge was stopped. The standard error (i.e., the root mean squared error) of the measurements made under wet conditions was found to be about 0.5 cm (the bed elevation being roughly 30 cm thick with variations mostly between ±5 cm).

3 Bedload transport rate fluctuations

In this chapter, we investigate the bedload transport rates measured at the flume outlet during each of the three experiments. More specifically, we are interested in the fluctuations observed in the corresponding time series. Note that the results obtained are analyzed making references to the bed slope and morphology, which are investigated in details in Chapter 4. Moreover, the effect of the sediment feed rate is discussed throughout the chapter highlighting the differences in the results obtained for each experiment.

Our analysis starts with the definition of three fluctuation regimes, each associated with a sediment feeding condition and characterized by its intermittency and intensity. We then further discuss the time scales and the periodic character of the bedload pulses, and investigate the effect of the sampling time on their characteristics. Finally, we relate the bedload transport measurements to sediment storage in the bed, and conclude on the equilibrium state of the system before discussing the results.

3.1 Preliminary considerations

The bedload transport rate (BTR) was measured continuously at the flume outlet during each experiment. The corresponding time series can therefore be investigated over a wide range of time scales, depending on the related physical processes that are of interest (Gomez et al., 1989). Two extreme examples are the motion of individual particles and the migration of mega-scale bedforms (Hoey, 1992). In this this study, we focus on the propagation of macro-scale bedforms (i.e., that scale with the flume width). After a first analysis of the data collected, a sampling time of one minute was found to be relevant given our objectives. We make it clear that, unless stated otherwise, all the results concerning the BTRs presented in this chapter are associated to this time scale. The average BTRs over one minute (Q_s) are plotted in figure 3.1; and the main characteristics of the time series are given in the first part of table 3.1.

3.1.1 Bedload pulses and low transport phases

The BTR time series in figure 3.1 are characterized by large fluctuations, which indicates a succession of low and intense bedload transport events during the experiments. This
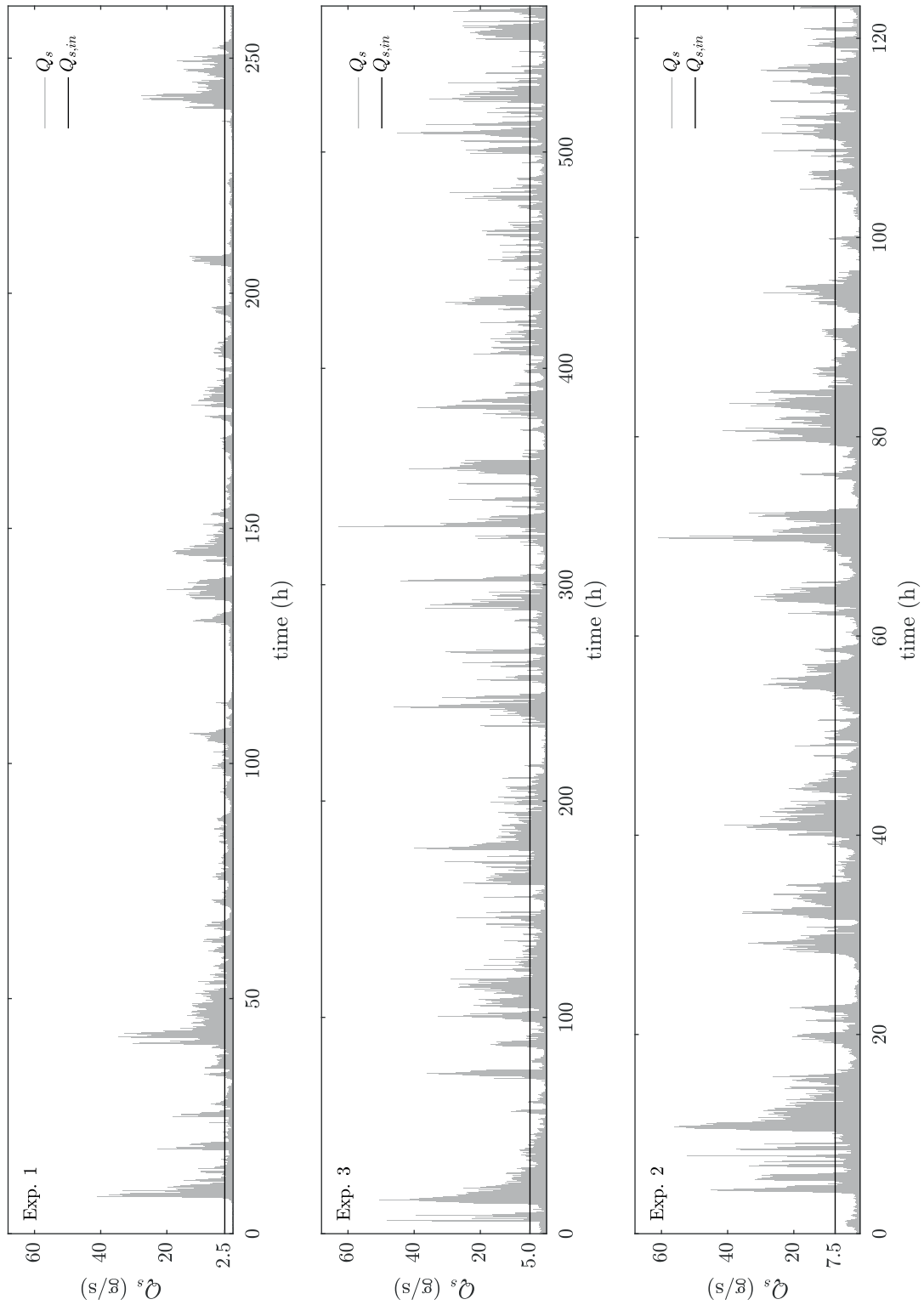
Figure 3.1: Time series of the bedload transport rates averaged over one minute Q_s measured at the flume outlet during experiment 1, 2 and 3. The black lines indicate the sediment feed rates $Q_{s,in}$, which are about equal to the average BTR values $\bar{Q}_s$.

Table 3.1: Summary values of the bedload transport rate measurements averaged over one minute during experiment 1, 2 and 3.

		Units	Exp. 1	Exp. 3	Exp. 2
flow rate	Q_l	l/s	15	15	15
flume slope		%	1.6	1.6	1.7
sediment feed rate	$Q_{s,in}$	g/s	2.5	5.0	7.5
average bedload transport rate		g/s	2.65	4.82	7.85
standard deviation		g/s	3.86	6.11	8.11
relative standard deviation			1.46	1.27	1.03
maximum value		g/s	41.12	62.89	61.04
number of samples			15666	34050	7395
experiment duration		h	261.1	567.5	123.2
ignoring the adjustment time at the beginning of the experiments [*]					
adjustment time	t_a	min	678	713	292
average bedload transport rate	$\bar{Q}_s$	g/s	2.57	4.84	7.97
standard deviation		g/s	3.54	6.08	8.05
relative standard deviation			1.38	1.26	1.01
maximum value		g/s	34.62	62.89	61.04
number of samples			14988	33337	7103
experiment duration	T_{exp}	h	249.8	555.6	118.4

[*] see section 3.1.2.1

variability is stressed by the values given in table 3.1: the standard deviation of the time series is larger than 100% and the BTRs can be up to one order of magnitude higher than their average values. Our measurements are therefore consistent with the numerous studies that have described the inherent variability of bedload transport, even under steady flow conditions (Gomez et al., 1989).

The fluctuating behavior of the BTR time series reflects the *intermittent* character of bedload transport, in the sense that the fluctuations show heterogeneity in their magnitude and in their temporal distribution (Singh et al., 2009). To avoid any confusion, we clarify that this terminology is sometimes used in another sense, not employed here, to describe particle motion and the alternation between moving and resting phases (e.g., in Ancey et al., 2014). We also make it clear that the BTRs averaged over one minute in figure 3.1 never drop to zero as the term *intermittent* may suggest.

The peaks in the BTR time series are referred to as *bedload pulses*, following the terminology used by Gomez et al. (1989). From a morphological perspective, the occurrence of bedload pulses implies that, in the bed, large sediment volumes are transferred in the downstream direction. During these intense transport phases, the bed is therefore on the whole eroded. In between bedload pulses, the BTRs are low compared to the sediment feed rates as illustrated in figure 3.1. These *low transport phases* inversely indicate a global aggradation of the bed

(i.e., a general increase in bed elevation due to sediment deposition).

3.1.2 Adjustment time at the beginning of the experiments

3.1.2.1 Definition

The beginning of each BTR time series is characterized by a time period of low bedload transport (i.e., close to zero) followed by large bedload pulses (see figure 3.1). This period is termed the *adjustment time* and noted t_a: it is the time necessary for the bed to evolve from a flat configuration (the initial condition) to a formed configuration (i.e., with bedforms).

During the adjustment time, the bed slope (S_b) comes close to its average value over the entire experiment duration ($\bar{S}_b$), as illustrated in figure 3.2 (section 4.2.1 for details about the bed slope calculation). Note that, in the literature, $\bar{S}_b$ is sometimes referred to as the *equilibrium slope* (Frey et al., 2003; Recking et al., 2009), under the assumption that the experiment duration is long enough and that an equilibrium state is reached. The complete bed slope time series are investigated in section 4.2.
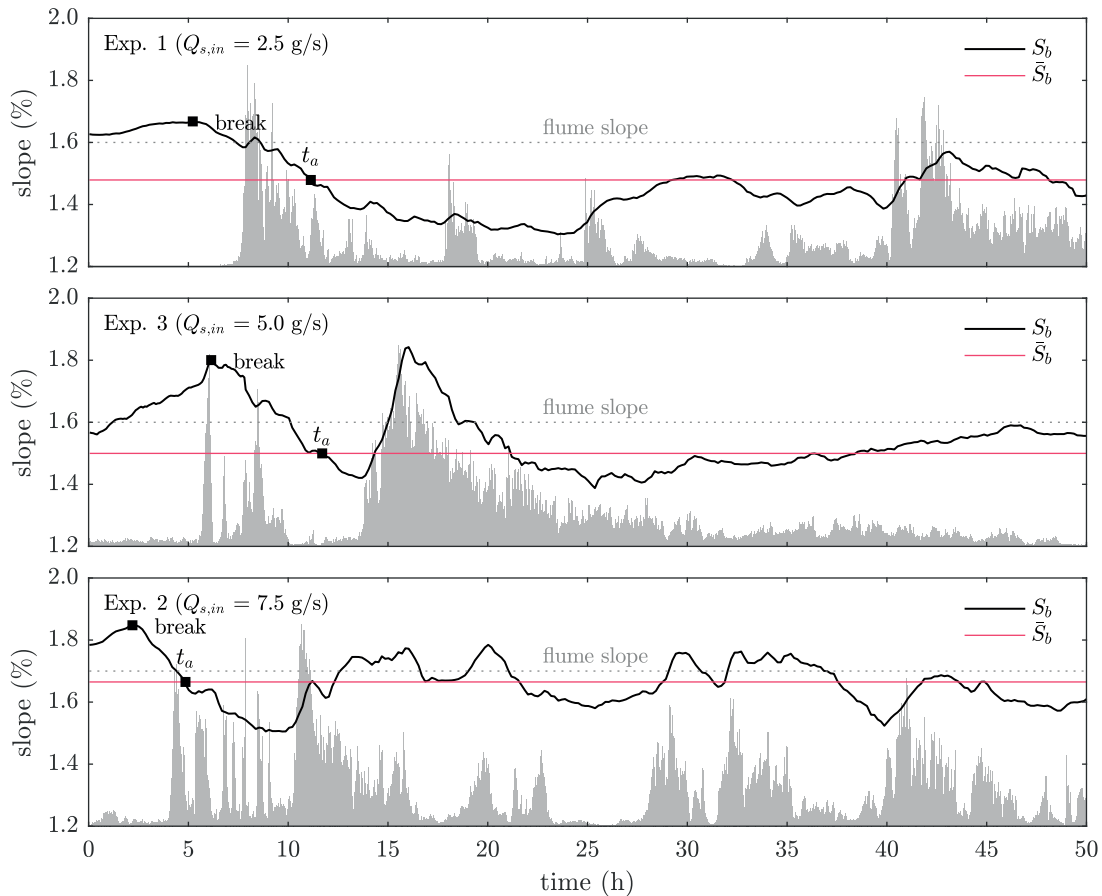
Figure 3.2: Temporal evolution of the bed slope S_b at the beginning of experiment 1, 2 and 3. The filled area plots represent the bedload transport rates on an arbitrary scale.

In each experiment, the initial value of S_b is larger than $\bar{S}_b$ (see figure 3.2). When the experiments start, S_b increases until a certain breaking point. This raise in the bed slope indicates that the sediment fed in the flume is deposited in its upstream part. During this phase, we observed that alternate bars form in the bed, progressively from the upstream to the downstream part of the flume.

After the breaking point, S_b drops below $\bar{S}_b$ and large bedload pulses occur: the bed is eroded and the slope decreases. Alternate bars are then present over the entire flume length, as illustrated in figure 3.3. We therefore define the adjustment time t_a as the time necessary for S_b to meet $\bar{S}_b$ for the first time.
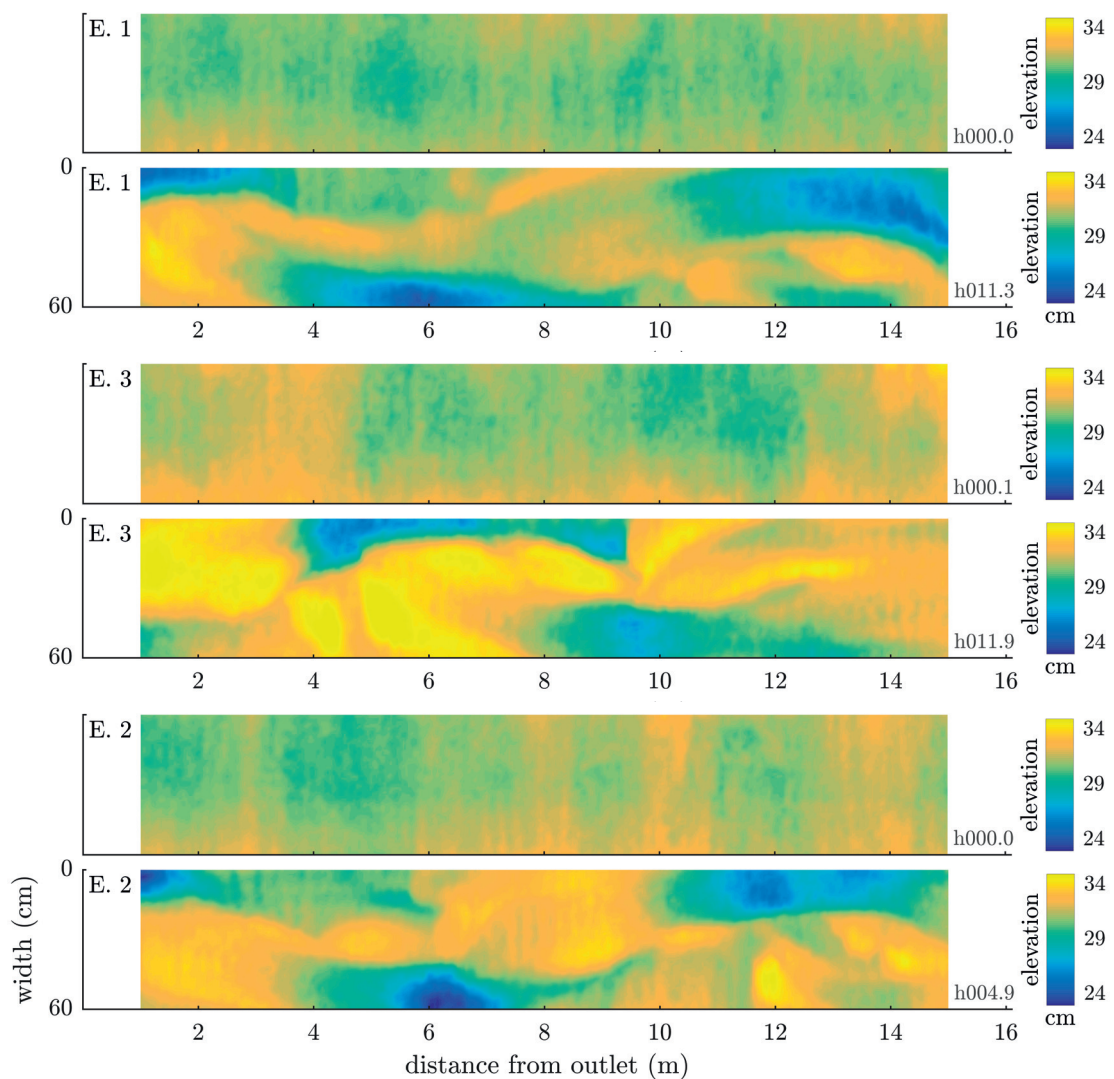
Figure 3.3: Bed topography at the beginning of each experiment (flat) and after the adjustment time (with alternate bars). See section 4.1 for more details about the topographical data.

27

3.1.2.2 Evolution of the system

In the following, we consider the system constituted of the mobile bed and the water flow. It is therefore bounded by the flume components (walls, bottom, inlet and outlet) and the free surface; and its initial state is characterized by a flat bed with a uniform thickness.

During the experiments, the system is fed with water and sediment at a constant rate (steady feeding) and the bed topography varies over time through the processes of erosion, transport and deposition of the bed material. As a result, the hydraulic conditions in the system also vary over time since they are linked to the bed morphology through a feedback loop driven by bedload transport (Griffiths, 1993).

Although the initial bed slope was set close to the theoretical equilibrium slope (which depends on the sediment feed rate, the flow rate and the bed roughness), the initial flat configuration is not stable. Consequently, during the adjustment time, the system evolves toward more stable configuration, closer to the ones found in natural systems. In our experiments, it consists of alternate bars.

The transport capacity of the system also changes during the adjustment time, and evolves toward a value close to the imposed sediment feed rate in order to ensure a neutral sediment balance (Wainwright et al., 2015). Note that this mass-balance equilibrium is verified at the experiment time scales since $\bar{Q}_s$ matches $Q_{s,in}$ in each experiment (see table 3.1).

The adjustment time is therefore related to the concept of system equilibrium. However, the criterion used above to define t_a is not sufficient to guarantee that equilibrium conditions are achieved. As discussed in section 3.3, the latter are likely to be reached after longer time periods.

The characteristics of the BTR time series computed ignoring the adjustment time are given in the second part of table 3.1. Since t_a is short compared to the experiment durations, they show only slight differences with the ones of the whole time series. However, in the following analyses, we choose to ignore this first part of the experiments which is not representative of the system when the bed is formed.

3.2 Fluctuation regimes

The BTR fluctuations during the experiments reflect, as discussed in the previous section, the alternation between bedload pulses, which are intense transport events, and low transport phases. In the following, we characterize this fluctuating behavior of the time series quantifying its intensity and intermittency. Moreover, based on the result obtained, we define three fluctuation regimes related the different sediment feed rates in the experiments.

3.2.1 Data preparation

The BTRs presented in figure 3.1 fluctuate about their mean value, which matches the sediment feed rate in each experiment. In the following, we therefore assess the fluctuating behavior of the time series using without distinction $\bar{Q}_s$ and $Q_{s,in}$ as reference values.

In order to compare the time series of each experiment, the BTRs are normalized with respect to $\bar{Q}_s$, and the normalized sediment feed rates $Q^\star_{s,in}$ are rounded to 1 for convenience purposes. The normalized BTRs ($Q^\star_s$) plotted in figure 3.4 therefore indicate the relative magnitude of the fluctuations. Their main characteristics are given in table 3.2.

Bedload pulses, as discussed in section 3.1.1, refer to intense sediment transport events. They can be therefore identified in figure 3.4 as batches of large BTR values. In order to investigate their characteristics, we define bedload pulses more accurately as any consecutive set of $Q^\star_s$ values above $Q^\star_{s,in}$, and of which the maximum value is above a given threshold. The average pulse frequency and the average pulse duration, related to bedload pulses larger than one time the standard deviation, are given in table 3.2 for each experiment.

Table 3.2: Characteristics of the normalized bedload transport rates for experiment 1, 2 and 3. The adjustment times are not taken into account.

		Units	Exp. 1	Exp. 3	Exp. 2
sediment feed rate	$Q_{s,in}$	g/s	2.5	5.0	7.5
average bedload transport rate	$\bar{Q}_s$	g/s	2.57	4.84	7.97
normalized sediment feed rate	$Q^\star_{s,in}$		~1	~1	~1
experiment duration	T_{exp}	h	249.8	555.6	118.4
normalized bedload transport rates					
average value	$\bar{Q}^\star_s$		1	1	1
range			~0 –13.50	~0 –13.00	~0 –7.66
standard deviation	$\sigma^\star$		1.38	1.26	1.01
statistics related to pulses larger than one time the standard deviation					
average pulse frequency		h^{-1}	0.2	0.3	0.5
average pulse period		h	5.2	3.5	2.1
range			10 min–32 h	6 min–44 h	6 min–10 h
standard deviation		h	7.0	5.3	2.2
average pulse duration		h	1.2	0.9	0.6
range			4 min–5 h	2 min–7 h	4 min–3 h
standard deviation		h	1.3	1.0	0.6

3.2.2 Global characteristics

The values given in table 3.2 provide a global characterization of the fluctuations in the BTR time series. Indeed, the relative standard deviation of the BTRs quantifies the intensity of the fluctuating behavior, and the average pulse frequency (along with the related standard deviation) measures its intermittency.

In this way, it appears that in all three experiments at least 30% the BTR measurements are greater than two times the sediment feed rate (i.e., the coefficients of variation, which are equal to $\sigma^{\star}$, are larger than 1). Moreover, as pointed by the range of the BTR values, the fluctuations can be one order of magnitude higher or lower than their average value.

The intermittent character of the fluctuations is stressed by their relative high average frequency compared to the experiment durations and by the variability in the pulse periods. Indeed, a bedload pulse is observed in average at least every 5 h and the pulse spacing can vary within two orders of magnitude (from few minutes to more than ten hours). Note also that the average pulse duration is in the order of 1 h, which is much lower than the average pulse spacing.

The values above highlight the fluctuating behavior of all three BTR time series. However, comparing the characteristics of each experiment, they appear to be each associated with a different fluctuation regime depending on the sediment feed rate. Indeed, when $Q_{s,in}$ increases, bedload pulses tend to be shorter, more frequent, and of lower magnitude.

Note that the increase in sediment feed rate between the experiments is equivalent to an increase in flow rate, which is a common way to test different hydraulic conditions (Ashmore, 1991; Singh et al., 2009; Ghilardi et al., 2014a), in the sense that both result in an increase in the stream power

$$\omega = \rho g q S_b \tag{3.1}$$

with ρ the water density (kg m^{-3}), g the acceleration due to gravity (m s^{-2}), q the unit water discharge (m^2 s^{-1} m^{-1}) and S_b the bed slope (-). Indeed, as discussed in section 3.1.2, an increase in the feed rate induces a raise in the slope to ensure a sufficient transport capacity (Iseya and Ikeda, 1987).

The stream power estimated using the average bed slope in the above equation is respectively 3.61, 3.65 and 4.07 W m^{-2} in experiment 1 ($Q_{s,in} = 2.5$ g/s), experiment 3 ($Q_{s,in} = 5.0$ g/s) and experiment 2 ($Q_{s,in} = 7.5$ g/s). The corresponding dimensionless stream power indexes, computed by using $\omega^{\star} = q S_b / ((\rho_{s,app}/\rho - 1) g d_{50}{}^3)^{0.5}$ with $\rho_{s,app}$ the sediment apparent density and d_{50} the median grain diameter (Hoey, 1992), are 0.36, 0.37 and 0.41.
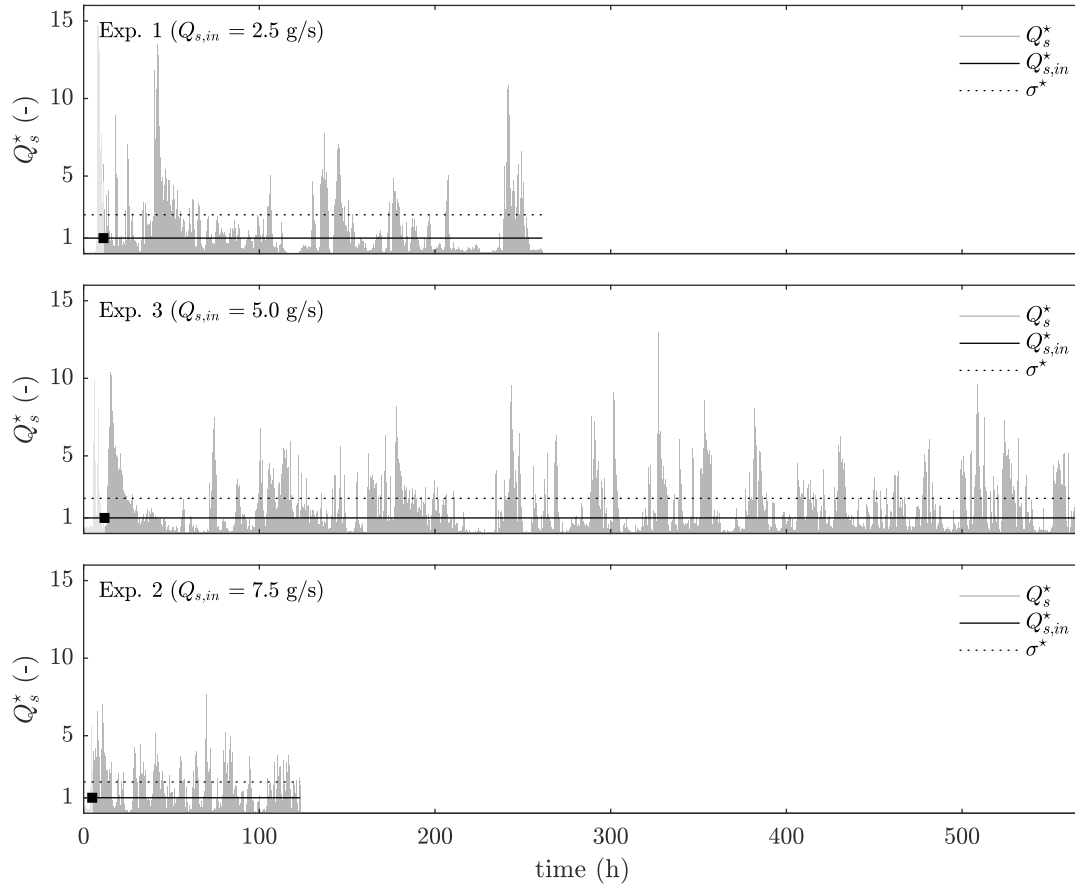
Figure 3.4: Time series of the normalized bedload transport rates $Q_s^\star$ for experiment 1, 2 and 3. The solid lines indicate the normalized sediment feed rates $Q_{s,in}^\star$ and the dashed lines the standard deviations $\sigma^\star$.

3.2.3 Dependency on pulse magnitude

In the definition given above, bedload pulses are characterized by their duration and frequency, which depend on their magnitude. For instance, the values given in table 3.2 are only related to pulses higher than one time the standard deviation. In the following, we characterize the bedload pulses associated with each fluctuation regime describing the dependency of their average frequency and average duration on their magnitude.

For each experiment, the average pulse frequency and the average pulse duration are computed by considering bedload pulses larger than different threshold values, ranging from 1.5 to 4. The dependency of these three variables on each other is plotted in figure 3.5. Note that threshold values larger than 4 are ignored because the number of corresponding pulses is too low for the related statistics to be significant. Moreover, we remind that a threshold of 1.5 implies that all pulses larger than 1.5 times the sediment feed rate are considered.
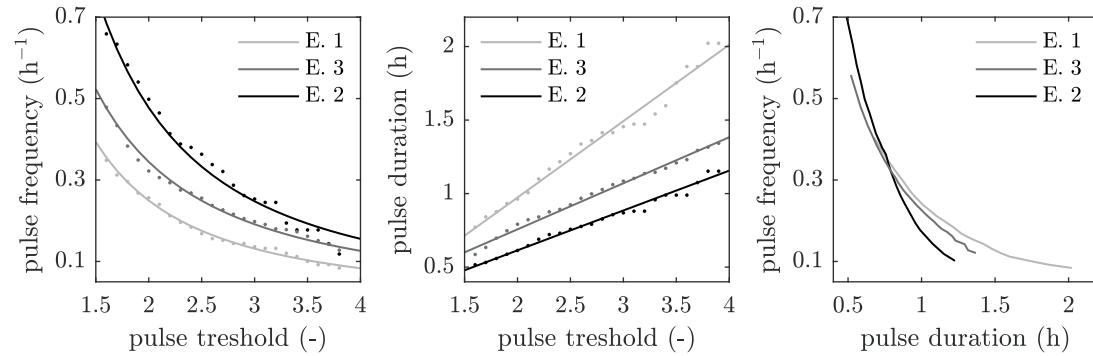
Figure 3.5: Relationships between the average pulse frequency, the average pulse duration, and the threshold used to define bedload pulses for experiment 1, 2 and 3.

In each experiment, as shown in figure 3.5(left), the pulse frequency decreases with increasing threshold value: large bedload pulses occur less frequently than lower ones. The decrease follows a power law $f(x) = ax^b$ with

– $a = 0.75$ and $b = -1.58$ in experiment 1 ($R^2 = 0.99$, $SE = 0.01$);

– $a = 0.94$ and $b = -1.45$ in experiment 3 ($R^2 = 0.99$, $SE = 0.01$);

– $a = 1.47$ and $b = -1.62$ in experiment 2 ($R^2 = 0.98$, $SE = 0.03$);

with R^2 the coefficient of determination of and SE the standard error of the estimate. Moreover, bedload pulses tend to be more frequent in experiments with larger sediment feed rates, regardless the threshold value. Note that, however, the average frequency of the largest pulses in each experiment converges toward the same value (close to zero).

The average pulse durations plotted in figure 3.5(middle) increase linearly with increasing threshold value in each experiment, which indicates that large pulses tend to last longer than lower ones. The coefficients of the linear functions $ax + b$ describing the increase are

– $a = 0.52$ and $b = -0.06$ in experiment 1 ($R^2 = 0.98$, $SE = 0.06$);

– $a = 0.31$ and $b = 0.13$ in experiment 3 ($R^2 = 0.99$, $SE = 0.03$);

– $a = 0.27$ and $b = -0.07$ in experiment 2 ($R^2 = 0.98$, $SE = 0.03$).

It is interesting to note that the slopes are similar in experiment 2 and 3, whereas the increase is almost twice faster in experiment 1 (which has the lowest sediment feed rate). It appears also that, for any threshold value, the average pulse duration is larger in experiments with lower sediment feed rates.

The two relationships above are summarized in figure 3.5(right) where we show that the average pulse frequency decreases with increasing average pulse duration. It appears that the relationship is similar in experiment 1 and 3, which are associated with comparable stream

power values. In experiment 2, which has a higher stream power value, the pulse frequency decreases faster with increasing duration. Note that, however, the ranges of values visited in each experiment are different.

In summary, the results above support the existence of three fluctuation regimes associated with the different sediment feed rates. The tendency described in section 3.2.2 is verified and extended to all fluctuations: bedload pulses tend to be shorter and more frequent, regardless their magnitude, when $Q_{s,in}$ (and therefore the stream power) increases.

3.2.4 Variability in bedload pulses

As discussed above, the average pulse frequencies and durations given in table 3.2 depend on pulse magnitude (figure 3.5). In order to complete our analysis on the intermittent character of bedload pulses, the relative standard deviations of the pulse durations and of their inter-arrival times (i.e., their spacings in time) are plotted in figure 3.6 versus the pulse threshold.
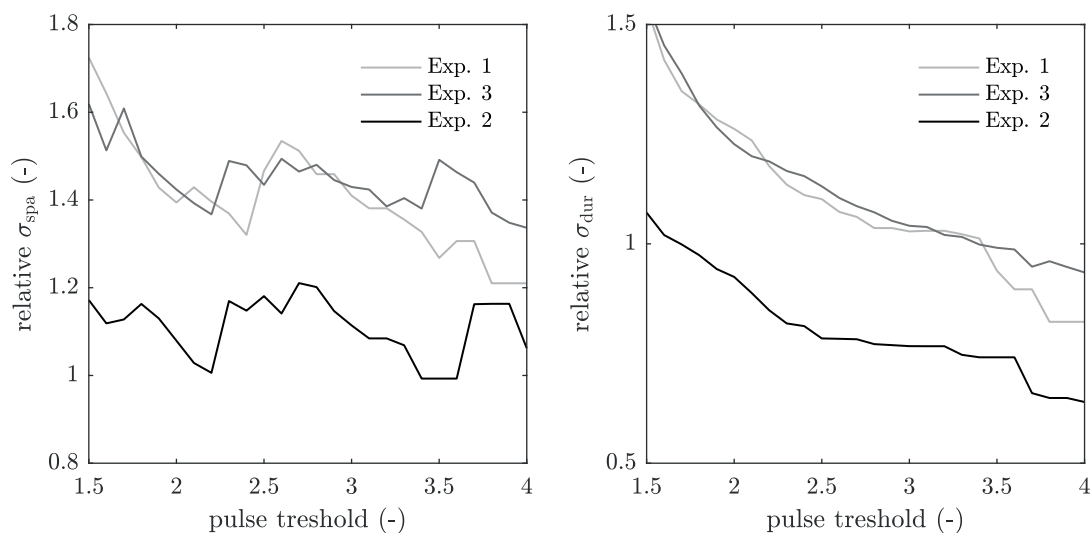
Figure 3.6: Relative standard deviations of the pulse spacings (left) and of the pulse durations (right) versus the threshold value used to define bedload pulses in experiment 1, 2 and 3.

The variability in pulse spacings changes little with increasing pulse threshold, although it shows a slight tendency to decrease as illustrated in figure 3.6(left). The average value of the relative standard deviation is 1.4, 1.4 and 1.1 in experiment 1, 3 and 2, which is high (i.e., > 100%). Our conclusions in section 3.2.2 about the intermittent character of bedload pulses are therefore supported.

Regarding the relative variability in pulse durations, it remains important (at least > 60%) although the decrease with increasing threshold value plotted in figure 3.6(right) is more pronounced than for the pulse spacings. Comparing the relative standard deviations to the average values in figure 3.5(middle), it appears that the pulse durations vary between few

minutes and few hours which generalizes the results in table 3.2 to all pulse thresholds.

It is interesting to note that the fluctuation regime in experiment 2 in differentiated from the two others in figure 3.6 by a generally lower variability in pulse durations and spacings. In other words, its intermittent character is less marked. Moreover, the high variability in the characteristics of bedload pulses commented above, in addition to highlight their intermittent character, implies that BTR fluctuations occur at different time scales.

3.3 Time scales of bedload pulses

The fluctuation regimes discussed in the previous section are characterized by intermittent bedload pulses: BTR fluctuations show heterogeneity in their magnitude, duration and inter-arrival time. We also demonstrated that, in regimes with larger sediment feed rates, fluctuations tend to be of lower magnitude, of shorter duration and closer in time. In this section, we determine the range of time scales over which bedload pulses occur investigating the convergence time and the power spectrum associated with each fluctuation regime.

3.3.1 Convergence time

In each experiment, the average BTR matches the sediment feed rate (see table 3.1), which can be interpreted as a sign of equilibrium since it indicates a neutral sediment balance at the experiment time scale (Iseya and Ikeda, 1987). However, given the long experiment durations (more than 100 h), such equilibrium conditions are likely to be reached after a shorter time period. More generally, we are here interested in the minimum observation time (regardless the experiment portion considered) for which mass-balance equilibrium is achieved.

This issue is addressed in the following computing the *convergence time* in each experiment. It is defined as the minimum sampling time for which the averaged BTRs are contained within a limited range of values close to the sediment feed rate. Two ranges are considered hereafter: $Q_{s,in} \pm 50\%$ and $Q_{s,in} \pm 25\%$, and the corresponding convergence times are noted $T_{c,50}$ and $T_{c,25}$. The latter are determined computing the temporal averages of the normalized BTRs for different sampling times T_s and starting times t_0 as follow:

$$\bar{Q}_s^\star(T_s; t_0) = \frac{1}{T_s} \sum_{t=t_0}^{t_0+T_s-1} Q_s^\star(t), \quad t_0 \in [1, T_{exp}] \quad \text{and} \quad T_s \in [1, T_{exp} - t_0 + 1], \tag{3.2}$$

with T_{exp} the experiment duration. For convenience purposes, the sampling times were chosen as multiples of 30 min; and the starting times as multiples of 1 h in experiment 1 and 2, and of 4 h in experiment 3. We remind that in each experiment the adjustment time is ignored.

The time-averaged BTRs are plotted as a function of T_s and t_0 in figure 3.7 for each experiment. Note that, in the following, we are mostly interested in the envelopes of the curves which indicate the range of values visited by the BTRs for a given sampling time. We first comment on the upper envelopes, related to bedload pulses, and then on the lower ones which reflect the effect of low transport phases on the time-averaged BTRs.
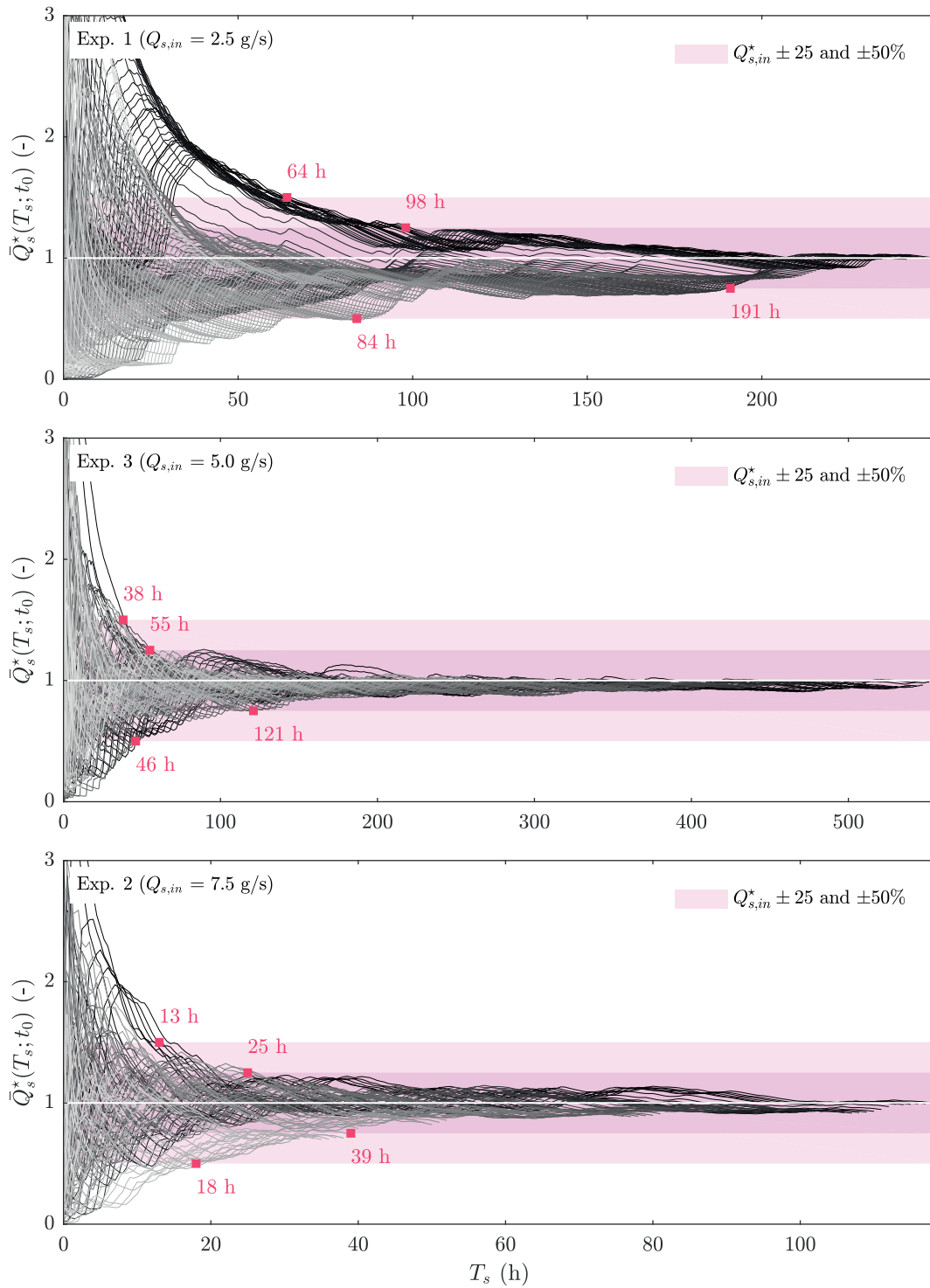
Figure 3.7: Temporal averages of the normalized bedload transport rates as a function of the sampling time T_s and the starting time t_0 for experiment 1, 2 and 3. Each curve corresponds to a different starting time (light shades of gray stand for large starting times).

3.3.1.1   Convergence time associated with bedload pulses

We are here interested in the effect of the sampling time on bedload pulses (i.e., on large BTR values). We therefore focus on the time-averaged BTRs larger than the sediment feed rates in figure 3.7. For clarity purposes, the upper envelope of each experiment is reported in figure 3.8. They indicate the maximum BTR measured during the experiments as a function of the sampling time.
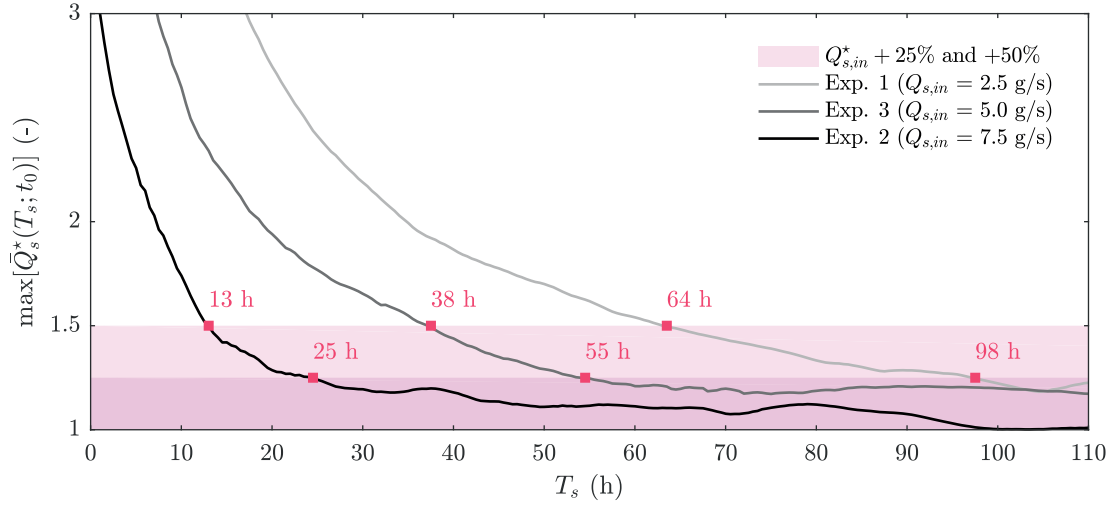
Figure 3.8: Maximum normalized bedload transport rates as a function of the sampling time T_s for experiment 1, 2 and 3.

The time-averaged BTRs in figure 3.8 converge slowly to the sediment feed rates with increasing sampling time, and the convergence time is shorter in experiments with larger sediment feed rates. This result is consistent with section 3.2 where we showed that bedload pulses in fluctuation regimes associated with larger $Q_{s,in}$ are of lower magnitude and closer in time. The convergence times characterising the different fluctuation regimes are summarized in table 3.3.

Table 3.3: Convergence times associated with bedload pulses in experiment 1, 2 and 3.

		Units	Exp. 1	Exp. 3	Exp. 2
sediment feed rate	$Q_{s,in}$	g/s	2.5	5.0	7.5
experiment duration	T_{exp}	h	249.8	555.6	118.4
convergence time (pulses $< Q_{s,in} + 50\%$)	$T_{c,50}$	h	64	38	13
$T_{exp}/T_{c,50}$			4	15	9
convergence time (pulses $< Q_{s,in} + 25\%$)	$T_{c,25}$	h	98	55	25
$T_{exp}/T_{c,25}$			3	10	5

The convergence times in table 3.3 are shorter than the experiment durations which indicates that neutral sediment balance is likely to be achieved before the end of the experiments. However, they are defined based on criteria (e.g., pulses lower than $Q_{s,in} + 25\%$) which only indicate that sediment balance is close to zero. In addition, as illustrated in figure 3.8, the convergence becomes very slow when the time-averaged BTRs come very close to $Q_{s,in}$ (i.e., less than 25% away). Therefore, in order to ensure mass-balance equilibrium, the experiments must be much longer than the convergence times, for instance by one order of magnitude. Such a criterion is met only in experiment 2 and 3 (see the relative convergence times in table 3.3).

3.3.1.2 Effect of low transport phases on convergence

The convergence of the time-averaged BTRs in figure 3.7 is asymmetrical on both side of the reference line representing the sediment feed rate. As discussed above, the convergence of the upper envelope reflects the effect of the sampling time on the bedload pulses. Inversely, the convergence of the lower envelope illustrates how low bedload transport phases affect the time-averaged BTRs. The upper and lower envelopes of the time-averaged BTRs, as plotted in figure 3.7, are compared in figure 3.9 for each experiment.
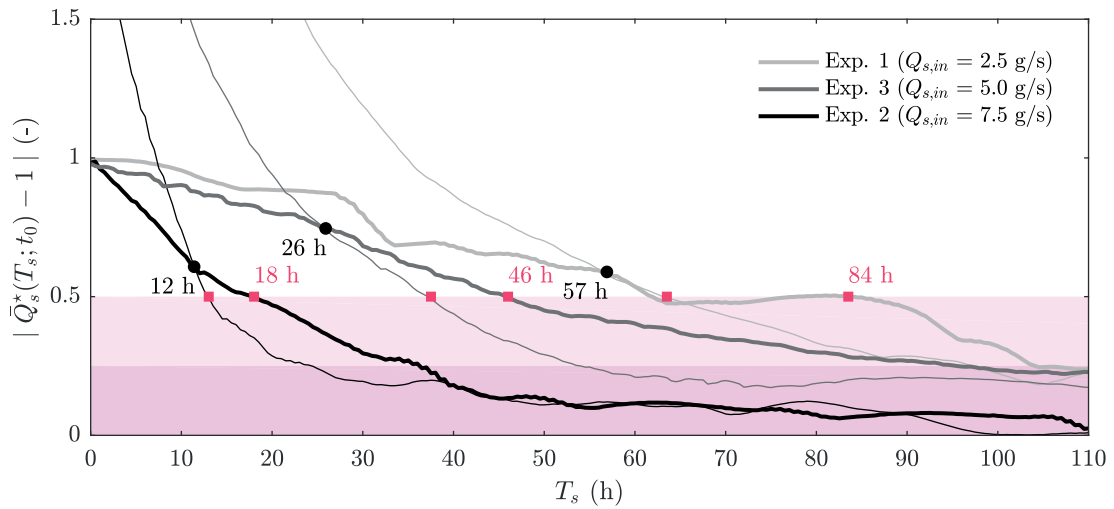
Figure 3.9: Upper (fine curves) and lower (thick curves) envelopes of the normalized bedload transport rates as a function of the sampling time T_s for experiment 1, 2 and 3.

For low sampling times, the deviation of the time-averaged BTRs from $Q_{s,in}^{\star}$ is much larger for the upper envelopes than for the lower envelopes (see figure 3.9). This difference in magnitude is consistent with what can be observed in the time series in figure 3.4: the deviation of the BTRs from $Q_{s,in}$ is much larger during bedload pulses than between them (i.e., during low transport phases).

However, this tendency gets inverted for sampling times greater than respectively 57 h, 26 h and 12 h in experiment 1, 3 and 2 (see figure 3.9). Low transport phases become then the limiting factor for convergence. It is interesting to note that this change occurs while fluctuations are

still relatively important (i.e., larger than $Q^{\star}_{s,in} \pm 50\%$).

As a consequence, the convergence times of the lower envelopes given in figure 3.9 are longer than the ones in table 3.3 (related to bedload pulses). This slower convergence means that bedload pulses are generally of shorter duration than low transport phases, which is consistent with the conclusions drawn in section 3.2.

The results above stress the importance of taking into account low bedload transport phases when studying BTR fluctuations, although, unlike bedload pulses, they do not directly imply the transport of large sediment amounts. Indeed, as shown in figure 3.4, the BTRs between bedload pulses can be much lower than the sediment feed rates for relatively long time periods compared to the pulse durations. The large sediment volumes stored in the bed during these low transport phases, and the morphological changes that necessarily occur, are thus likely to be related to the generation of bedload pulses (as further discussed in section 3.6).

3.3.2 Fluctuations across time scales

3.3.2.1 Considerations regarding the convergence time

The various shapes of the time-averaged BTRs curves in figure 3.7, and the slow convergence times discussed above, indicate that BTR fluctuations occur across a wide range of time scales. This conclusion is illustrated in figure 3.10, where fluctuations associated with time scales ranging from one minute to ten hours are presented using an example from experiment 3.
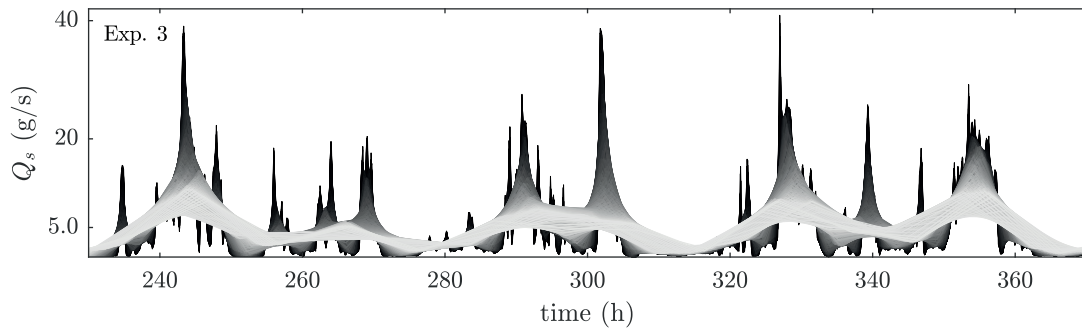
Figure 3.10: Bedload transport rates averaged over sampling times ranging from 10 min to 10 h for a portion of experiment 3. Each curve corresponds to a different sampling time (light shades of gray stand for large sampling times).

The convergence time is therefore a measure of the time necessary to capture all the fluctuations in the system. As a consequence, it can be seen as an upper bound of the time scales at which fluctuations occur. Indeed, the latter cannot be infinite: they are bounded by the system size and the feeding conditions (Jerolmack and Paola, 2010).

This measure of the maximum time scale is useful to assess the duration of the time series in the view of studying BTR fluctuations: the observation time should be much larger, at least

by about one order of magnitude, than the convergence time. As a consequence, whereas experiment 2 and 3 appear to be long enough, experiment 1 seems too short to capture the entire system dynamics. The data collected during the latter should therefore be interpreted carefully.

3.3.2.2 Analysis in the frequency domain

The results above indicate that BTR fluctuations occur over time scales ranging from few minutes to more than then hours. In the following, we evaluate this frequency range more accurately investigating the time series in the frequency domain. Our analysis is based on the Thomson's multitaper and the wavelet power spectra of the BTR time series plotted in figure 3.11.

At low frequencies, the spectra saturate: the power spectral density is constant which is characteristic from white noise and indicates stationarity (Jerolmack and Paola, 2010). The characteristic time scale associated with saturation is respectively 33 h, 27 h and 13 h in experiment 1, 3 and 2.

These saturation time scales indicate the maximum time scale associated with the BTR fluctuations. Note that they are consistent with the convergence times computed in section 3.3.1, although slightly shorter. Moreover, they also decrease with increasing sediment feed rate. The spectral analysis therefore supports and refines our previous conclusions.
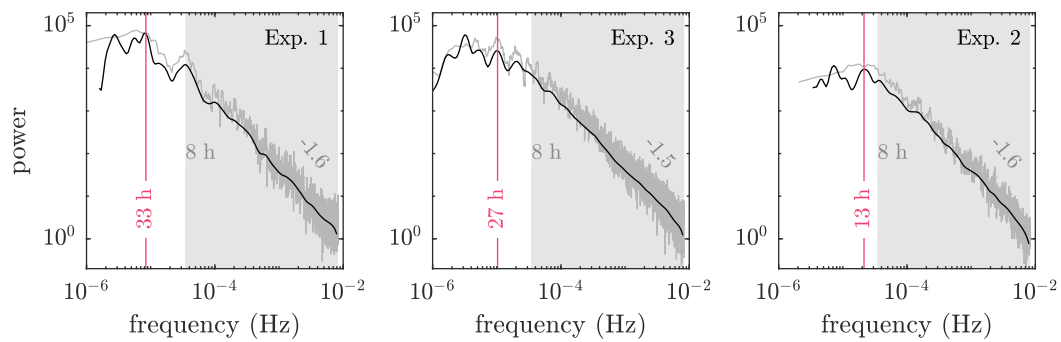
Figure 3.11: Power spectra of the bedload transport rates measured at the flume outlet during experiment 1, 2 and 3. The grey curves represent the multitaper spectrum and the black curves the wavelet spectrum. The scaling ranges are indicated in light grey and the corresponding spectral slopes are given. The vertical lines indicate the saturation time scales.

At frequencies higher than the saturation time scale, the power spectral density decreases with increasing frequency (see figure 3.11). The log-log linearity that is observed is indicative of a scaling range, which suggests a scale dependence of the fluctuation characteristics (Singh et al., 2009): the corresponding spectral slopes are respectively -1.59, -1.55 and -1.54 in experiment 1, 2 and 3. The energy contained in the fluctuations therefore decreases with increasing frequency similarly in each fluctuation regime. Note also that, in the scaling ranges, some

frequencies are more energetic (see figure 3.12): they indicate the most prevalent periods of the fluctuations (Kuhnle and Southard, 1988).

The considerations above raise the issue concerning the scale-dependence of BTR statistics. Indeed, several authors (Bunte and Abt, 2005; Ancey et al., 2008; Singh et al., 2009; Campagnol et al., 2012; Recking et al., 2012) reported that the characteristics of BTR fluctuations depend on the sampling time. We therefore address this issue in the next sections.
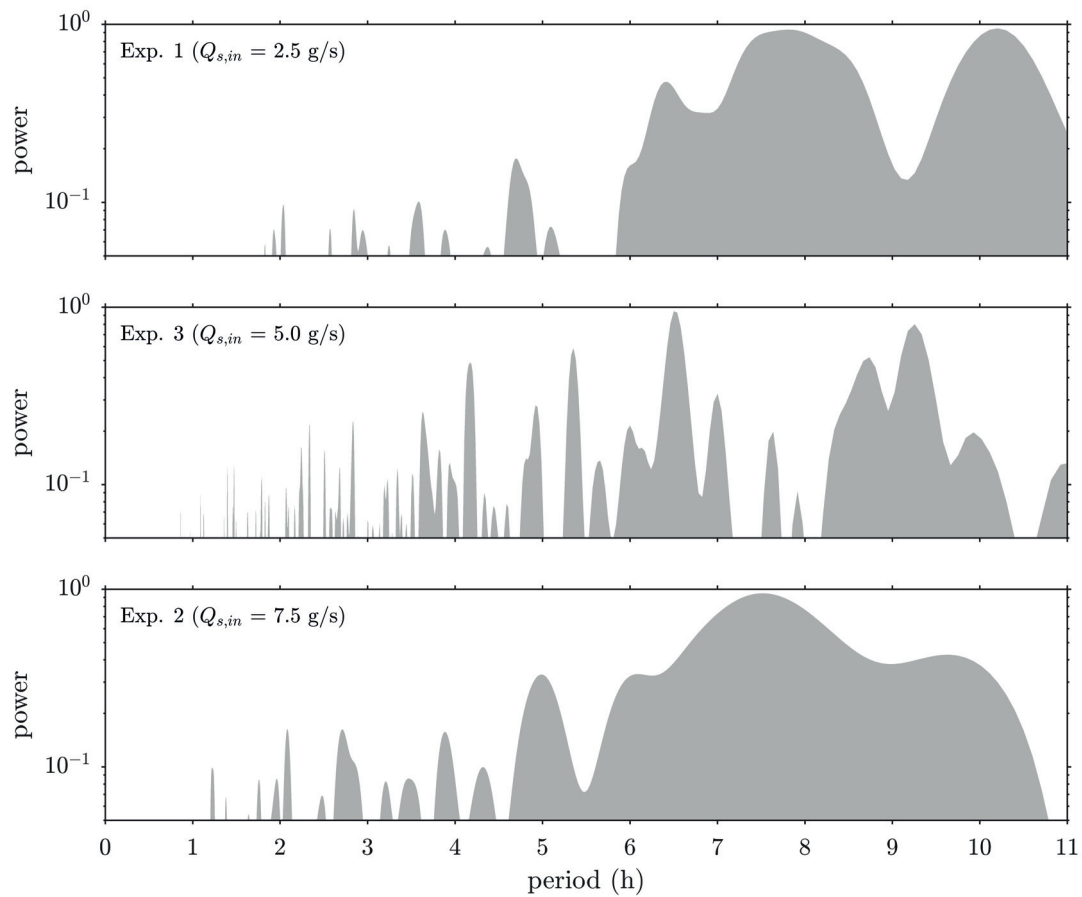
Figure 3.12: Normalized periodograms of the bedload transport rates measured at the flume outlet during experiment 1, 2 and 3. The periodograms were computed based on a Fourier transform of the time series, and only the frequencies higher than $1/11 \text{ h}^{-1}$ were considered.

3.4 Periodicity of bedload pulses

The bedload pulses observed during the experiment occur over a wide range of time scales, from few minutes to more than ten hours. In this section, we are interested in their potential periodic character, which has been reported in several study (Iseya and Ikeda, 1987; Ghilardi et al., 2014b), across these time scales. We clarify that the term *periodic* is used here to describe regular fluctuations over time, whereas some authors (Gomez, 1991; Hoey, 1992) use it in reference to any fluctuating behavior about a mean value. The analysis hereafter is based on the autocorrelation function of the BTR time series (Cudden and Hoey, 2003), which indicates their correlation with themselves for different time lags.

3.4.1 Data preparation

The autocorrelation function is computed for each BTR time series plotted in figure 3.1 ignoring the adjustment time (we remind that their temporal resolution is 1 min). In order to account for the effect of the sampling time, the autocorrelation function is also computed for the BTRs aggregated over different time periods ranging from 1 h to 5 h.

For experiment 3, which is particularly long (~560 h), an additional autocorrelation analysis is performed removing the first 230 h of the experiment. Indeed, examining the corresponding time series in figure 3.1, the fluctuating behavior seems different during the first part and the last part of the experiment. The results of the autocorrelation analysis for each experiment are presented in figure 3.13.

The autocorrelation functions in figure 3.13 get smoother as the sampling time increases, which is a direct effect of averaging. However, the general shape of the curves, including the peaks, remain similar even for sampling times as large as 5 h. The most prominent peaks in the autocorrelation functions therefore indicate the frequencies of bedload pulses associated with long time scales (i.e., several hours). Note that, since fluctuations occurring at different time scales can overlap, the potential periodic character of shorter pulses (as suggested by figure 3.12) cannot be assessed in the following.

3.4.2 Bedload pulse duration

The time lag when the autocorrelation function is zero for the first time is indicative of the duration of large-scale pulses (Campagnol et al., 2012). It is respectively 10 h, 8 h and 3 h for experiment 1, 3 and 2, which is consistent with the values given in section 3.2.3. In addition, it confirms that bedload pulses have a tendency to be shorter when the sediment feed rate increases.

If the experiment 3 is truncated, the time lag associated with zero autocorrelation drops from 8 h to 5 h. This difference suggests that the fluctuation regime in the last part of the experiment is characterized by shorter pulse durations compared to the first part.
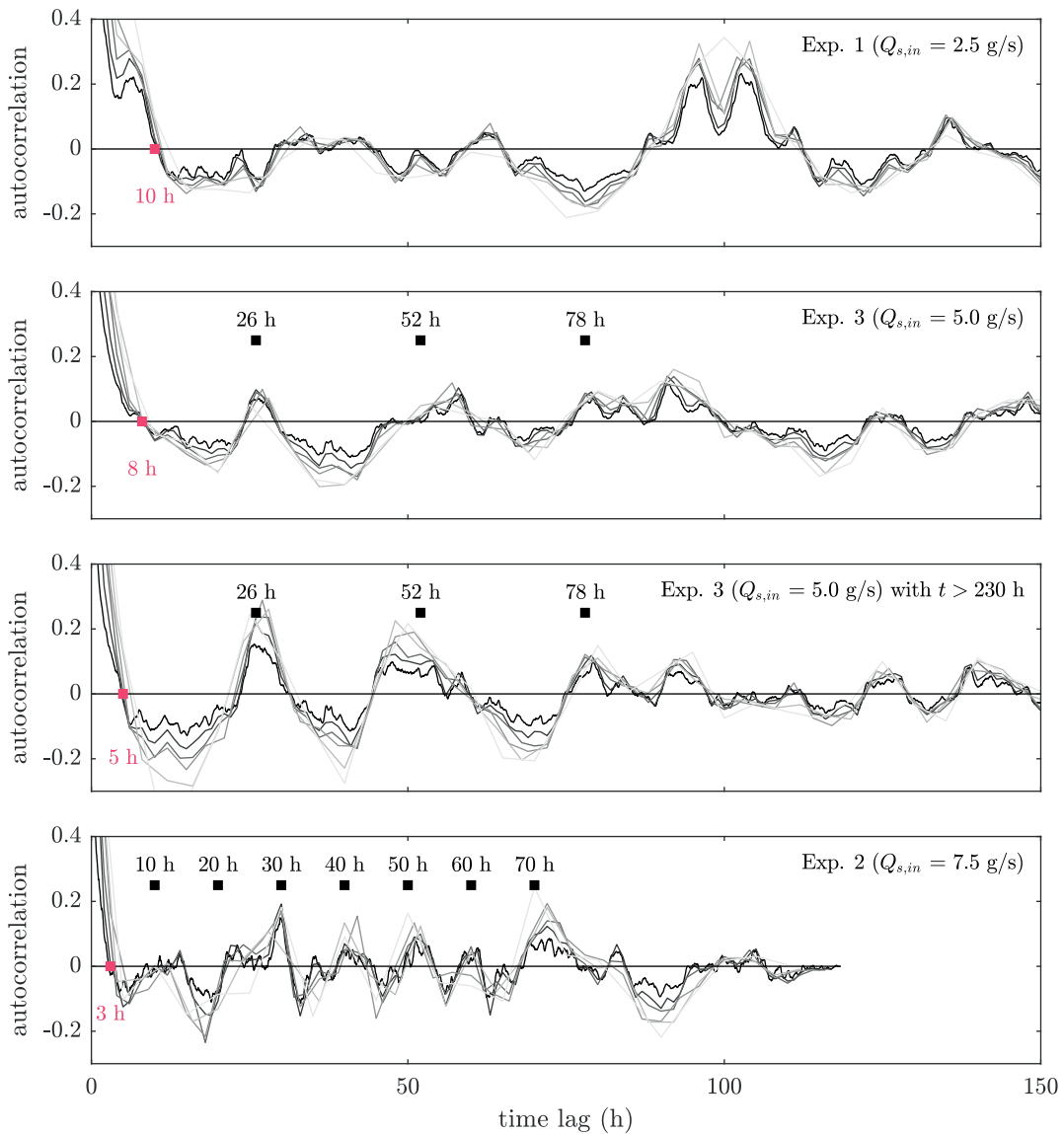
Figure 3.13: Autocorrelation functions of the bedload transport rates averaged over different sampling times for experiment 1, 2 and 3. The black curves correspond to a 1-min sampling time. The grey curves correspond to sampling times within 1 h and 5 h (light shades stand for large sampling times). For experiment 3, the autocorrelation analysis is performed over the whole time series and removing the first 230 h.

3.4.3 Bedload pulse frequency

The autocorrelation function in experiment 2 features several prominent peaks that are fairly evenly spaced by about 10 h. This regularity in the peak spacing suggests that large-scale bedload pulses have a periodic behavior characterized by a period of about 10 h, which is is consistent with the pulse frequencies given in section 3.2.3.

In experiment 3, a prominent peak occurs at a time lag of 26 h. At time lags multiples of 26 h, the autocorrelation function also features peaks, but less marked. However, if the first 230 h of the BTR time series are removed, two peaks appear clearly at 52 h and 78 h. Large-scale bedload pulses seem therefore to have a periodic behavior, particularly during the second part of the experiment, characterized by a period of about 26 h.

In experiment 1, a first peak occurs at 6 h, before the autocorrelation function drops to zero. Some bedload pulses are therefore likely to occur regularly with a period of about 6 h. However, the peak vanishes for larger sampling times, which means that these pulses are associated with time scales shorter than few hours.

The most prominent peak in experiment 1 occurs at a time lag of about 100 h. Given the experiment duration (~260 h), no conclusion about periodicity can be drawn based on this observation. Moreover, the peaks observed at shorter time lags are not enough marked, and the corresponding autocorrelation coefficients are too low, to draw any conclusion either. This result was expected since, inspecting visually the time series in figure 3.13, any periodic behavior in major BTR fluctuations seems to be unlikely.

In summary, only the fluctuation regimes associated with $Q_{s,in} = 7.5$ and 5.0 g/s are characterized by a periodic behavior of the large-scale fluctuations. However, this periodicity is less marked and of lower frequency when the sediment feed rate is lower.

3.5 Distribution of the bedload transport rates

Probability distributions are frequently used to described the variability of BTRs (Turowski, 2010). In the following, we characterize the fluctuations in the BTR time series using such tools, and we examine the effect of the sampling time on the distribution characteristics.

3.5.1 Effect of intermittency

The probability density function (PDF) of the BTRs averaged over one minute is plotted for each experiment in figure 3.14. It appears that, in each fluctuation regime, the PDF is asymmetric and decreases with increasing Q_s: large BTR values are less frequent than lower ones. However, the distributions are stretched toward the right, which reflects the occurrence of bedload pulses during the experiments.

The Gamma distributions plotted in figure 3.14 fit well the PDFs, including their tails, which is consistent with the findings of several studies on similar topics (Campagnol et al., 2012). However, note that the Gamma distribution slightly underestimates the frequency of the lowest BTR values in experiment 1 and 3.

The cumulative distribution function (CDF) and the PDF of the normalized BTRs of each experiment are compared in figure 3.15. They show that the distribution of the BTRs in experiment 2, which has the largest sediment feed rate, is different from the two others. Indeed, it appears that, in this experiment, low BTR values ($Q_s^\star < 0.5$) are less frequent, and
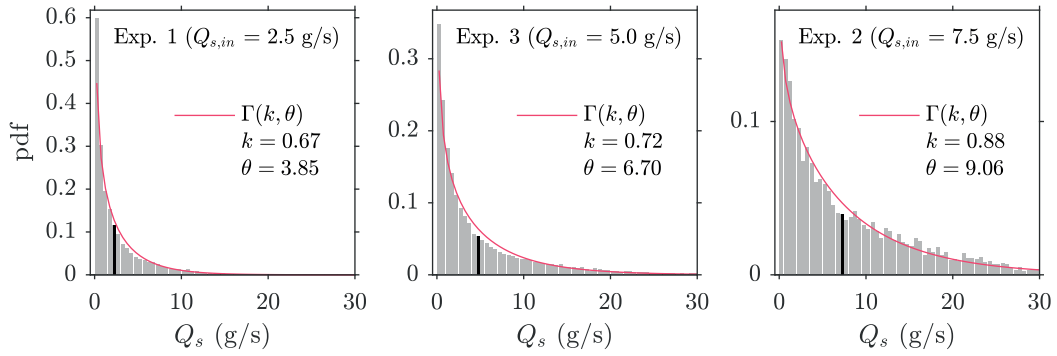
Figure 3.14: Probability density function of the bedload transport rates averaged over one minute for experiment 1, 2 and 3. The bin width is 0.5 g/s and the bins containing the sediment feed rates are indicated in black. The curves represent the Gamma distribution Γ fitted to the data.

high values ($Q_s^\star > 2$) more frequent. This finding is consistent with the results presented in section 3.2.3. More generally, the comments above show that the distribution of the BTRs reflects well the intermittent character of the fluctuation regimes discussed in section 3.2.

It is interesting to note that the BTR values close to $\bar{Q}_s$ are rarely observed (see figure 3.14). For instance, the observation frequency of values within $\bar{Q}_s \pm 0.25$ g/s is respectively 5.7 %, 2.0 % and 2.7 % in experiment 1, 2 and 3. This observation highlights the intermittent character of BTR fluctuations: the system switches between low transport phases and intense transport phases (i.e., bedload pulses). In other words, the mass-balance equilibrium state defined by $Q_s = Q_{s,in}$ is rarely visited (Iseya and Ikeda, 1987).
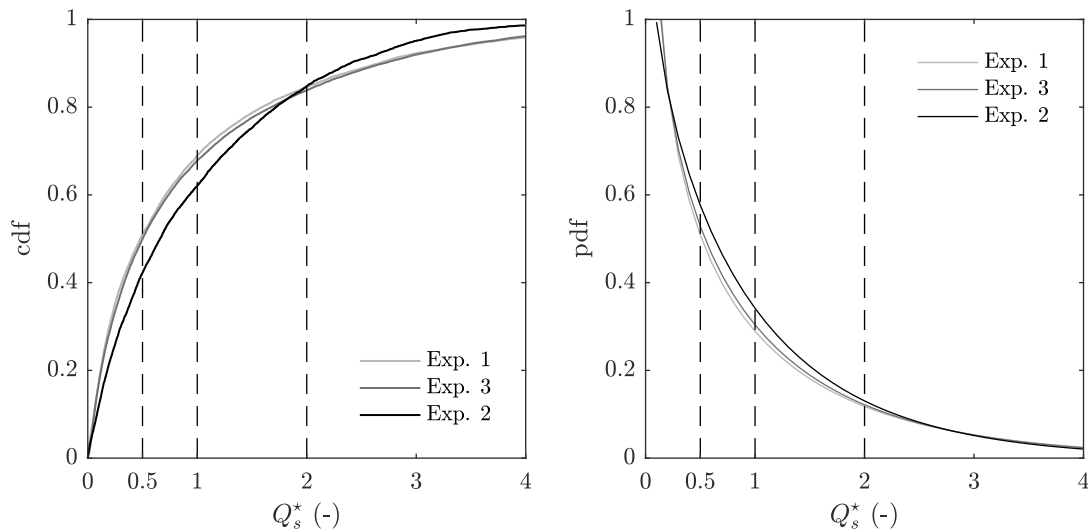
Figure 3.15: Cumulative distribution function and probability density function of the normalized bedload transport rates averaged over one minute for experiment 1, 2 and 3.

3.5.2 Effect of sampling time

The CDFs of the normalized BTRs averaged over sampling times (T_s) ranging from one minute to ten hours are plotted in figure 3.16. The effect of the sampling time on the shape of the distributions appears clearly: the CDFs evolve progressively from an inverted L-shape to a S-shape. Indeed, the very low and very large values are less frequently observed, and the range of observed BTR values is narrowed, when averaging the time series (Singh et al., 2009). Moreover, the median of the distributions increases toward the mean, which is equal to 1 when considering $Q_s^\star$.
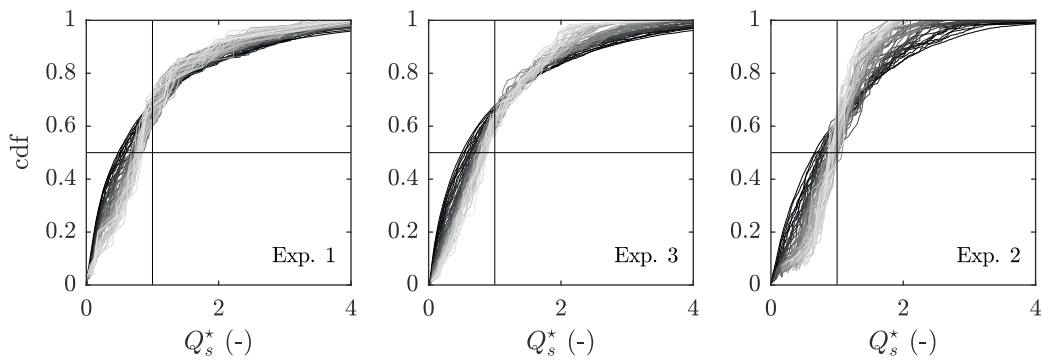
Figure 3.16: Cumulative distribution function of the normalized bedload transport rates as a function of the sampling time for experiment 1, 2 and 3. Each curve corresponds to a different sampling time (light shades of grey stand for large sampling times) ranging from one minute to ten hours.
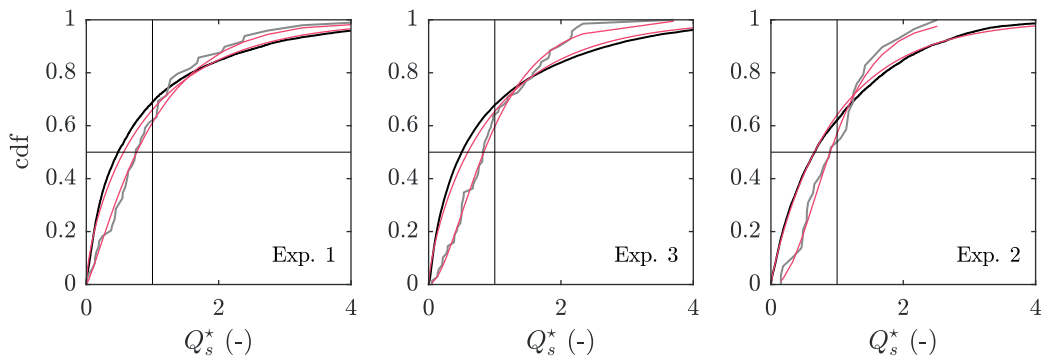
Figure 3.17: Cumulative distribution function of the normalized bedload transport rates for experiment 1, 2 and 3. The black curves represent the CDFs of the rates averaged over one minute. The grey curves represent the CDFs of the rates averaged over respectively 5, 4 and 8 hours for experiment 1, 2 and 3. The thin curves represent the Gamma distributions fitted to the data.

In order to further investigate the changes in the distribution characteristics described above, the Gamma distribution was fitted to the averaged BTRs for each sampling time. Indeed, as shown in figure 3.17, the Gamma distribution also fits well the CDFs of the normalized BTRs averaged over several hours. The effect of the sampling time on the Gamma PDF is illustrated in 3.18.
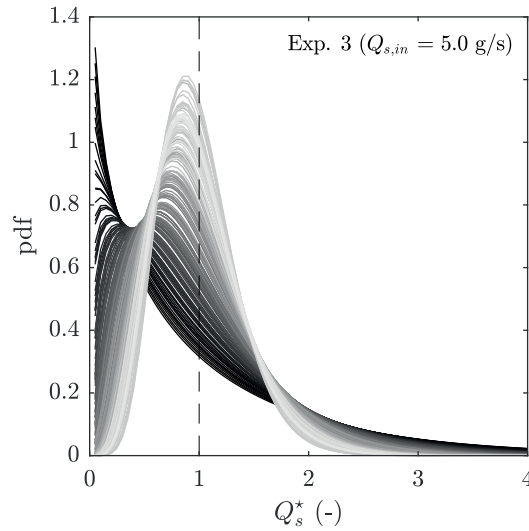
Figure 3.18: Probability density function of the Gamma distribution fitted to the normalized bedload transport rates as a function of the sampling time for experiment 3. Each curve corresponds to a different sampling time ranging from 1 min to 30 h (light shades of grey stand for large sampling times).

For low sampling times, the distribution shows no mode (it is L-shaped). Then, as the sampling time increases, a mode appears close to zero and moves slowly toward the mean (which is equal to 1). In the meanwhile, the tail of the distribution gets shorter. These changes in the PDF correspond to the ones discussed above for the CDF.

We remind that the Gamma distribution $\Gamma(k, \theta)$ depends on a shape (k) and a scale (θ) parameter; and that its mode and skewness (which describes its tail) are respectively equal to $(k-1)\theta$ (for $k \geqslant 1$) and $2/\sqrt{k}$. The changes in shape commented above are therefore quantified in figure 3.19, which presents the mode and the skewness of the fitted Gamma distributions as a function of the sampling time.

It is interesting to note that the fluctuation regimes associated with each experiment are differentiated in figure 3.19. Indeed, in experiments with larger sediment feed rates, the tail is shorter (lower skewness) and shortens faster with increasing sampling time, and the mode appears for shorter sampling times and moves faster toward the mean.
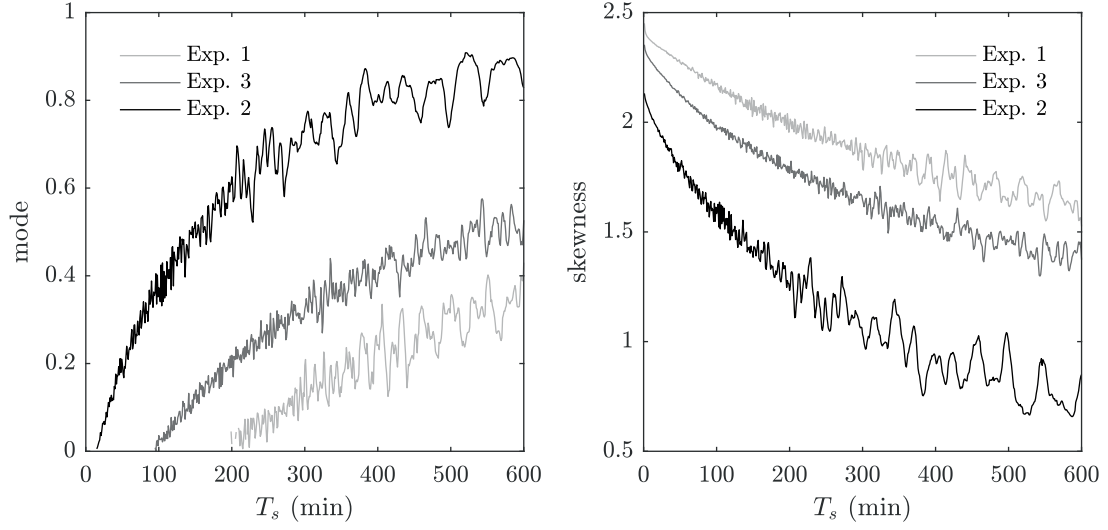
Figure 3.19: Mode and skewness of the Gamma distribution fitted to the normalized bedload transport rates as a function of the sampling time T_s for experiment 1, 2 and 3.

We show in figure 3.20 that the effect of the sampling time T_s on the shape parameter k of the fitted Gamma distribution can be approximated using the following linear relationships:

– $k = 0.0014 T_s + 0.72$ in experiment 1, for T_s within 1 min and 10 h ($R^2 = 0.95$, $SE = 0.05$);

– $k = 0.0023 T_s + 0.73$ in experiment 3, for T_s within 1 min and 10 h ($R^2 = 0.97$, $SE = 0.07$);

– $k = 0.0078 T_s + 0.85$ in experiment 2, for T_s within 1 min and 4 h ($R^2 = 0.93$, $SE = 0.15$).

Note that the goodness-of-fit of each regression curve is assessed using the coefficient of determination R^2 and the standard error of the estimate SE. Moreover, these equations can be used with T_s expressed in minutes or as its ratio with respect to the smallest sampling time (since the latter is one minute).

The relationships above also describe the effect of the sampling time on the scale parameter θ, the mode, the skewness and the variance of the distribution since they can all be expressed as functions of k. Indeed, since the mean of the Gamma distribution is equal to $k\theta$, and as $\bar{Q}_s^\star = 1$ for any sampling time (averaging is a linear process), we have the relationship $\theta = 1/k$. From the latter, we can derive that:

– the mode is given by $1 - \frac{1}{k}$ for $k \geqslant 1$;

– the variance is given by $\frac{1}{k}$.

As stated above, the skewness is by definition equal to $2/\sqrt{k}$.

47
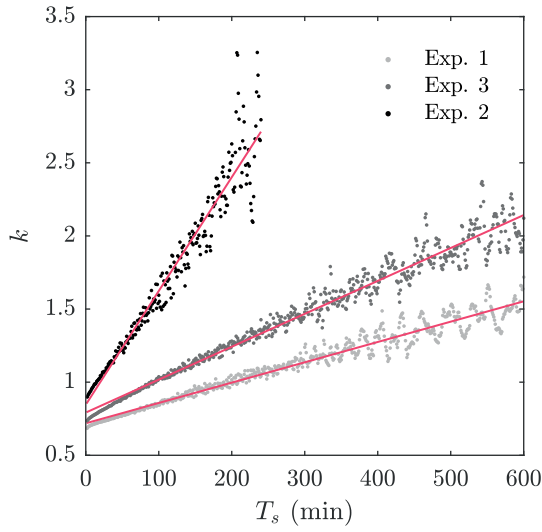
Figure 3.20: Shape parameter k of the Gamma distribution fitted to the normalized bedload transport rates as a function of the sampling time T_s for experiment 1, 2 and 3.
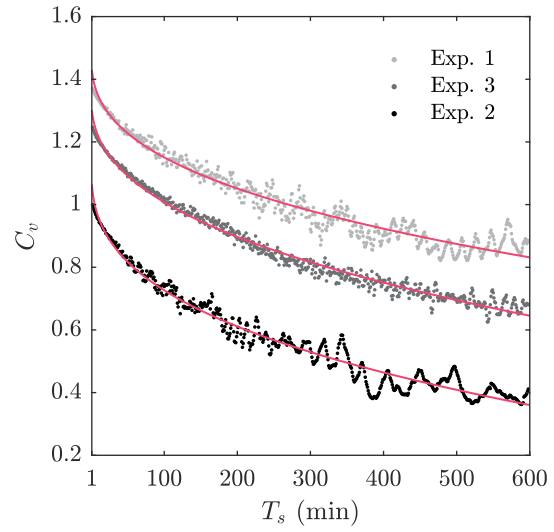
Figure 3.21: Effect of the sampling time T_s on the coefficient of variation C_v, for T_s within 1 min and 10 h, in experiment 1, 2 and 3.

3.5.3 Coefficient of variation

The effect of the sampling time on the characteristics of the fluctuations is often assessed examining its effect on the coefficient of variation $C_v = \sigma / \bar{Q}_s$ (e.g., in Kuhnle and Southard, 1988; Singh et al., 2009; Mettra, 2014), which is simply the relative standard deviation of the BTRs ($\sigma^\star$) discussed previously. As in the studies mentioned above, C_v decreases with increasing sampling time (see figure 3.21) which reflects the effect on the PDFs discussed previously: their width gets narrower as the sampling time increases (i.e., the fluctuations are of lower magnitude). The decrease in C_v is parametrized using a function $ax^b + c$ of which coefficients are given in table 3.4.

The regression curves in figure 3.21 describe well the effect of the sampling time on C_v as indicated by the goodness-of-fit statistics. However, they are slightly shifted from the computed values for low sampling times. Indeed it appears that C_v is related to T_s by different scaling laws for T_s values lower and larger than 2 h (see table 3.4 and figure 3.22). These two scaling regimes seem respectively associated to fluctuations within large bedload pulses (intra-event) and to the large pulses themselves (inter-event).
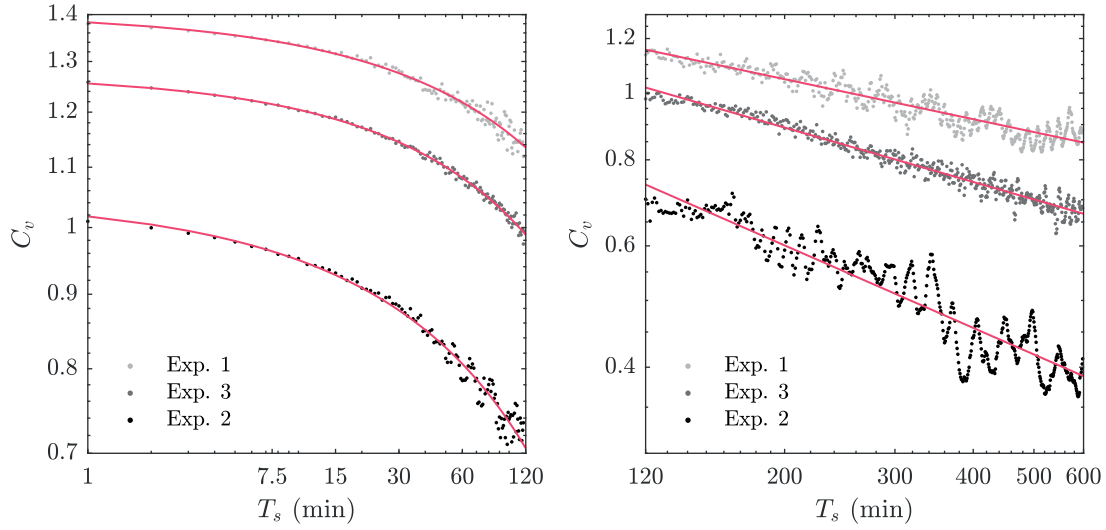
Figure 3.22: Effect of the sampling time T_s on the coefficient of variation C_v (log-log scale), for T_s within 1 min and 2 h (left) and within 2 h and 10 h (right), in experiment 1, 2 and 3.

Table 3.4: Coefficients of the regression curves describing the coefficient of variation C_v as a function of the sampling time T_s for experiment 1, 2 and 3. The goodness-of-fit is assessed using R^2 (the coefficient of determination) and SE (the standard error of the estimate).

	a	b	c	R^2	SE
$f(x) = ax^b + c$, $T_s \in$ [1 min, 10 h]					
experiment 1	-0.06	0.37	1.49	0.95	0.030
experiment 3	-0.06	0.40	1.36	0.98	0.018
experiment 2	-0.08	0.35	1.15	0.96	0.030
					see figure 3.21
$f(x) = ax^b + c$, $T_s \in$ [1 min, 2 h]					
experiment 1	-0.02	0.54	1.40	0.97	0.012
experiment 3	-0.02	0.57	1.27	0.99	0.005
experiment 2	-0.03	0.50	1.05	0.97	0.013
					see figure 3.22(left)
$f(x) = ax^b$, $T_s \in$ [2 h, 10 h]					
experiment 1	2.91	-0.19		0.89	0.031
experiment 3	3.57	-0.26		0.97	0.017
experiment 2	4.95	-0.40		0.89	0.033
					see figure 3.22(right)

3.6 Bedload pulses and sediment storage

As we characterized the fluctuation regimes associated with each experiment in the previous sections, we discussed the issue of system equilibrium several times. In the following, we conclude on this topic investigating the relationship between bedload pulses and the sediment volume stored in the bed.

3.6.1 Stationarity of the time series

As discussed in section 3.3.1, equilibrium conditions are likely to be achieved in the system only after very long times (in the order of 10 h to 100 h). In the following, we further investigate this issue examining the stationarity of the BTR time series. To do so, we compute the cumulative mass of sediment measured at the flume outlet (M_s^{cum}) integrating Q_s over time. The temporal evolution of M_s^{cum} during each experiment (including the adjustment time) is plotted in figure 3.23.

The cumulative mass increases over time following an overall linear trend, which is given by the integration of $\bar{Q}_s$ over time ($M_{s,av}^{cum}$). This behavior suggests that, at the experiment time scales, the BTR time series are stationary.

The cumulative mass of sediment fed in the flume ($M_{s,in}^{cum}$), which increases linearly in time because of the steady feeding conditions, is also plotted in figure 3.23. It closely matches $M_{s,av}^{cum}$, which indicates a neutral sediment balance at the end of the experiments (the slight differences observed are attributed to some inaccuracy in the sediment feeding system).

However, as illustrated in figure 3.23, M_s^{cum} diverges from the linear trend during most of experiment 1 and 2. It appears that neutral sediment balance is only achieved at their very end. As a consequence, system equilibrium seems to be reached only in experiment 3.
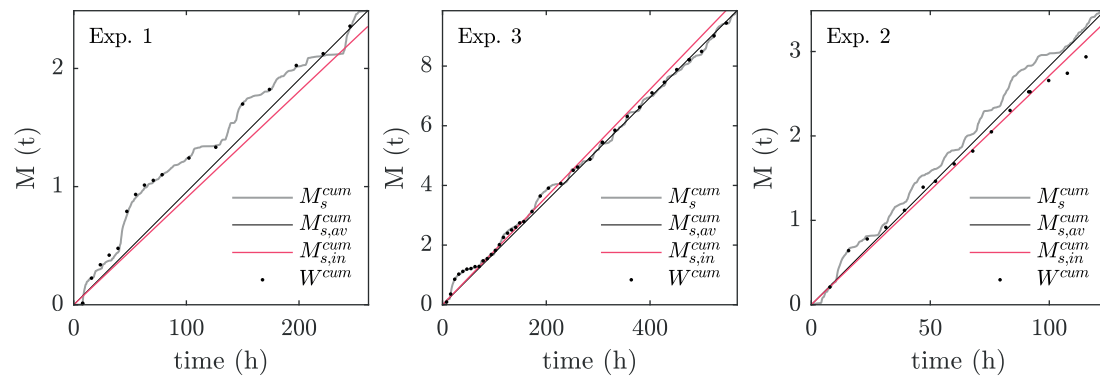
Figure 3.23: Cumulative mass of sediment measured at the flume outlet M_s^{cum}, cumulative mass of sediment fed in the flume $M_{s,in}^{cum}$, and cumulative mass of sediment collected at the flume outlet at the end of each run W^{cum} during experiment 1, 2 and 3.

During each experiment, the sediment collected at the flume outlet was weighted at the end

of each run. The corresponding cumulative masses (W^{cum}) plotted in figure 3.23 closely match with M_s^{cum}: the two measurement methods are therefore consistent. Note that the shift observed in experiment 2 is due to sediment loss during the collection process.

3.6.2 Changes in bed volume

3.6.2.1 Data preparation

The cumulated mass of sediment evacuated from the flume reflects the state of the system in term of sediment storage. Indeed, making a simple mass balance, the mass of sediment stored in the bed compared to its initial value is given by

$$\Delta M_{bed} = M_s^{cum} - M_{s,av}^{cum} \tag{3.3}$$

where $M_{s,av}^{cum}$ approximates the actual amount of sediment fed in the system. Note that we do not estimate the latter by $M_{s,in}^{cum}$, which is the theoretical value, because of the difficulty to build a perfectly steady sediment feeding system. The equation above therefore consists in removing the linear trend in the M_s^{cum} curves plotted in figure 3.23.

The relative sediment stock can also be computed from the bed topography measurements performed during the experiments. The results of the two methods were found to be in good agreement, which validates the approach used here.

The temporal evolution of the relative sediment stock (ΔM_{bed}) in the bed is plotted in figure 3.24 for each experiment. It appears that the amount of sediment stored in the bed fluctuates over time: the average values of ΔM_{bed} are -161.5 kg, -125.7 kg and -72.8 kg, and the standard deviations are 135.8 kg, 84.8 kg and 160.6 kg, in experiment 1, 2 and 3.

The average ΔM_{bed} values are therefore lower than zero by about 100 kg, which implies that the average sediment stock in the bed during the experiments is significantly lower than the initial stock. This overall bed erosion explains why the average bed slope in each experiment is lower than the initial bed slope, as mentioned in section 3.1.2.1. Indeed, the mass of sediment corresponding to the difference between these two slopes (assuming no change in bed elevation at the flume outlet) is 175 kg, 144 kg and 90 kg for experiment 1, 2 and 3, which is consistent with the values above.

3.6.2.2 System equilibrium

The fluctuations of ΔM_{bed} in figure 3.24 indicate that the bed undergoes a succession sediment deficit and sediment surplus phases. The time scale associated with these fluctuations is much larger that the one associated with bedload pulses (which are also plotted in figure 3.24 for comparison purposes). Moreover, the fluctuations feature an hysteretic behavior: the sediment stock decreases much more faster than it increases. The sudden stock decreases correspond to major sediment transport events. Then, the stock increases slowly toward the reference value. In the meanwhile, bedload pulses of lower magnitude still occur.
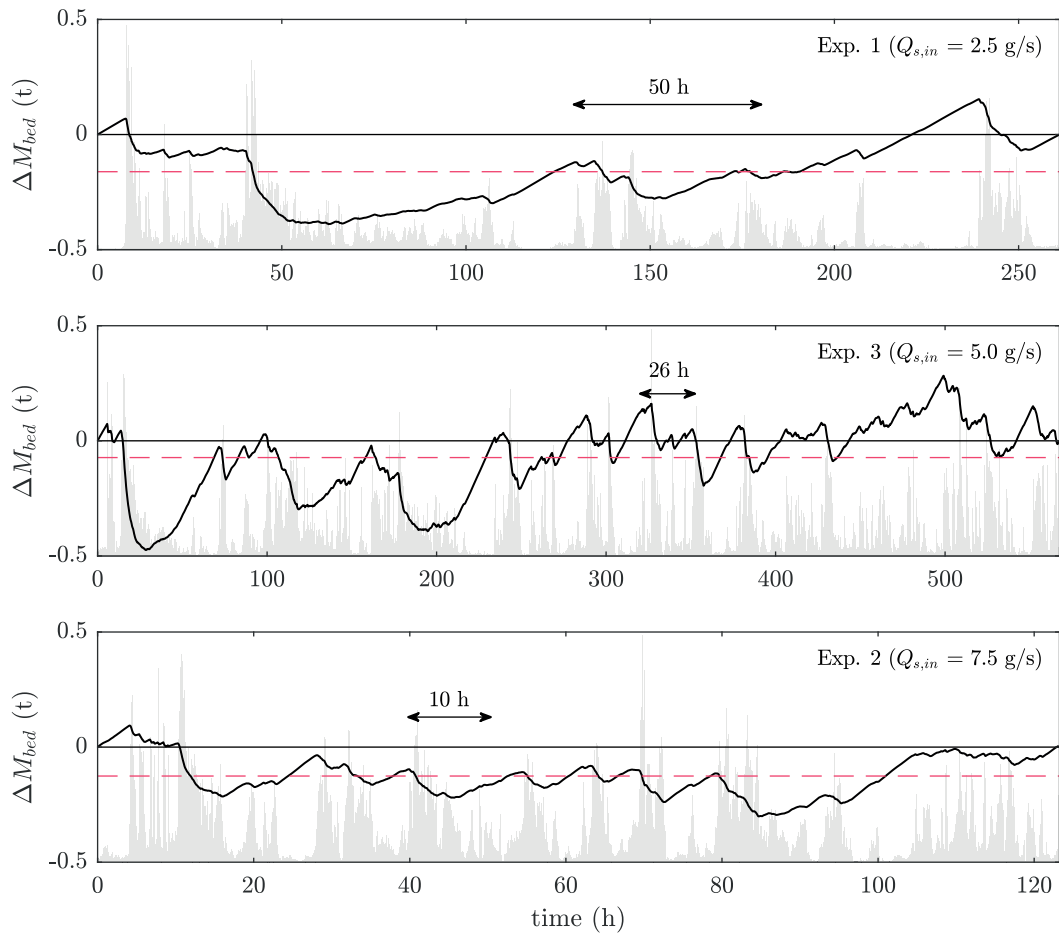
Figure 3.24: Temporal evolution of the relative sediment stock (in tonnes) stored in the bed ΔM_{bed} during experiment 1, 2 and 3. The dashed curves represent the average values and the filled area plots represent the bedload transport rates on an arbitrary scale.

In section 3.4.3, the characteristic period associated with large-scale pulses was found to be 50 h, 10 h and 26 h in experiment 1, 2 and 3. These frequencies are consistent with the time scale associated with the ΔM_{bed} fluctuations (see figure 3.24), which supports the above observation that the major pulses are related to the large decreases in bed volume.

As commented at the beginning of this section, stationarity is only observed in experiment 3 which is much longer than the two other experiments. Examining the corresponding ΔM_{bed} graph in figure 3.24, two fluctuation regimes appear. During the first part of the experiment (≈ 230 h), the fluctuations are of much larger magnitude and duration than in the second part. This observation lead us to conclude that system equilibrium is reached only in the second part, since it is generally defined by gentle fluctuations about a mean value (Recking et al., 2009; Ancey et al., 2015). Note that this latter equilibrium state is often referred to as *dynamic equilibrium* as discussed in section 3.7.4.

Large decreases in bed volume, similar to the ones in the first part of experiment 3, are also observed during most of experiment 1. In addition, as mentioned in section 3.3.1, equilibrium is expected to be achieved after a longer time period in experiment 1 than in experiment 3 (because of the lower sediment feed rate). Given these considerations, we conclude that equilibrium conditions are not reached in experiment 1.

Inversely, equilibrium is expected to be reached sooner in experiment 2 than in experiment 3. Examining the corresponding ΔM_{bed} graph in figure 3.24, it appears that neutral sediment balance is only achieved during the last 20 h of the experiment. Although this neutral balance is indicative of equilibrium, the experiment is not long enough to draw any clear conclusion.

3.7 Discussion

3.7.1 Bedload transport rate fluctuations

The bedload transport rates (BTRs) measured at the flume outlet during the experiments vary within one order of magnitude about their mean values, which is consistent with other experimental studies performed under steady flow conditions (Hubbell, 1987; Iseya and Ikeda, 1987; Kuhnle and Southard, 1988; Gomez et al., 1989; Hoey, 1992; Frey et al., 2003; Recking et al., 2009; Singh et al., 2009; Ghilardi et al., 2014a). Moreover, the L-shaped and right-skewed probability distributions of the BTRs reflect the pulsating (Reid et al., 1985), or bursty (Singh et al., 2009), nature of bedload transport: low and intense transport phases alternate in the bed. We refer to the latter as bedload pulses following the terminology used by several authors (Iseya and Ikeda, 1987; Gomez et al., 1989; Ashmore, 1991; Hoey, 1992; Ghilardi et al., 2014a). An interesting consequence of this fluctuating behavior is that the average BTR values are rarely visited although they are key characteristics of the fluctuation regimes, used for instance to assess the intensity of the pulses (Kuhnle and Southard, 1988) and the mass-balance equilibrium state (Iseya and Ikeda, 1987).

When describing large BTR fluctuations as bedload pulses, one refers to the concept of transport events: fluctuations are viewed as clusters of large values, assuming memory in the time series (Saletti et al., 2015), rather than instantaneous variations at the measurement time scale. Bedload pulses are therefore defined by their duration along with their frequency and magnitude.

The bedload pulses in our experiments are characterized by a strong temporal heterogeneity, with inter-arrival times varying between few minutes and more than ten hours, which denotes their intermittent character. According to Singh et al. (2009), this intermittency arises from the stochastic nature of bedload transport, which has also been reported at the particle scale (Einstein, 1950; Paintal, 1971; Papanicolaou et al., 2002; Ancey et al., 2008).

Paradoxically, we also observed an autoregressive behavior in the BTR time series, which indicates periodic patterns in the fluctuations (Cudden and Hoey, 2003; Ghilardi et al., 2014b). This coexistence of stochastic and periodic behaviors implies that BTR fluctuations are not only random realizations of stochastic processes (Singh et al., 2009), but can also originate

from deterministic mechanisms occurring in the bed (Cudden and Hoey, 2003).

The periodic patterns observed are characterized by temporal scales larger than ten hours, which corresponds roughly to the period of the largest bedload pulses. Moreover, this periodicity in the BTR time series was also found to be associated with global changes in bed volume. This regular succession of sediment deficit and surplus phases in the bed suggests that a maximum storage capacity, associated to a given bed configuration, governs the periodic behavior of the large-scale fluctuations.

Periodicity in the BTR fluctuations at higher frequencies, corresponding to periods of few hours, was also demonstrated performing a Fourier analysis (Kuhnle and Southard, 1988). This finding is in agreement with other studies (Kuhnle and Southard, 1988; Gomez et al., 1989; Ashmore, 1991; Hoey, 1992; Ghilardi et al., 2014b), described in table 3.5, which related the periodic character of bedload pulses to migrating bedforms (e.g., bars and sediment waves). An overview is given in Kuhnle (1996). Such bed structures, which can generate bedload pulses, were also observed in our experiments. They are investigated in details in the next chapters.

We described quantitatively the fluctuations in each experiment based on the intensity and intermittency of the bedload pulses. Three fluctuation regimes arise from the results obtained, each associated with one of the sediment feed rate tested. It appears that bedload pulses tend to be shorter, more frequent and of lower magnitude as the feed rate increases. Note that the global hydraulic conditions vary from one experiment to another because of the changes observed in the average bed slope: the average stream power (i.e., computed based on the average slope) is larger in experiments with larger sediment feed rates.

The tendencies mentioned above are consistent with the findings of other authors who describe in general "smoother" BTR time series (i.e., less bursty) at higher flow rates (Singh et al., 2009). For instance, Kuhnle and Southard (1988) report that BTR fluctuations are of lower magnitude when the sediment feed rate in their experiments with poorly-sorted gravel is increased. More generally, Ghilardi et al. (2014b), who tested various combinations of water discharges and sediment feed rates in a gravel-bed flume with large boulders, observed that the magnitude, period and duration of the pulses decrease with increasing stream power.

3.7.2 Sampling time

Some of the authors cited above (Kuhnle and Southard, 1988; Gomez et al., 1989; Hoey, 1992) have raised the issue of the effect of the sampling time on the characteristics of the BTR time series. Indeed, it appears that the coefficient of variation decreases with increasing temporal scale (Kuhnle and Southard, 1988; Fienberg et al., 2010), which denotes a decrease in the relative magnitude of the fluctuations (i.e., a "smoothing" of the time series). This effect implies that the choice of the optimal sampling time is not trivial (Gomez et al., 1989), and makes BTR time series recorded with different sampling times difficult to compare (Kuhnle, 1996). As a consequence, several authors investigated the change in the statistics of fluctuations across temporal scales, both at the particle scale (Campagnol et al., 2012; Ma et al., 2014; Ancey et al.,

Table 3.5: Flume experiments under steady flow conditions reporting bedload pulses. The following characteristics are given: the flume length L, the flume width W, the experiment duration T_{exp}, the sampling time T_s, the period of the pulses, the bed slope and the grain size.

	$L \times W$ m	T_{exp} h	T_s min	period min	slope %	bed material and features
Iseya and Ikeda (1987)	4×0.1	1/3	1/6	4	2–4	gravel and sand (d_{50} = 2.6 and 0.37 mm) single channel, bedload sheets & grain sorting
Kuhnle and Southard (1988) *L1 & L2 runs*	11×0.74	2.5	0.5	6–25	1.9	poorly-sorted gravel (d_m = 3 mm) single channel, bedload sheets & grain sorting
Gomez et al. (1989) *ERC run*	160×4	19.5	5	168	0.7	well-sorted gravel (d_{50} = 3.97 mm) single channel, migrating bars
Ashmore (1991)	10×2	60	15	hrs	1.0–1.5	poorly-sorted sand (d_{50} = 1.2 mm) braided, sediment wave & bars
Hoey (1992)	14×3	50	15	60–120	1	sand (d_{50} = 0.57 mm) braided, bed wave
Frey et al. (2003) *run 4*	4×0.1	< 1/6	< 1/6	1–2	15	poorly-sorted gravel (3–15 mm) single channel, grain sorting
Recking et al. (2009)	2-8×~0.1	0.5–64	-	min–hrs	0.8–9	poorly-sorted gravel (2.3–9 mm) single channel, bedload sheets & grain sorting
Singh et al. (2009)	20×2.74	20	2	NR	0.2–0.5	poorly-sorted gravel (d_{50} = 11.3 mm) sediment patches & grain sorting
Ghilardi et al. (2014b)	7×0.25	a few	1	min–hrs	> 6	poorly-sorted gravel (d_m = 11.9 mm) & boulders single channel, bedform migration & grain sorting

2015) and at larger scale (Singh et al., 2009; Fienberg et al., 2010).

We investigated this issue examining the effect of the sampling time, from minutes to hours, on the BTR probability distributions approximated by a Gamma law. We showed that the scale parameter of the distributions increases roughly linearly with the sampling time and that the evolution of the second and third statistical moments (i.e., the variance and the skewness) can be deduced from these linear relationships.

Moreover, we demonstrated that the coefficient of variation C_v decreases with increasing sampling time T_s in this way: $(C_v - cst) \propto T_s^b$. This result is in agreement with Singh et al. (2009) and Fienberg et al. (2010) who report that scaling laws related to BTRs often follow power functions. However, in our experiments, these laws cover a larger range of time scales, which is a motivation to further investigate the scaling properties in BTR time series. Note that the scaling laws parametrized were found to depend on the stream power (i.e., they are different for each experiment). However this dependence requires more experimental runs to be quantified.

Closely related to the considerations above, about the effect of the sampling time on the statistics of the BTR fluctuations, is the issue of the total measurement duration required to measure the "true" average BTR (Bunte and Abt, 2005). Indeed, because of the inherent variability of bedload transport (Singh et al., 2009), such a measure can take a long period of time, which can be challenging in field studies (Bunte and Abt, 2005). This issue stresses further the need to better understand the BTR scaling properties discussed above.

3.7.3 Mass-balance equilibrium

In flume studies, which are often performed under steady or periodic feeding conditions (see the citations above), the "true" average BTR matches the average sediment feed rate since the experimental procedures generally ensure mass-balance equilibrium (Recking et al., 2009). To do so, the common procedure is to wait that the average BTR stabilizes close to the average sediment feed rate before starting the measurement campaign (Singh et al., 2009).

We addressed this issue introducing the *convergence time* which is a measure of the minimum observation time necessary to guarantee mass-balance equilibrium in the system regardless the experiment portion that is observed. The convergence time can thus also be seen as the time necessary to capture all fluctuations types in the system, including the largest ones.

In addition, the convergence time indicates how bedload pulses and low transport phases respectively affect the average BTR measured. It appears that, in our experiments, low transport phases become the limiting factor making this measure shift from the expected value after a certain observation time (i.e., that retards the moment when mass-balance equilibrium is achieved). This observation highlights the importance of taking into account low transport phases, although they do not directly imply the transport of large amounts of sediment. Indeed, the sediment stored in the bed during such phases is likely to play a key role in the generation of bedload pulses. In summary, we argue that the convergence time is a useful tool to characterize fluctuation regimes.

3.7.4 Dynamic equilibrium

In many studies, when mass-balance equilibrium is observed, dynamic equilibrium is assumed to be reached in the system (Iseya and Ikeda, 1987; Kuhnle and Southard, 1988; Singh et al., 2009). We remind that dynamic equilibrium refers to an equilibrium state in which the variables of interest fluctuate about a mean value (Recking et al., 2009). This assumption is probably verified is most experiments performed under steady feeding conditions and starting from a flat bed configuration. Indeed, we observed that in such conditions particularly large BTR fluctuations occur at the beginning of the experiments (as the bed gets progressively formed) which delays the time when mass-balance equilibrium is observed. The adjustment time at the beginning of the experiments is therefore likely to be long enough to ensure that dynamic equilibrium is achieved in the system.

However, mass-balance equilibrium is by definition only related to bedload transport (since it is the process observed) and is therefore only indicative of a potential global dynamic equilibrium in the system, which depends also on the temporal variability in the bed topography and hydraulic conditions. For these reasons, the stabilization of the average bed slope close to the equilibrium slope value is also often verified (Iseya and Ikeda, 1987; Gomez et al., 1989; Frey et al., 2003; Recking et al., 2009) as it is in general an available data (this issue is investigated in the next chapter).

The above considerations motivated us to further assess system equilibrium examining the variations in bed volume (i.e., in the sediment stock) computed from the cumulative BTRs, which is an approach derived from the stationarity analysis of the BTRs (Mettra, 2014; Ghilardi et al., 2014a). Doing so, it appeared that dynamic equilibrium is likely to be achieved only in experiment 3 (the longest of the three experiments), after 230 h which is about twice the time necessary for the average BTR to come close to the sediment feed rate within ±25%. Indeed, it is only after this time period that sediment stock fluctuations become "gentle" about their mean value. A key outcome of our results is thus that dynamic equilibrium in flume experiments is possibly achieved after a much longer time than mass-balance equilibrium.

The variability in sediment stock discussed above suggests that the dynamic equilibrium in the system is controlled by a certain storage capacity of the bed, associated to a given bed configuration. As the system is fed with sediment, the bed alternately stores and releases bed material, which results in a succession of sediment surplus and deficit phases (with respect to an average sediment storage state). In this view, bedload pulses are the result of the evacuation of large sediment volumes when the maximum storage capacity is reached.

However, the two regimes observed in experiment 3 indicate that such an equilibrium state may not be unique, although some may be more stable than others. For instance a transitional equilibrium state may appear after a strong perturbation (e.g., that flattens the bed) before the system switches to a more persistent equilibrium state once the resilience time is over. However, further experiments are required to better address this issue.

4 Evolution of the bed topography

We investigate in this chapter the topographical changes the bed undergoes during the experiments. More specifically, we are interested in the dynamics of the alternate bars characterizing the bed topography, and in the physical processes involved in the transfer of sediment along the flume length. The motivation of the analyses performed hereafter relies on the better understanding of the mechanisms generating the bedload pulses discussed in Chapter 3.

In the first sections of the chapter we investigate how sediment is transferred in the bed, through the erosion and deposition of bed material. We then relate these processes to the alternate bar system observed in the bed, before characterizing separately the evolution of the bars and the pools during the experiments. Finally, we describe qualitatively how sediment is transferred from pool to pool, in a wave-like behavior, before discussing our results.

4.1   Topographical data

The bed and the water elevations are measured about every 10 min during each experiment. A single measurement takes about 3 min to be completed, which is the time necessary to scan the flume over its entire length. Based on the observations made during the experiments, it is assumed that the topography and the water height do not vary significantly during this time period. The bed and the water elevation data can therefore be seen as instantaneous measurements of the system geometry. The system dynamics are, for their part, reflected by the evolution of the geometry between the scans. We remind that the post-processed elevation data have a spatial resolution of 1 cm in the cross-sectional direction and 5 cm in the longitudinal direction, and that the measurement accuracy is finer than 1 cm. Moreover, the first and the last meter of the flume were not scanned because of technical limitations (see Chapter 2).

The elevation data are three-dimensional. They are analyzed in the coordinate system shown in figure 4.1 which is defined by: an x-axis in the longitudinal direction of the flume, an y-axis in the cross-sectional direction of the flume, and a z-axis in the vertical direction (perpendicular to the flume bottom). The x-axis is oriented in the upstream direction and its origin is the flume outlet. The y-axis is oriented from right to left with respect to the flow direction and its origin is the right wall. The z-axis is oriented upward and its origin is the flume bottom.
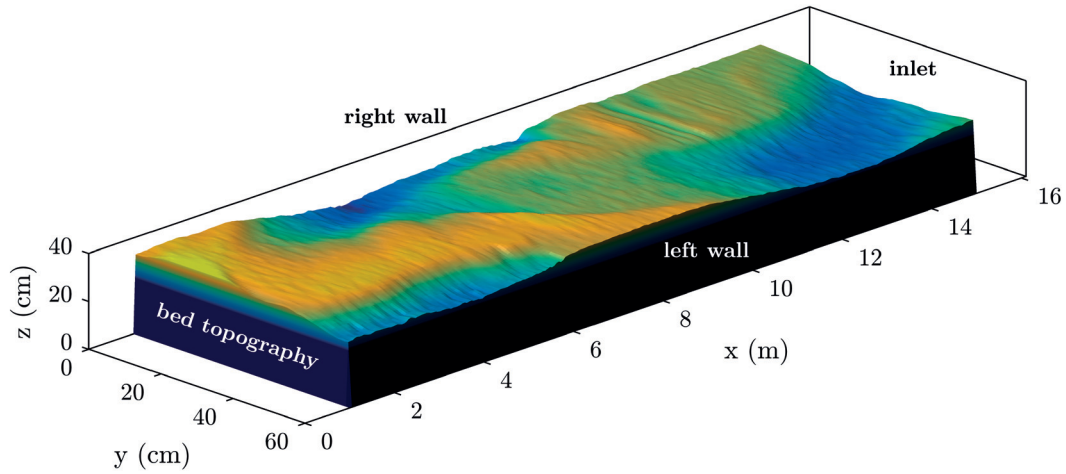
Figure 4.1: Example of the bed elevation data, the x-axis being the distance from the flume outlet, the y-axis the distance from the right wall of the flume, and the z-axis the elevation from the bottom of the flume.

The bed topography is characterized by single-row alternate bars which consist of a succession of bars and pools on both sides of the flume. An example is shown in figure 4.2 using the same bed elevation measurements than in figure 4.1. The pools are the low elevation areas where the water height is significant compared to where the bars are located. Indeed, in our experiments, the bars are most of the time in flush with the water surface. Their downstream limits are referred to as *bar heads* which are usually the highest point of the bars and mark the transition with the pools observed after them. Note that during the experiments the pool depths were found to be in the order 10 cm, the flow velocities in the order of 1 m/s, and the flow regimes close to critical with a Froude number varying about 1.
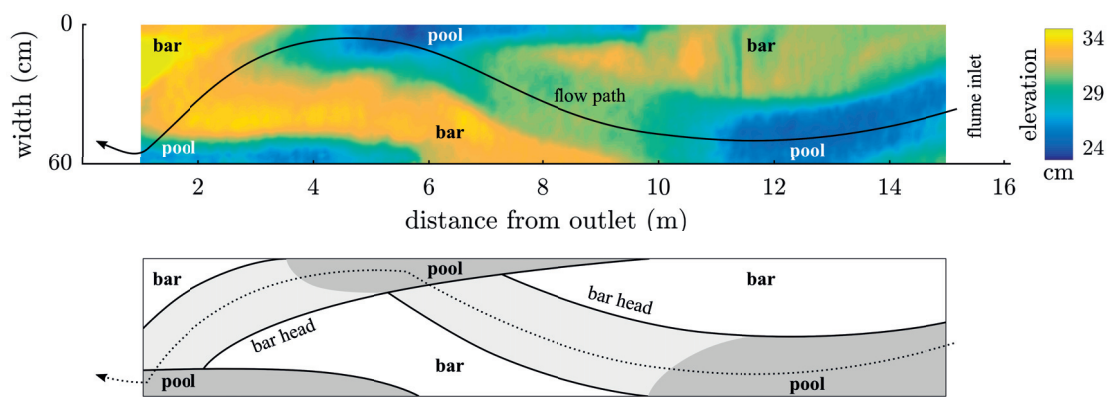
Figure 4.2: Example of alternate bars in the bed (top-view).

The geometry of the alternate bars observed in our experiments (see figure 4.2) corresponds to the one described in the related literature (Jaeggi, 1984; Ikeda, 1984; Chang, 1985; Yalin, 1992),
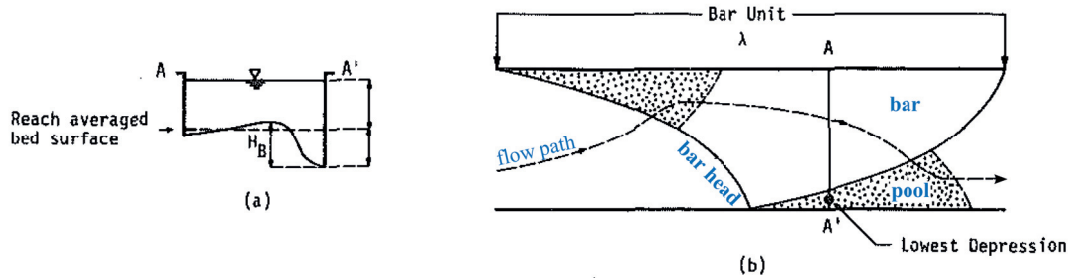
Figure 4.3: Common representation of single-row alternate bars in straight channels, modified from Ikeda (1984).

as illustrated in figure 4.3. We clarify that the mechanisms leading to bar formation, which have been the subject of numerous studies (Colombini et al., 1987; Seminara, 1998; Tubino et al., 1999), are beyond the scope of this study. Indeed, our interest is focused on the relation between the alternate bars, which characterize the bed morphology in our experiments, and the bedload pulses discussed in Chapter 3.

The bed and the water elevation data have rather fine spatial (~1 cm) and temporal (~10 min) resolutions given the flume size and the duration of the experiments. The dataset collected contains therefore a large amount of information about the evolution of the bed and the hydraulic conditions during the experiments. However, the evolution of a topographic surface over a long period of time is difficult to represent graphically, and can be complex to analyze. A simple approach is to reduce the number of dimensions in the dataset in such a way it is easier to examine. For instance, in the following, we often choose to study the bed elevation along given longitudinal profiles which reflect well the bar-and-pool system (e.g., in section 4.4.2). However, when doing so, one has to bear in mind that part of the information contained in the original dataset is lost.

4.2 Bed slope time series

The bed slope, which can be computed from the topographical data presented in section 4.1, is a widely used variable to evaluate the changes in bed topography. In the following, we first verify that it is in phase with the water-surface slope before discussing its temporal evolution during the experiments. We then relate the bed slope fluctuations to bedload transport in a first step linking the BTR fluctuations discussed in Chapter 3 to the bed morphodynamics.

4.2.1 Comparison of the bed and water slopes

The bed slope and the water-surface slope are two common variables used to describe the system constituted of the bed and the water flow (see definition in section 3.1.2.2) in flume experiments (Iseya and Ikeda, 1987; Recking et al., 2009). We compute both averaging the bed elevation and the water elevation in the cross-sectional direction and calculating the slope of

the bed and water profile obtained. The latter are computed by performing a linear regression on the averaged profiles. Note that the flume inclination is taken into account in the final computation of the bed slope and the water-surface slope, and that the emerged parts of the bed are ignored in both cases.

The water elevation is relatively homogeneous along each cross section and varies gently in the longitudinal direction. Therefore, little information is lost during the water-surface slope calculation. However, the bed elevation can vary significantly in both the cross-sectional and longitudinal direction because of the alternate bars in the bed. Indeed, the bars are generally in flush with the water surface whereas the pools can be up to about 10 cm deep with respect to the bar heads. As a consequence, a large amount of information about the bed elevation variability in space is lost when computing the bed slope. It is therefore important to keep in mind that the local bed slope can differ significantly from the average value when analysing the bed slope time series in the following.
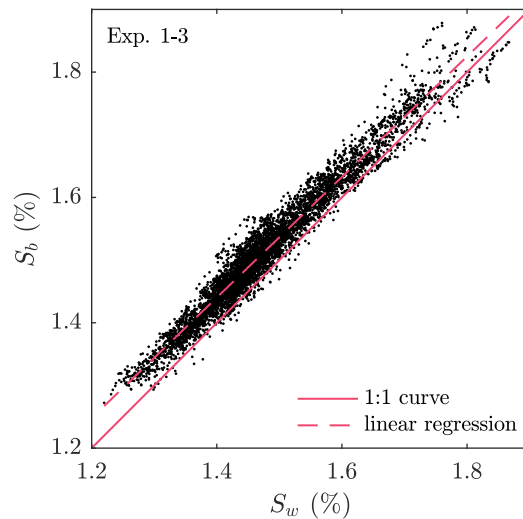
Figure 4.4: Bed slope S_b measurements versus water-surface slope S_w measurements during experiment 1, 2 and 3 combined. The coefficient of determination R^2 and the standard error of the linear regression are 0.96 and 0.02%.

The bed slope (S_b) and the water-surface slope (S_w) are compared in figure 4.4. They are linearly correlated and S_b is in average steeper by 0.04% than S_w which is negligible. We can therefore consider that the water surface is in phase with the bed or, in other words, that the water surface adjusts instantaneously to changes in bed topography (Recking et al., 2009). Therefore, in the following, we only consider the bed slope time series which are directly related to bed topography.

4.2.2 Characteristics of the bed slope time series

The temporal evolution of the bed slope during each experiment is plotted in figure 4.5, along with the BTR time series for comparison purposes. The main characteristics of the bed slope time series are summarized in table 4.1.

The bed slope fluctuations about the mean values in figure 4.5 are much more limited than the BTR ones (see figure 3.1). Indeed, the relative standard deviations are lower than 5% in each experiment, whereas they were larger than 100% for the BTRs. As a consequence, given the long experiment durations and the discussion in section 3.7 about system equilibrium, we can consider that dynamic equilibrium regarding the bed slope is achieved in the experiments. The average bed slopes in table 4.1 can therefore be seen as the *equilibrium slopes* mentionned is section 3.1.2.1. Note that the latter are in agreement with the theory since they are close to the flume slopes which were set based on the bedload tranport formula proposed by Recking (2006).

The average bed slopes given in table 4.1 are steeper in experiments with larger sediment feed rates (see table 4.1) which is in agreement with the theory. Indeed, the transport capacity, which increases with increasing bed slope, has to match the input sediment feed rate to achieve mass-balance equilibrium (Wainwright et al., 2015).

However, it is interesting to note that $\bar{S}_b$ in experiment 1 and 3 are very close (the difference is 0.02% in absolute value) although $Q_{s,in}$ doubles. In comparison $\bar{S}_b$ in experiment 3, of which $Q_{s,in}$ is three times larger than in experiment 1, is larger by about 0.18% (in absolute value). Since the granulometry (skin roughness) and the flow rate are the same in each experiment, this observation highlights that bed morphology (which affects form roughness) plays a fundamental role in the transport capacity of the system.

4.2.3 Bed slope fluctuations and bedload transport rates

The bed slope fluctuates over time, as illustrated in figure 4.5. In the following, we relate these fluctuations to bedload transport, first discussing how they are induced by sediment erosion and deposition in the bed, and then investigating their correlation with the BTR fluctuations described in Chapter 3. More specifically, we compare the spectral signature (see section 3.3.2.2) and the autoregressive behavior (see section 3.4) of both time series, before evaluating their cross-correlation coefficients.

4.2.3.1 Bed aggradation and degradation

Local erosion and deposition of bed material directly impact bed slope. For instance, aggradation in the upstream part of the bed, or degradation in its downstream part, induces a raise in bed slope. Inversely, degradation in the upstream part, or aggradation in the downstream part, induces a decline in bed slope. The fluctuating behavior of the bed slope (see figure 4.5) therefore indicates that the bed undergoes constantly local aggradation and degradation.
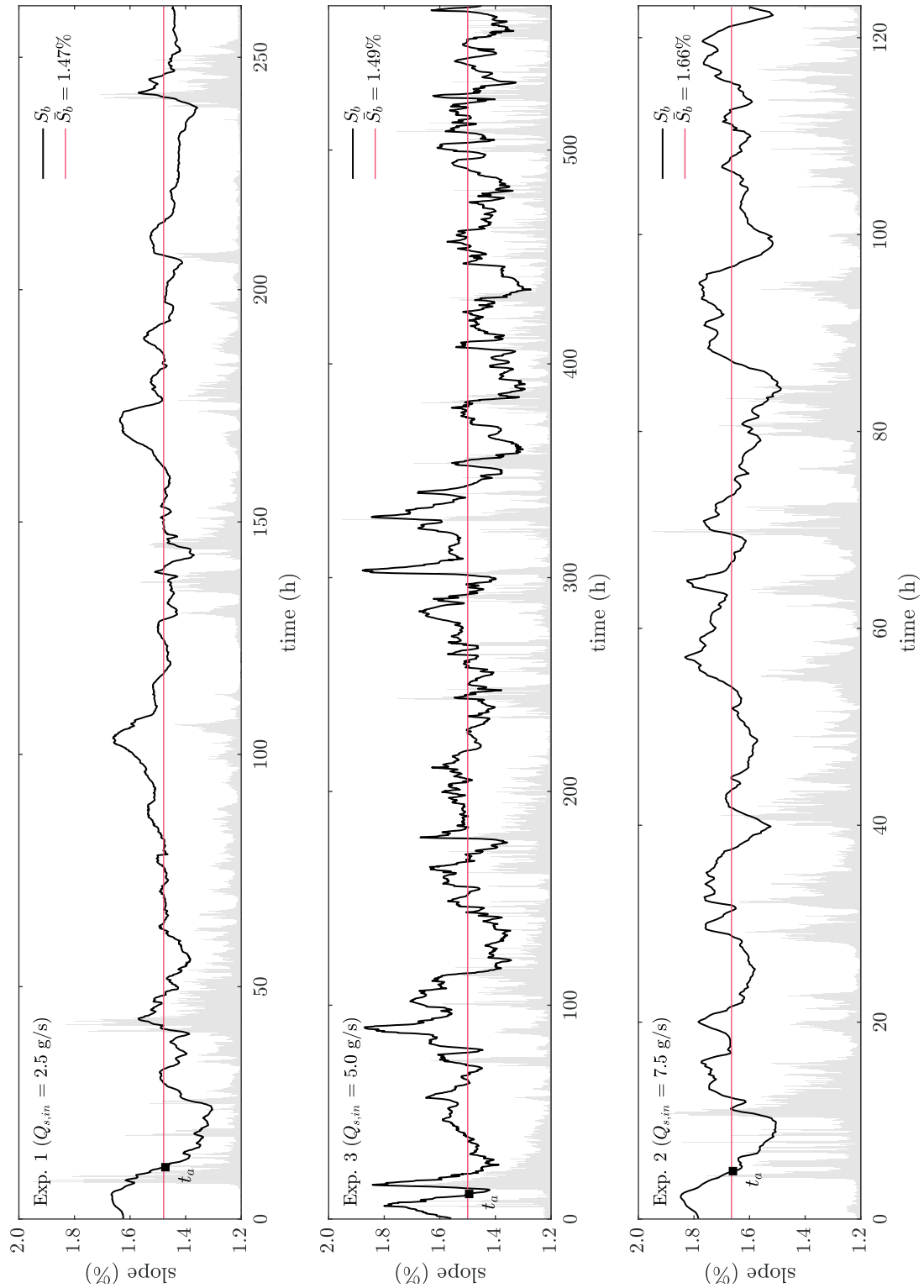
Figure 4.5: Time series of the bed slope S_b for experiment 1, 2 and 3. The solid lines represent the average bed slopes $\bar{S}_b$ and the filled area plots represent the bedload transport rates on an arbitrary scale.

Table 4.1: Summary values of the bed slope measurements during experiment 1, 2 and 3.

		Units	Exp. 1	Exp. 3	Exp. 2
flow rate	Q_l	l/s	15	15	15
flume slope		%	1.6	1.6	1.7
sediment feed rate	$Q_{s,in}$	g/s	2.5	5.0	7.5
initial bed slope ($t = 0$)		%	1.63	1.57	1.78
average bed slope		%	1.48	1.50	1.66
absolute standard deviation		%	0.07	0.10	0.08
number of observations			1566	3435	740
experiment duration		h	261.1	567.5	123.2
ignoring the adjustment time at the beginning of the experiments					
adjustment time	t_a	min	669	703	292
average stream power	ω	W/m^2	3.61	3.65	4.07
average bed slope	$\bar{S}_b$	%	1.47	1.49	1.66
absolute standard deviation		%	0.06	0.07	0.09
relative standard deviation			0.04	0.05	0.05
number of observations			1498	3326	710
experiment duration	T_{exp}	h	249.9	555.8	118.4

We observed that the sediment fed upstream was not directly transported toward the flume outlet, but was first deposited in the upstream part of the bed. However, at some point, sediment has to be transferred in the downstream direction to maintain a certain mass balance, which occurs through the processes of erosion, transport and deposition of bed material. As a consequence, the bed topography is continuously disturbed which is reflected in the bed slope fluctuations commented above.

As shown in figure 4.5, large increases in bed slope are generally associated with large bedload pulses (e.g., in experiment 3 at $t = 300$ h) which means that large amounts of sediment is eroded in the downstream part of the flume and subsequently evacuated. During low bedload transport phases, the bed slope can also increase (e.g., in experiment 3 at $t = 25$ h). In that case, it indicates sediment deposition in the upstream part of the flume. If, on the contrary, the slope decreases (e.g., in experiment 1 at $t = 210$ h), it means that sediment is eroded in the upstream part and deposited in the downstream part. Note that sometimes the slope remains relatively stable about a given value (e.g., in experiment 1 at $t = 60$ h). Aggradation and degradation of bed material then occur uniformly along the flume length.

In summary, the bed slope fluctuations reflect the transfer of sediment in the downstream direction, which results in bedload pulses. Moreover, this transfer appears to occur through local bed aggradation and degradation processes, rather than continuously over the entire flume length, which is consistent with the intermittent character of bedload pulses. This correlation between the slope and BTR fluctuations is further investigated below.

4.2.3.2 Spectral signature

In order the compare the spectral signatures of the BTR and the slope time series, the power spectra of the latter are plotted in figure 4.6 in the same way they were for the BTRs in figure 3.11. It appears that the saturation time scales associated with the BTRs also indicate when the slope power spectra saturate: the largest scales of fluctuations are similar for both variables. This result is a first evidence that the slope and the BTR fluctuations are correlated.
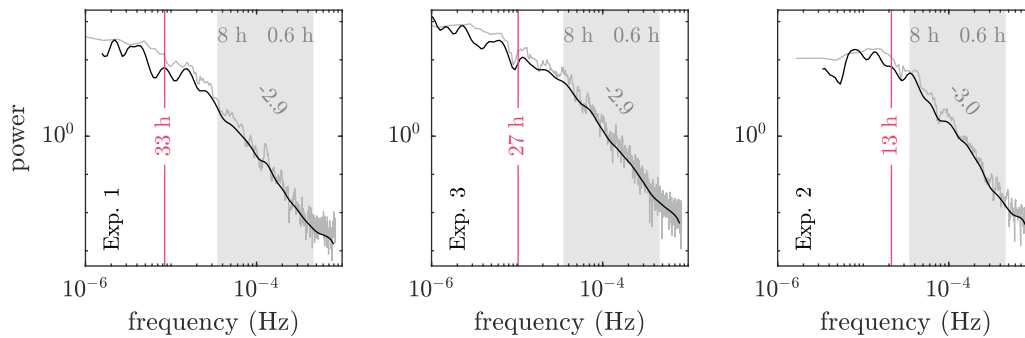
Figure 4.6: Power spectra of the bed slope time series for experiment 1, 2 and 3. The grey curves represent the multitaper spectra and the black curves the wavelet spectra. The scaling ranges are indicated in light grey and the spectral slopes are given. The solid vertical lines indicate the saturation time scales computed for the time series of the bedload transport rates.

The exact bounds of the scaling ranges appearing in figure 4.6 (log-log linearity) are difficult to determine precisely, but are about 8 h-0.6 h in each experiment. They are therefore similar to the ones computed for the BTRs (note that the bounds corresponding to high frequencies must be compared with caution since the temporal resolution of the bed slope measurements is ~10 min whereas it is 1 min for the BTRs). However, the spectral slopes are about -3 in each experiment, which is roughly two times the ones calculated for the BTR time series: the energy contained in the fluctuations decreases faster with decreasing temporal scale for the bed slope time series. This result was expected since the slope time series in figure 4.5 are smoother than the BTR time series.

To complete the comparison of the spectral signatures, the periodograms of the slope and BTR time series are plotted in figure 4.7 (as they were in figure 3.12 for the BTRs only). They show that most of the predominant periods in the slope time series (which are all larger than two hours, in agreement with the considerations above) correspond to a peak in the BTR periodograms. These similarities in the spectral signatures reinforce our conclusion above that the fluctuations in the slope and BTR time series are correlated, which is consistent with the findings of Recking et al. (2009).
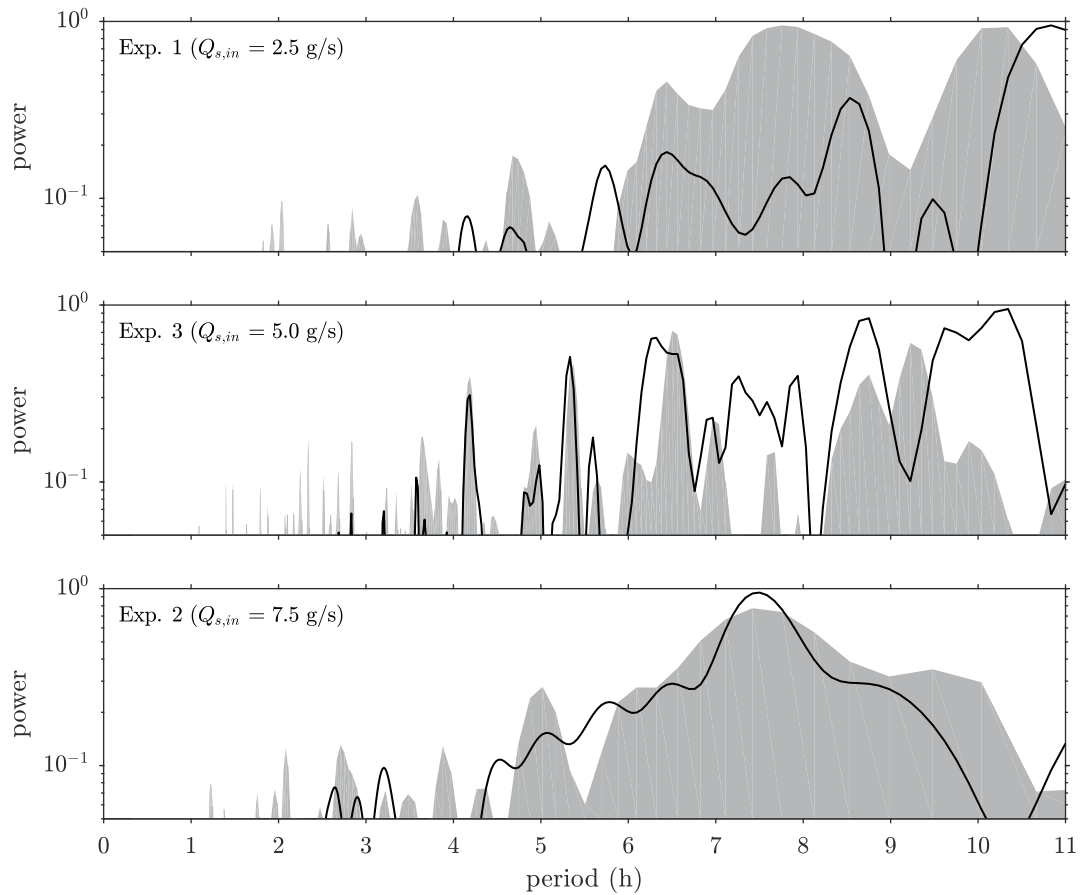
Figure 4.7: Normalized periodograms of the bedload transport rates (filled area plot) and the slope time series (black curve) for experiment 1, 2 and 3 (they were computed based on a Fourier transform of the time series, and only the frequencies higher than $1/11$ h^{-1} were considered).

4.2.3.3 Autocorrelation

As expected from the results above that the spectral signatures of the slope and BTR time series are similar for low frequencies, the bed slope autocorrelation functions plotted in figure 4.8 show similar features to the BTR ones plotted in figure 3.13.

Indeed, in experiment 1, no prominent peaks are observed as for the corresponding BTR time series. In experiment 3, bedload pulses were found to have a certain periodicity characterized by a period of about 26 h. For corresponding time lags, the bed slope time series shows also significant autocorrelation. Finally, the periodicity of the bed slope fluctuations in experiment 2 appears clearly for time lags of about 15 h. This period is of the same order of magnitude as the one identified for the BTR fluctuations (~10 h), although slightly larger. These observations therefore support the conclusion in section 4.2.3.2 that the large fluctuations in the bed slope and the BTR measurements are related.
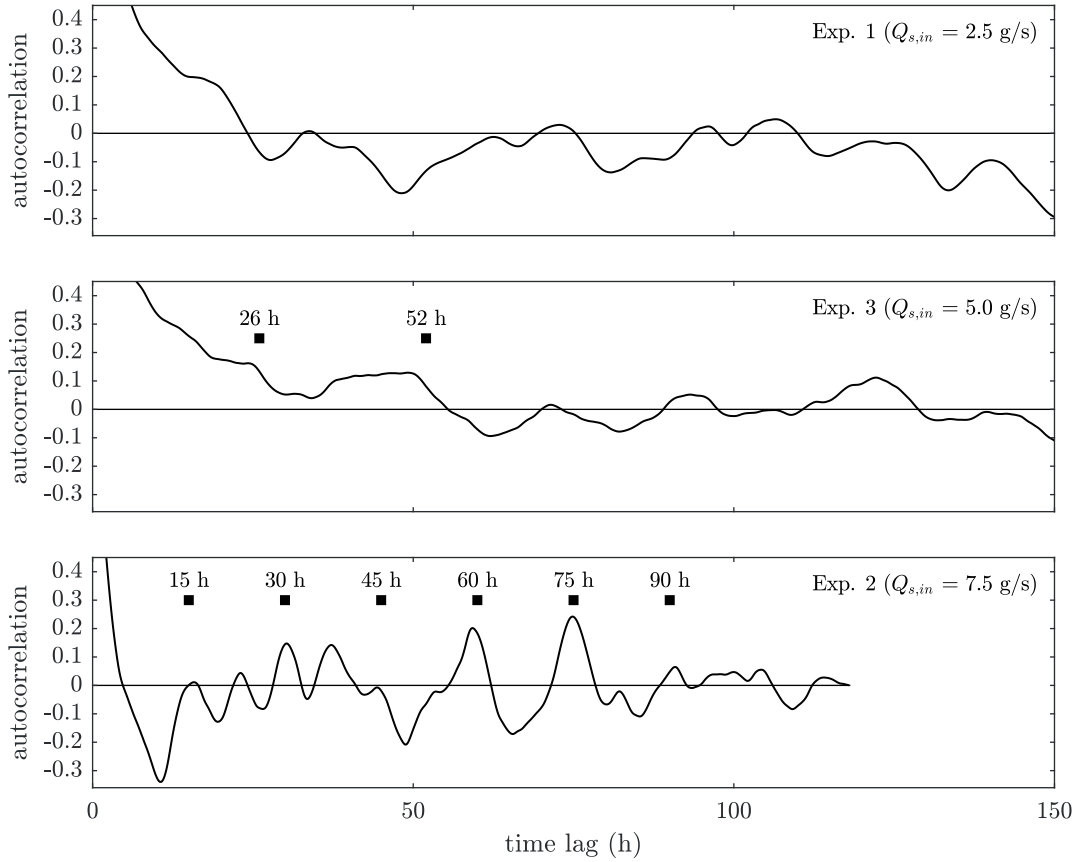
Figure 4.8: Autocorrelation functions of the bed slope time series for experiment 1, 2 and 3.

4.2.3.4 Cross-correlation

In order to quantify the correlation between the bed slope and the BTR time series, of which evidences are given above, we compute their cross-correlation coefficients hereafter. To do so, the BTRs are first averaged over 10 min, in order to match the temporal resolution of the slope measurements, and then the bed slope measurements are linearly interpolated to match exactly the BTR measurements in time.

The cross-correlation coefficients computed are respectively 0.60, 0.73 and 0.65 for experiment 1, 2 and 3. They indicate that the bed slope and the BTR fluctuations are significantly correlated, and that this link is stronger in experiments with larger sediment feed rates. Moreover, the cross-correlation was found to be maximum for time lags (with respect to the bed slope time series) of respectively about -60 min, -30 min and -20 min. This phase shift means that, during bedload pulses, the maximum slope value is often reached after the maximum BTR value. Indeed, once the peak in BTR is measured, the bedload pulse usually still last for some time: the bed continues to be eroded in its downstream part, inducing a raise in the bed slope.

In summary, the results above bear evidence that the bedload pulses observed in our exper-

iments are closely related to physical processes occurring in the bed. In the following, we further investigate this link in consideration of the alternate bars which characterize the bed topography.

4.3 Bed erosion and bedload pulses

The bedload pulses measured at the flume outlet involve sediment volumes much larger than the quantities fed in the flume. Therefore, they necessarily result from the erosion of large amounts of bed material that are subsequently evacuated from the flume. The analysis of the bed slope fluctuations performed in section 4.2 points that the bed aggradation and degradation processes are localized in space, at least in the longitudinal direction. More specifically, bedload pulses appear to be often associated with erosion in the downstream part of the bed. This supports the intuition that sediment evacuated during bedload pulses originates from the downstream part of the flume, close to the outlet, rather than from further upstream.

Based on this observation, we define the *active length* as the downstream portion of the bed of which overall erosion matches the amount of sediment evacuated at the flume outlet. It is computed by aggregating first the bed elevation measurements in the cross-sectional direction. Then, for each measurement, the change in bed mass since the last measurement is computed at each cross section. In other words, the mass balance is computed between each bed scans (every ~10 min) and summed in the y-axis direction. Finally, the change in bed mass is integrated along the flume length, starting from the outlet, until it matches the amount of sediment evacuated from the flume during the same period of time.

Note that the active length is computed only when the mass evacuated is larger than the mass fed by 1.5 times (i.e., during intense bedload transport events). Moreover, we clarify that the change in bed mass at the beginning of the flume ($x = 0$–1 m), where measurements are not available, was approximated using the measurements at $x = 1$ m.

The histogram of the active lengths during bedload pulses is plotted in figure 4.9 for each experiment. The active length seems bounded by a value corresponding to 75% of the flume length (12 m). However, the remaining 25% of the length (between 12 m and 16 m) are likely to be affected by the flume upper boundary condition (i.e., the flume inlet). Therefore, no conclusion about an upper bound of the active length can be drawn: the entire flume length is possibly involved in bedload pulses generation.

Nevertheless, the active length shows preferential values. In experiment 1 and 3, three values multiples of ~4 m are observed. Examining the corresponding bed topography measurements, these values match the location of three bars and their adjacent pools (referred to as bar-pool pairs in the following). Note that the theoretical bar length (Yalin, 1992) is about 6 times the flume width (i.e., 3.6 m) which is in agreement with the values given above.

One can also notice that in experiment 3, which is the longest one (~600 h), bedload pulses
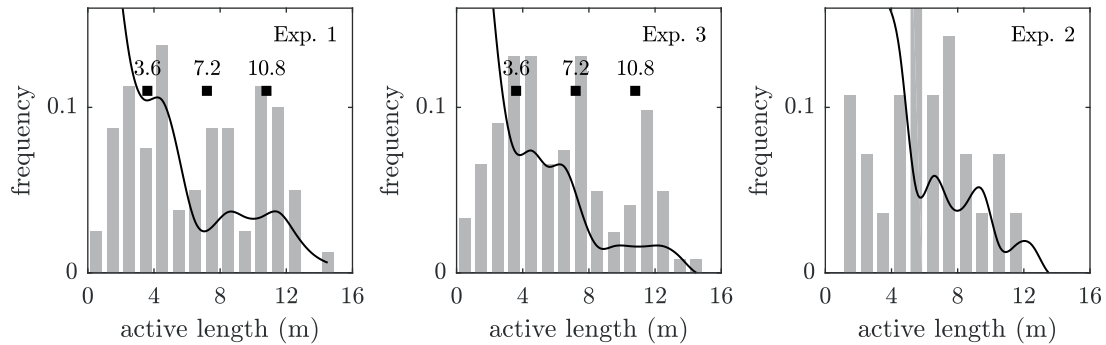
Figure 4.9: Distribution of the bed active lengths measured from the flume outlet for experiment 1, 2 and 3. The bar plots show the distribution during intense bedload transport phases, and the solid lines show the distribution during low bedload transport phases. The black squares represent the theoretical locations of alternate bars.

have a tendency to be produced in the most downstream bar-pool pair rather than in more upstream ones. In experiment 2, the preferential values taken by the active length are less uniformly spaced. We explain this difference by the larger variability in bar features (number, location and shape) observed during this experiment. In summary, the active length seems to be a function of the number of bar-pool pairs involved in sediment mobilization.

The active lengths during low transport phases (i.e., when the mass evacuated is lower than the mass fed) are also plotted in figure 4.9. In that case, the predominant values of the active lengths are within 0-4 m: when the bed undergoes overall aggradation, the low bedload pulses registered are generated by erosion in the most downstream bar-pool pair.

The fate of the sediment fed in the flume was also investigated using the same method: the change in bed mass was integrated starting from the flume inlet until it met the amount of sediment fed since the last topographical measurement. It appeared that the sediment fed upstream are preferentially deposited within the first meter from the flume inlet (16-15 m).

The above observations indicate that the transfer of sediment from the upstream part of the flume, where it is fed, to the downstream part is discontinuous and affected by the bar-and-pool system. Indeed, the sediment fed is first deposited close to the flume inlet, increasing the bed total volume asymmetrically, before being transported further downstream. The bed therefore behaves like a system that is constantly disturbed positively in its upstream part (i.e., by increases in volume), and of which spatially delimited zones participate in the transfer of sediment, rather than like a sediment toboggan where incoming material is simply transferred in the downstream direction.

4.4 Bar-and-pool system

In this section, we investigate the alternate bars observed in the bed which seem to play a key role in the transfer of sediment as discussed in section 4.3. The bars and the pools forming the *system of alternate bars* are studied as distinct entities, and both their geometry and dynamics are characterized based on the topographical measurements performed. Note that, in the following, the results are often interpreted in the light of the visual observations made during the experiments.

4.4.1 Spatial localization of the erosion and deposition processes

4.4.1.1 Method

The erosion and deposition of bed material between each scan, and at each bed location, can be computed by comparing the topographical measurements. In order to identify any preferential zone where bed degradation or aggradation occurs, the average erosion and deposition rates over the entire experiment durations are computed at each bed location.

To do so, the erosion and deposition in the bed are first computed between each scan. The total erosion and deposition during the experiments are then computed at each bed location. The corresponding rates are finally obtained by dividing by the respective experiment durations. The average erosion and deposition rates are shown in figure 4.10 for each experiment.

4.4.1.2 Degradation and aggradation zones

Zones of intense degradation and aggradation appear clearly in figure 4.10. They are stretched in the longitudinal direction and are located on both sides of the bed. Moreover, the degradation zones match the aggradation zones which means that the areas where the erosion process is concentrated also undergo intense sediment deposition during the experiments.

More generally, the average erosion and deposition rates compensate each other at each bed location. This zero sediment balance indicates that the bed volume is conserved at the experiment time scales (in agreement with the discussion in section 3.6).

The intense degradation/aggradation zones are located near the flume walls, either on the right or the left side, and are 15-20 cm wide. By way of comparison, the average erosion/deposition rates in the central region of the flume (which is ~20-30 cm wide) is approximately two to three times less. In the longitudinal direction, the intense degradation/aggradation zones are observed over the whole flume length, except in the very upstream part (the last ~2 m in experiment 2 and 3, and ~4 m in experiment 1). They are 4-6 m long and are alternatively located near the right or the left wall. The arrangement of the main zones is similar in each experiment: there are one on the right side and two (only one in experiment 1) on the left side. Note also that, near the flume inlet, the center of the channel undergoes intense erosion and deposition. This observation indicates that the sediment fed in the flume are first deposited before being transported further downstream, as already stated in section 4.3.
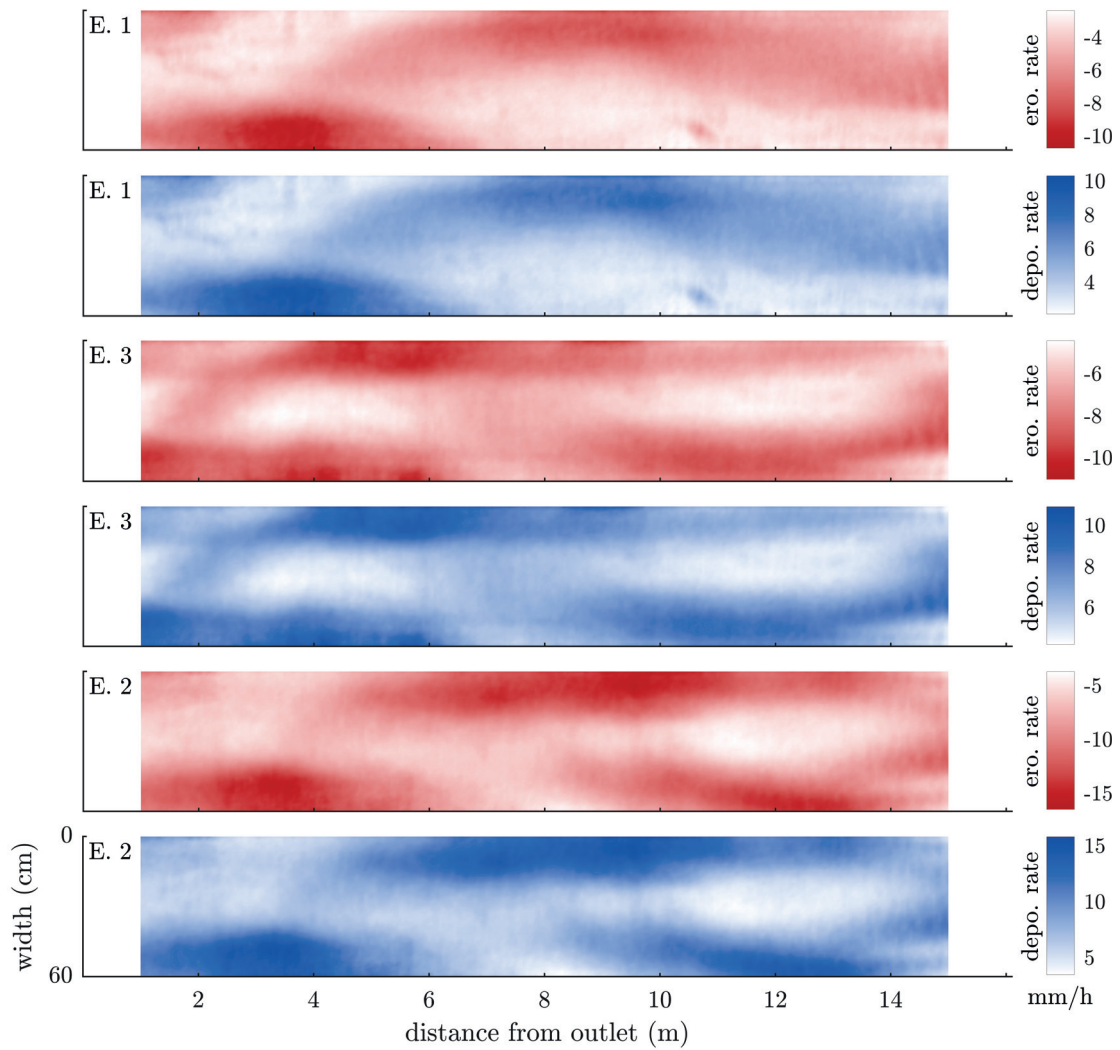
Figure 4.10: Average erosion and deposition rates in the bed during experiment 1, 2 and 3. Zones of intense degradation/aggradation are visible, alternately, on both sides of the bed.
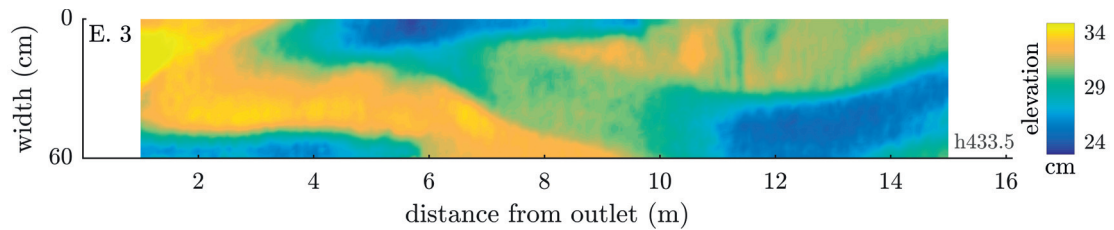
Figure 4.11: Example of the typical bed topography observed during experiment 3. Three pools, characterized by low bed elevations, are visible: one on the right side and two on the left side of the bed.

4.4.1.3   Effect of the sediment feed rate

The increase in the sediment feed rate between the experiments affects the characteristics of the degradation/aggradation zones observed in figure 4.10. As $Q_{s,in}$ increases from 2.5 to 5.0 g/s between experiment 1 and 3, a third zone appears in the upstream part of the flume. Moreover, the degradation/aggradation zones are more stretched longitudinally. Note that their maximum erosion rate remains however about -1.0 cm/h.

Between experiment 3 and 2, the sediment feed rate increases by 1.5, and so does the maximum erosion rate which increases to -1.5 cm/h. In summary, the erosion and deposition processes gain intensity as the sediment feed rate increases.

4.4.1.4   Comparison with the bar-and-pool system

The comparison of the average erosion/deposition rates (shown in figure 4.10) with the topographical data shows a high correspondence between the geometry of the degradation/aggradation zones and the alternate bars. For comparison purposes, an example of the typical bed topography observed during experiment 3 is given in figure 4.11.

The intense degradation/aggradation zones correspond to the most common locations of the pools. The latter therefore concentrate most of the bed erosion/deposition activity, which means that the pools store and release large amounts of sediment during the experiments. The system of alternate bars seems therefore to play a key role in the transfer of sediment (as pointed in section 4.3), the pools being the active part.

4.4.2   General considerations about alternate bar dynamics

The pools and the bars are located near the flume walls in the same way as in typical channels with alternate bars as discussed in section 4.4.1. Therefore, their dynamics can be investigated along the bed longitudinal profiles corresponding to these regions. Indeed, bar migration is essentially a longitudinal process. Two bed profiles are considered in the following: the *right profile* which is 5 cm away from the right wall, and the *left profile* which is 5 cm away from the left wall (we remind that the right and the left are defined with respect to the flow direction). Moreover, the joint analysis of these two profiles allows us to investigate the coupled dynamics of the bed structures on both sides of the bed.

The evolution of the right and left profiles during experiment 3 is shown in figure 4.12 which is a spatio-temporal representation of the bed topography. The evolution in time of the two profiles are plotted symmetrically for a better comparison. Only the results of experiment 3 are presented here for clarity purposes, which was chosen because it is the longest of the three experiments and the one where bar migration is the most often observed. However, the comments made in the following are also valid for experiment 1 and 2. The spatio-temporal plots of the latter are available in Appendix A.7.
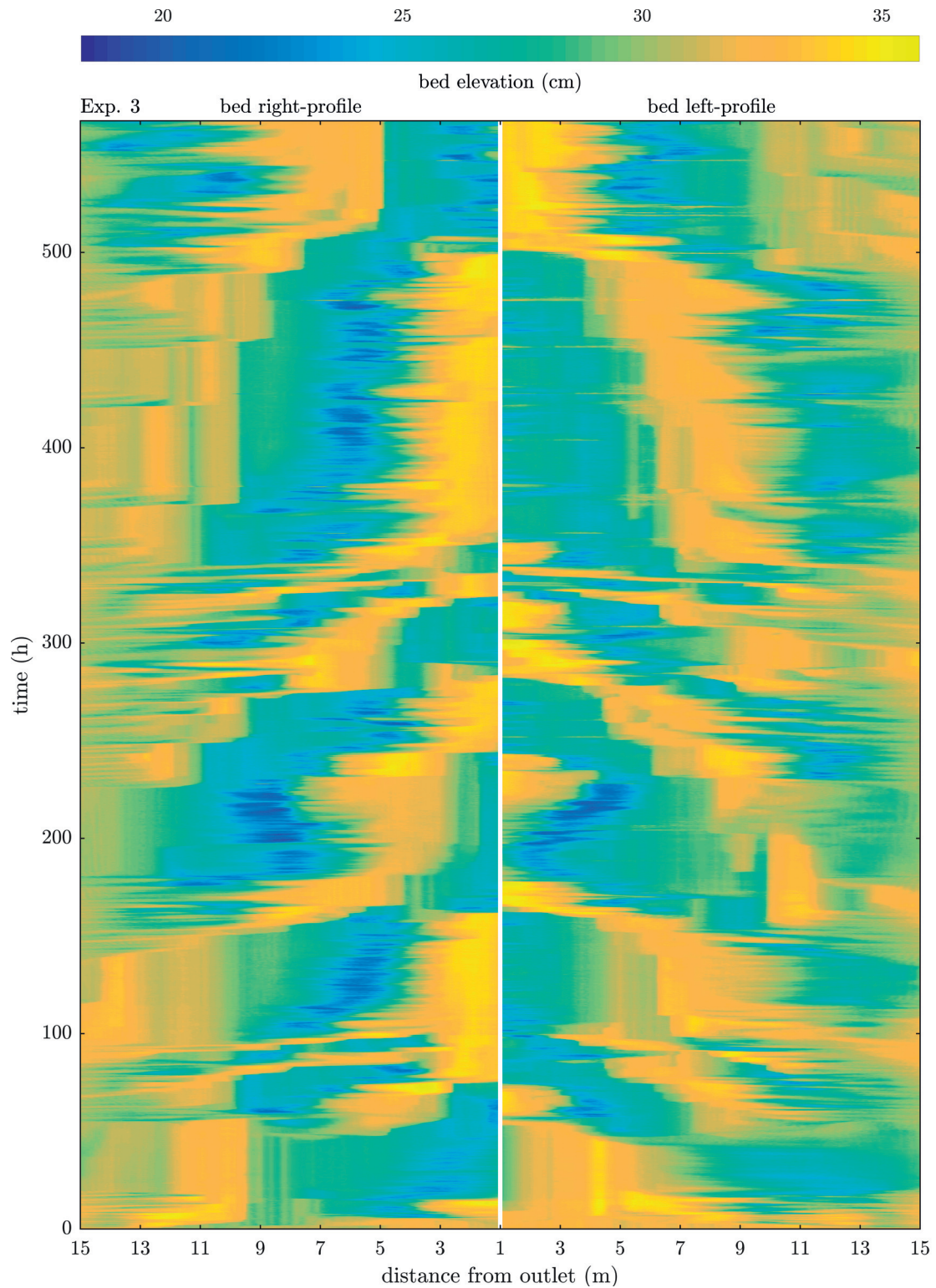
Figure 4.12: Temporal evolution of the right and left profiles of the bed during experiment 3. The two profiles are plotted symmetrically with respect to the flume outlet, which corresponds to the center of the figure.

4.4.2.1 Bed topography variations

As shown in figure 4.12, the bed topography continuously changes over time, although some part of the bed can remain stable for relatively long time periods compared to the experiment duration. Different structures, of various size and geometry, can be identified in the bed. They can appear or disappear, remain static, or move in either the downstream or upstream direction. These general observations illustrate the complexity of the bed topography variations and of the related physical processes in space and time.

However, the pools and the bars appear clearly in figure 4.12; and their dynamics seems to reflect the essential part of the topography variability. We remind that sediment transport also occurs in the cross-sectional direction. The bed mass is therefore not conserved along the longitudinal profiles which can cause discontinuities in the migration of the bed structures observed in figure 4.12.

4.4.2.2 Spatio-temporal characteristics of bars

Bar heads refer to the downstream end of bars, as stated in section 4.1. They are associated with abrupt drops in bed elevation, marking the transition between the bar and the pool that is generally observed after. Moreover, in our experiments, bar heads are most of the time in flush with the water surface (i.e., the water height above the bar heads is close to zero).

Bar heads can be clearly identified in figure 4.12 as high elevation areas. They are present on both sides of the bed and migrate intermittently in the downstream direction. The rest periods are much longer than the moving ones: the bar head locations can remain stable for up to several tens of hours. We investigate bar migration in more details in section 4.5.4.

The bar locations along the right and left profiles are shifted, which is a result of their alternate character. When a bar migrates on one side of the flume, the bars on the other side generally also migrate within a certain time window, which gives a symmetrical aspect to figure 4.12. This observation points the coupled dynamics of alternate bars, which is further discussed in section 4.5.4.

4.4.2.3 Spatio-temporal characteristics of pools

The pools can be identified in figure 4.12 by their bottom which are low elevation areas. Since they are delimited in space by the bars, they have a similar alternate configuration along the flume length. Moreover, their locations change when the bars migrate.

However, during the rest periods of the bars, the shape of the pools varies continuously, alternating between a *filled configuration* and an *empty configuration*. Moreover, the position of the bottom of the pools keeps oscillating within a certain range of values. This behavior of the pools is further discussed in section 4.6.

4.4.2.4   Link with bedload transport

At the flume end, a pool is present on either one of the bed sides, the other side being obstructed by a bar (see figure 4.12). The bed elevation fluctuations observed in this pool indicate that sediment is periodically evacuated toward the flume outlet. These aggradation-degradation cycles in the pool are therefore likely to be related to the BTR fluctuations measured at the flume outlet. When the pool changes side, the adjacent bar is destructed and the amount of sediment thus released is likely to generate a bedload pulse.

4.4.2.5   Additional comments

The results above indicate that the bars are stable structures in the bed. During the experiments, we observed that the bars are associated with low water heights and that they are circumvented by the stream flow which explains their stability. These observations therefore lead us to consider that the bars are stabilizing elements in the bed which constitute its "skeleton". When the bars migrate sufficiently, the overall configuration of the alternate bars is changed. As a result, the bars (and the pools) can seem to change side, whereas their are simply shifted in the downstream direction.

The stream flow, which is concentrated in the pools, changes side along the flume length, "jumping" from one pool to another. As a consequence, the pools ensure the transfer of water and sediment in the downstream direction. This role explains the frequent changes in shape that are observed: the erosion, transport and deposition of sediment modify constantly the geometry of the pools. In order to stress the role played by the pools in the transport of sediment, the alternate bars are sometimes referred to as the *bar-and-pool system* in this study.

The general considerations about the alternate bar dynamics made above constitute the framework for the detailed study of the bar-and-pool system performed in section 4.5 and section 4.6.

4.5   Bar characteristics

The system of alternate bars observed in the bed consists of a succession of bars and pools on both sides of the flume. As discussed in section 4.4.2, the bars are stable structures that can episodically migrate in the downstream direction. Their location can be computed by identifying the bar heads which appear clearly in the topographical data. Conversely, the geometry of the pools varies a lot over time making them more difficult to characterize. Therefore, in this section, the system of alternate bars observed during each experiment is characterized focusing on the bar structures. Both their geometry and their dynamics are investigated.

4.5.1   Data preparation

The bars are studied along the right and the left longitudinal profiles of the bed, each being 5 cm away from the corresponding flume wall. Since bars are prominent structures, the

profiles are smoothed using cubic spline functions to make them appear more clearly. In each experiment, the bars are defined with respect to a reference profile computed as follows: the mean of the two profiles is averaged over the total experiment duration, and the resulting profile is then approximated using a linear regression. The reference profile so obtained represents the average bed elevation along the flume.

We define the bars as the portions of the right and the left profiles above the reference profile, the bar heads being the highest points, as shown in figure 4.13. For each bar identified, the location is computed as the bar head location, the bar height as the bar head height with respect to the reference level, and the bar length as the length at the reference level. These definitions are illustrated in figure 4.13. Note that the bars located near the flume inlet or outlet are not taken into account since the boundary conditions interfere with them.
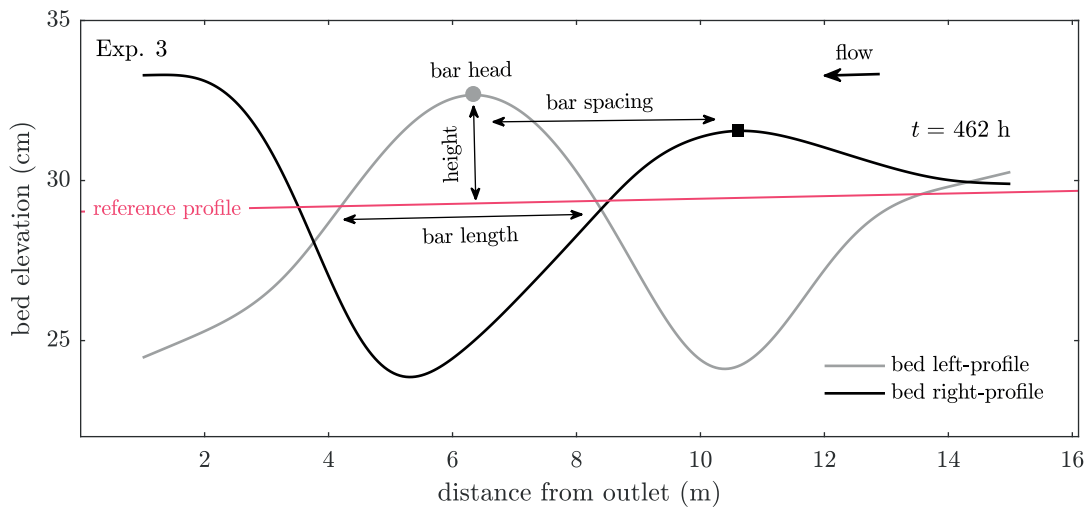
Figure 4.13: Example of alternate bars along the right and the left longitudinal profiles of the bed during experiment 3. The bed elevation is measured from the bottom of the flume.

4.5.2   Bar geometry

4.5.2.1   Bar length

The distributions of the bar lengths are plotted in figure 4.14(left). In each experiment, the bar lengths are bounded within 2 m and 8 m. However, the distribution in experiment 1 differs from the one in experiment 2 and 3: the respective dominant bar lengths are ~7 m and ~4 m, and the distributions are respectively stretched toward low and large values. It is interesting to note that, in experiment 1, bar lengths about 4 m are also observed frequently. The same observation can be made, to a smaller extent, for experiment 3 and bar lengths about 7 m.

In summary, two bar configurations can be observed in the bed: short bars (~4 m) and long bars (~7 m). As the sediment feed rate of the experiments decreases, the long bar configuration becomes progressively predominant. Note that the bar length definition used here differs

from the one in figure 4.3 which is generally used in other studies (Yalin, 1992).

4.5.2.2 Bar height

The distributions of the bar heights plotted in figure 4.14(right) are similar for each experiment: the bar heights vary between 1 cm and 5 cm and the distributions are bimodal. Comparing the bar heights against the bar locations, it appears that bars located downstream are generally higher than the ones upstream, which explains the bimodal character of the distributions.
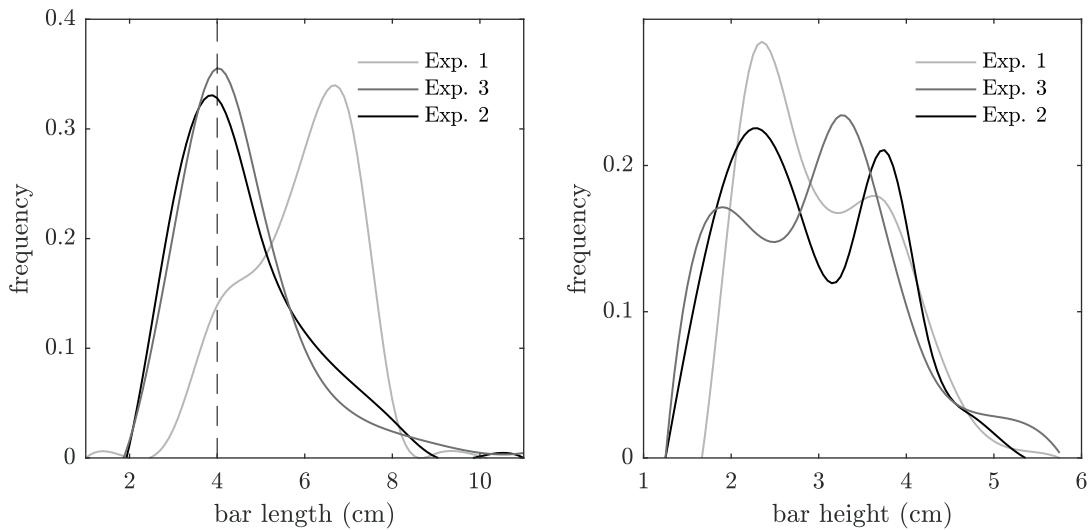
Figure 4.14: Distribution of the bar lengths (left) and the bar heights (right) in experiment 1, 2 and 3.

4.5.2.3 Bar spacing

The bar spacings is computed based on the bar locations on the both sides of the flume. Their distribution is plotted for each experiment in figure 4.15. They are consistent with the bar lengths computed above since, for each experiment, the distribution of the bar lengths and bar spacings are similar. Indeed, in alternate bar systems, the spacing between the bars is equal to the bar length by symmetry.

4.5.3 Bar location

The distributions of the bar locations along the right and the left profile of the bed are plotted in figure 4.16. They are commented below for each experiment.

In experiment 1, the bar positions vary little. On the right side of the bed, the preferred location is about 4 m away from the flume outlet. On the left side, the two preferred locations are about 8 m and 10 m away from the flume outlet. This low variability in the bar locations indicates that bars rarely migrate during the experiment. Note that the spacing between the preferred
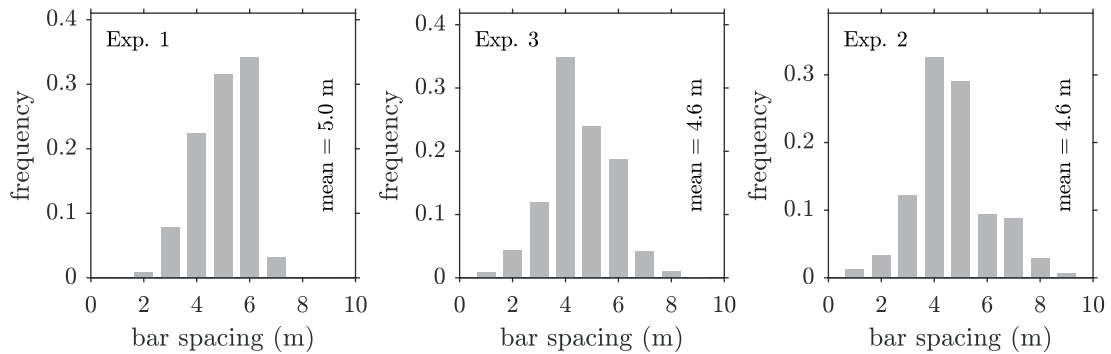
Figure 4.15: Distribution of the bar spacings, considering the bars on the both sides of the flume, in experiment 1, 2 and 3.

locations is consistent with the bar spacings plotted in figure 4.15.

Similar conclusions can be drawn for experiment 2, except that a bar on the right side can also be observed in the upstream part of the flume. Moreover, the wider distribution of the bar position about the preferred locations indicates that bar migration occurs more often than in experiment 1.

In experiment 3, although some preferred locations appear, bars are observed along the entire flume length. These various locations visited by the bars indicate that bars migrate during the experiment. Note that experiment 3 is about three times longer than the other experiments which is likely to increase the number of times bar migration occurs. However, no quantitative conclusion about the migration frequencies can be drawn based on the distribution of the bar locations.
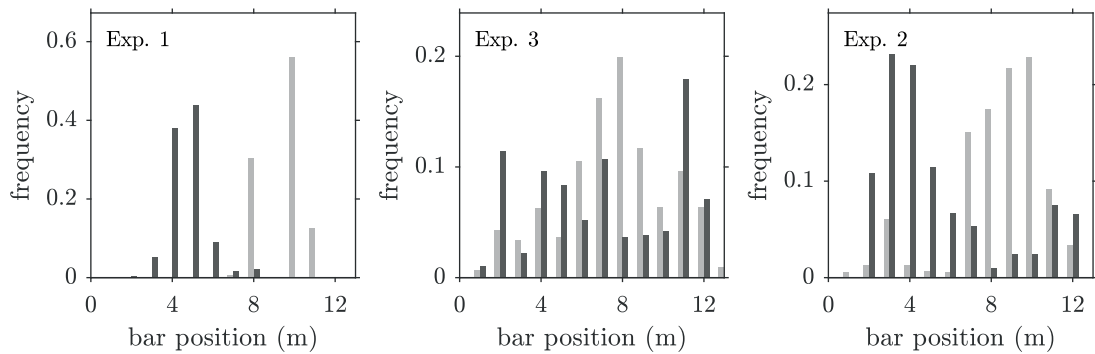
Figure 4.16: Distribution of the bar positions in experiment 1, 2 and 3. The light grey bar plots stand for the left profile, and the dark grey bar plots for the right profile of the bed.

4.5.4 Bar migration

In order to investigate bar migration, bar head trajectories along both bed profiles are computed by using a tracking algorithm. Each continuous displacement of at least 0.5 m in the downstream direction is recorded as a migration event, and the migration velocity is computed as the average velocity of the bar head displacement. The first ten hours of each experiment are not taken into account since, during this time period, the bed evolves from a flat configuration toward a formed one.

The summary values related to the migration of bars are given in table 4.2 for each experiment. The migration overlap provided is the ratio between the number of times simultaneous migration of at least two bars is observed and the total number of times bar migration is observed. The portion of the experiments during which no bar migration is observed is also indicated.

Table 4.2: Summary values of the bar migration characteristics during experiment 1, 2 and 3.

	Units	Exp. 1	Exp. 3	Exp. 2
sediment feed rate	g/s	2.5	5.0	7.5
experiment total duration	h	261.1	567.5	123.2
number of migration events		2	56	25
average migration velocity	cm/min	1.2	1.5	1.9
maximum migration velocity	cm/min	1.6	3.1	3.4
average migration duration	h	1.2	1.7	1.9
average migration distance	m	0.8	1.4	1.8
migration overlap	%	0.0	0.1	0.2
no migration	%	0.99	0.84	0.66

We make it clear that, using the methodology described above, only the migration events that are clearly identifiable and of major importance are recorded. The statistics presented in table 4.2 are related to these major events and must be interpreted as such. We also draw attention to the very small number of migration events recorded during experiment 1: the related statistics should therefore be interpreted with caution.

However, a visual analysis of the bed topography evolution shows that the computed bar trajectories are consistent with the ones than can be visually identified. We therefore consider that the values presented in table 4.2, and that the tendencies arising from them, are representative of the overall bar migration activity in the bed.

The results above (see table 4.2) indicate that bar migration activity is positively related to the sediment feed rate. Indeed, bar migration is nearly never observed in experiment 1 ($Q_{in} = 2.5$ g/s), and is about twice more frequent in experiment 2 ($Q_{in} = 7.5$ g/s) than in experiment 3 ($Q_{in} = 5.0$ g/s).

Bar migration can last for few hours, which gives an order of magnitude of the time scale associated with this process. The migration distance is in the order of few meters and the migration velocity of few centimeters per minute. Moreover, the duration, distance and velocity of bar migration tend to increase with increasing sediment feed rate.

The migration overlaps provided in table 4.2 indicate that the migration of the different bars in the bed occurs rarely simultaneously. Indeed, a complementary visual analysis of the bed topography evolution shows that, in many cases, bar migration is the result of a chain reaction initiated upstream. When a bar migrates in the downstream direction, the overall system of alternate bars is disturbed and the next bars migrate, one at a time, to maintain a stable configuration. Here, these chain reactions seem initiated by the formation of bars (i.e., sediment accumulation) near the flume inlet.
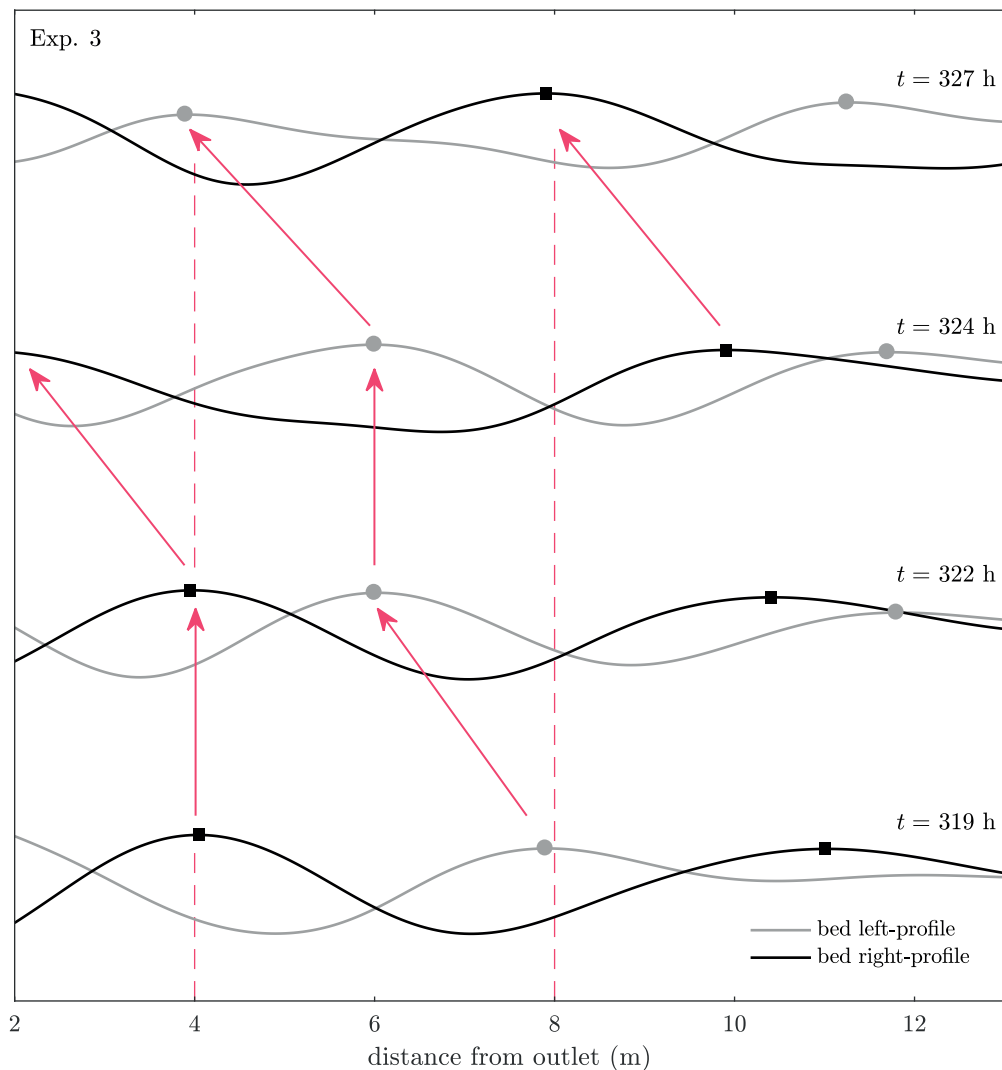
Figure 4.17: Example of bar migration during experiment 3. The right and the left longitudinal profiles of the bed are plotted at four different times. The markers represent the bar heads.

The bar migration process is illustrated in figure 4.17 which represents the evolution over time of the right and left profiles of the bed during a part of experiment 3. At the beginning, three bars are present in the bed: two on the right side and one on the left side. Then, a bar appears upstream, on the left side, and the other bars move progressively downstream.

The chain reaction from upstream to downstream is well illustrated by the two bars located at 8 m and 4 m from the flume outlet. They do not migrate simultaneously: the upstream bar moves first by 2 m, which is half the bar length, and then the downstream bar moves toward the flume outlet.

At the end of the migration process, the bars have moved by one bar length (4 m) and their configuration is inverted: there are one on the right side and two on the left side. The location of the bars, combining the two profiles, is almost exactly the same than at the beginning: they are located at 4 m, 8 m, and 11 m away form the flume outlet. Note that the whole migration process for the bars to take inverted configurations in this example last about 10 h which is significant compared to the experiment duration (~600 h).

4.6   Pool dynamics

The pools are delimited in space by the bars which are stable structures that can episodically migrate as discussed in section 4.4.2 and in section 4.5. In this section, the geometry and dynamics of the pools are investigated when the bars are static. Indeed, during bar migration, the whole system of alternate bars is disturbed which affects the characteristics of the pools.

4.6.1   Dead and active zones in pools

4.6.1.1   Pools bounded by two bar heads

In typical configurations, pools are located between two consecutive bars on a given side of the bed. These configurations can be observed in figure 4.12, in the central part of either the right or the left profiles. The bottom of the pools, which are regions of low elevation, are in most cases well marked. The two bar heads, located upstream and downstream the bottom of the pools, set the pool limits in the longitudinal direction. An example of a pool, in a typical configuration, is given in figure 4.18.

Each pool bounded by two bar heads is constituted of two parts having different dynamics: the *dead zone* and the *active zone* (see figure 4.18). The dead zone, referred to as inactive zone in Venditti et al. (2012), is located in the upstream part of the pool. In this area, the pool geometry is stable and the bed elevation does not vary over time. We observed during the experiments that the end of the dead zone corresponds to where the stream flow enters, laterally, into the pool (the entering stream flow originates from the pool located immediately upstream, on the other side of the flume). We also observed that, in dead zones, the stream velocity is close to zero and sediment transport is absent.

The active zone starts after the dead zone, where the stream flow enters the pool, and is bounded downstream by the next bar head (see figure 4.18). In this area, the bed elevation fluctuates continuously over time which means the pool undergoes successive phases of degradation and aggradation. When the active zone is aggraded, the pool bottom tends to move in the upstream direction, and inversely when it is degraded. As a consequence, the longitudinal position of the pool bottom fluctuates over time, as illustrated in figure 4.18. During the experiments, we observed that the stream flow entering the pool transports sediment that get deposited in the pool which explains the pool aggradation phases. When the pools are degraded, the sediment mobilized is evacuated, laterally, toward the next pool located on the opposite side of the flume.
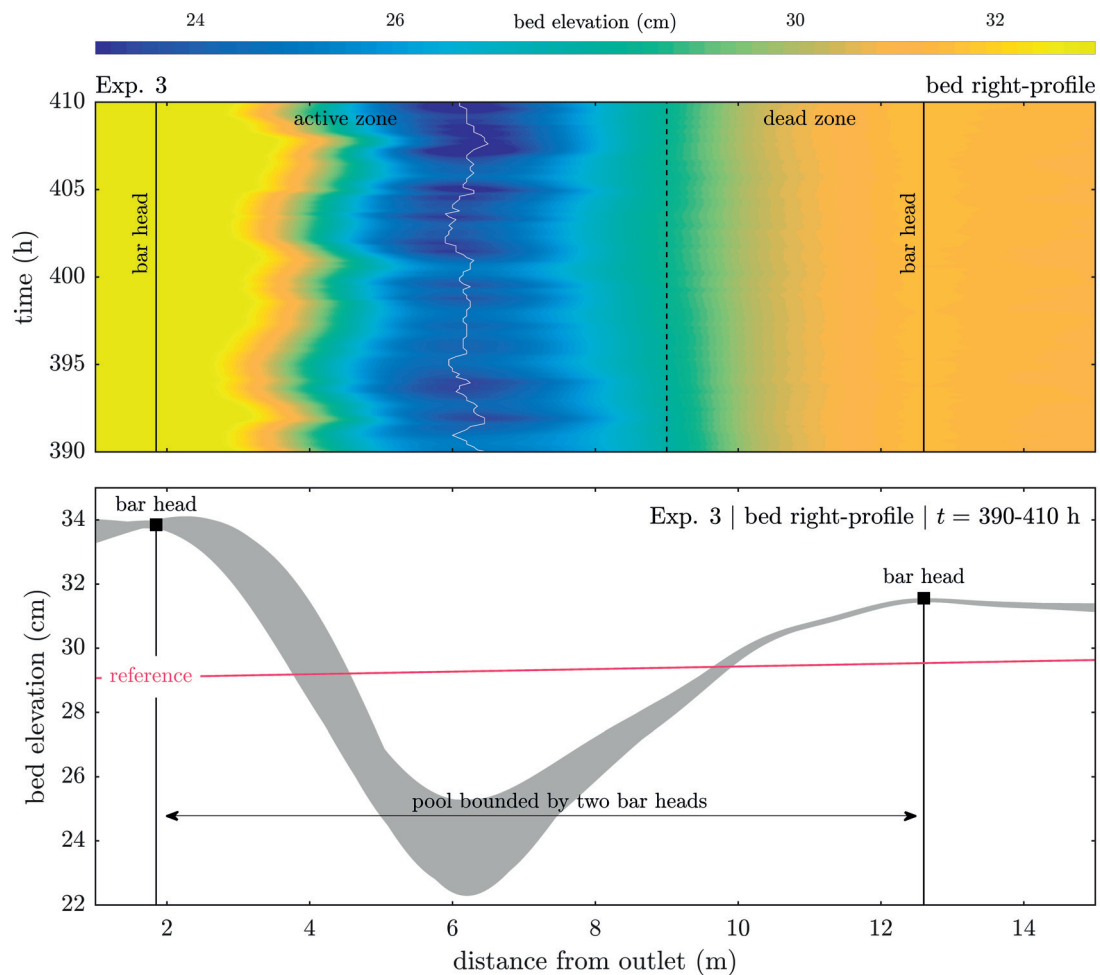
Figure 4.18: Example of a pool bounded by two bar heads, on the right side of the bed, during experiment 3. In the top part, the temporal evolution of the bed profile is presented. In the bottom part, a side view of the bed profile, representing the envelope of the bed elevation fluctuations, is plotted.

4.6.1.2 Pools with one open boundary

The pool described in figure 4.18 is bounded by two bar heads which is the typical configuration in the central part of the flume. However, near the flume inlet and outlet, the pools are open toward respectively the upstream and downstream directions. An example is given in figure 4.19. Note that the two pools shown in this example are located along the left profile, during the same time period when the pool in figure 4.18 is observed along the right profile.

In figure 4.19, the pool located in the upstream part of the flume is not bounded upstream by a bar head. In that case, the stream flow enters longitudinally into the pool at its beginning. As a consequence, there is no dead zone and the entire flume length is active. The pool undergoes the same succession of degradation and aggradation phases as the one described above. In figure 4.19 (top), the lower part of the pool appears to migrate successively in the
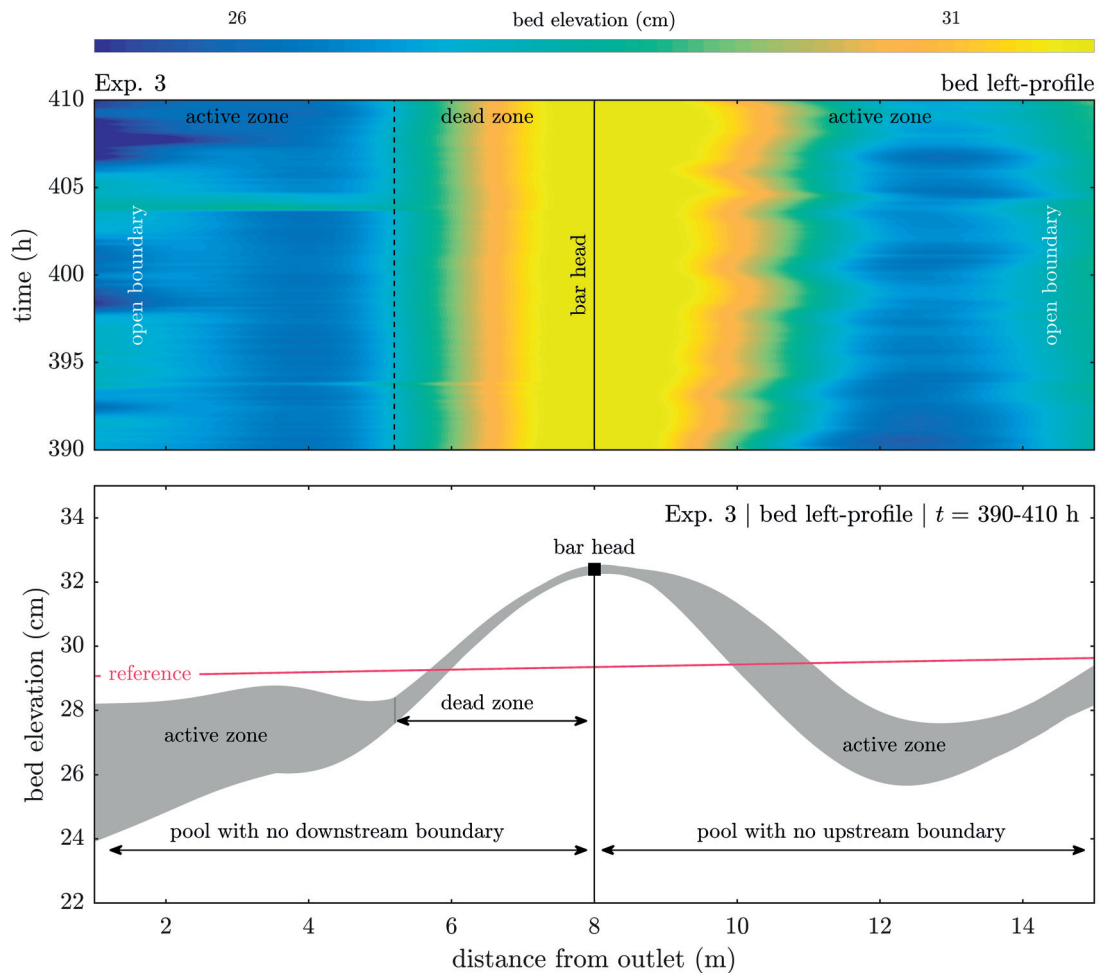
Figure 4.19: Example of pools open in the downstream or upstream direction, on the left side of the bed, during experiment 3. In the top part, the temporal evolution of the bed profile is presented. In the bottom part, a side view of the bed profile, representing the envelope of the bed elevation fluctuations, is plotted.

downstream and in the upstream direction. This periodic change in geometry suggests a wave-like sediment transfer in the pool.

The pool located near the flume outlet in figure 4.19 is not bounded downstream by a bar head. In that case, the pool characteristics are similar to the ones described for the typical configuration (see figure 4.18) with a dead zone and an active zone. The difference is that the sediment mobilized during the pool degradation phases is evacuated toward the flume outlet.

4.6.2 Sediment transfer in pools

The active zone in the pools undergoes successive phases of degradation and aggradation, as described in section 4.6.1. This fluctuating behavior of the bed elevation indicates that sediment volumes are transferred through the pools. In this section, the process of sediment transfer is investigated for the different pool configurations mentioned in section 4.6.1 (i.e., with open boundaries or not).

4.6.2.1 Pools bounded by two bar heads

In pools bounded by two bar heads, the degradation and aggradation phases modify their geometry as illustrated in figure 4.18. Pool degradation leads to an *empty configuration* and pool aggradation to a *filled configuration*. The evolution of the pool geometry during an aggradation-degradation cycle is described in figure 4.21 using an example from experiment 3.
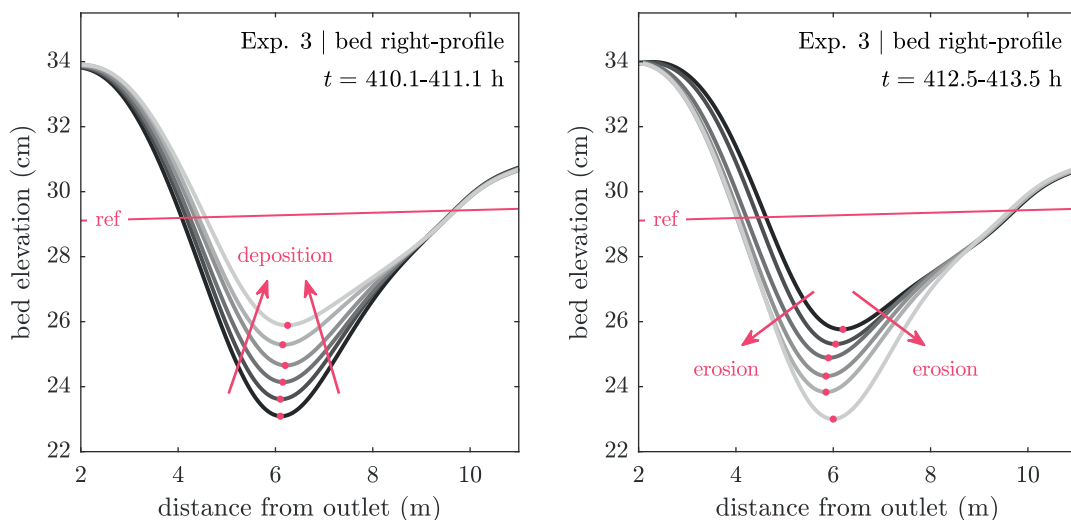
Figure 4.20: Illustration of the aggradation-degradation cycles in pools with closed boundaries using an example from experiment 3. The initial topography is plotted is black and the subsequent states are plotted in lighter shades of grey.

The aggradation phase is illustrated in figure 4.21(left). As sediment is deposited in the pool, the whole active length is aggraded. During this process, the pool bottom slightly moves in the upstream direction. However, the height and the position of the bounding bar heads remain the same. At the end of the aggradation phase, the pool has a *filled configuration*: it is shorter and shallower than in the original configuration. Moreover, the bed slope in the downstream part of the pool (between the pool bottom and the downstream bar head) is milder.

During the degradation phase, which is illustrated in figure 4.21(right), the pool is eroded and the sediment mobilized is evacuated further downstream. As the pool returns to its original geometry, the pool bottom moves first in the downstream direction before shifting upstream, toward its original location. This asymmetry indicates that the downstream part of the pool is eroded before the upstream part. As a consequence, when the sediment mobilized in the upstream part is evacuated from the pool, the bed slope in the downstream part has already returned to its steep configuration.

4.6.2.2 Pools with no upstream boundary

When the pools are not bounded upstream, sediment volumes can enter longitudinally into them, as discussed in section 4.6.1. As a consequence, the cycles of aggradation-degradation observed (see figure 4.19) seem related to a wave-like sediment transfer. The typical motion of such a sediment wave is illustrated in figure 4.21 using an example from experiment 3.
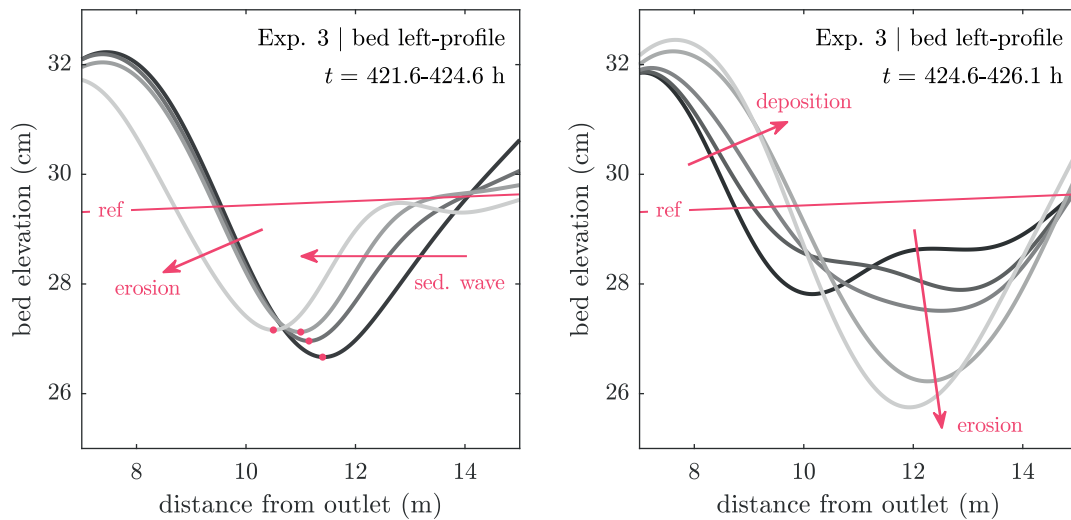
Figure 4.21: Illustration of the wave-like sediment transfer in pools with an open upstream boundary using an example from experiment 3. The initial topography is plotted is black and the subsequent states are plotted in lighter shades of grey.

The propagation of a sediment wave that progressively fills the pool is illustrated in figure 4.21(left). Once the pool is approximately half-filled, the downstream part of the pool is eroded and the corresponding bed slope is lowered. Moreover, the bar head moves slightly in

the downstream direction.

Then, as described in figure 4.21(right), the sediment wave travels through the pool and gets deposited in its downstream part. As a consequence, the downstream part of the pool is aggraded and returns to a steep configuration. During this process, the pool bottom gets first filled before being highly eroded.

Therefore, the wave does not travel through the entire pool. When it enters the pool, it modifies the pool geometry which certainly changes the hydraulic conditions. This change induces the erosion of the downstream part of the pool, which mobilizes sediment that is transported further downstream. The sediment transported in the wave is subsequently, in a large part, deposited in the pool. In this way, the latter returns to its initial geometry.

4.6.2.3 Pools with no downstream boundary

The pools located in the downstream part of the flume are "open" toward the flume outlet, as illustrated in (see figure 4.19). The aggradation-degradation cycles observed correspond to the deposition and erosion of sediment, in the same way as the case where the pools are bounded by two bar heads. However, the amount of sediment that can be accumulated locally is in general lower since there is no downstream boundary. As a consequence, the aggradation-degradation cycles are usually of lower amplitude. An aggradation-degradation cycle in the case of an important sediment arrival is described in figure 4.22 using an example from experiment 3.
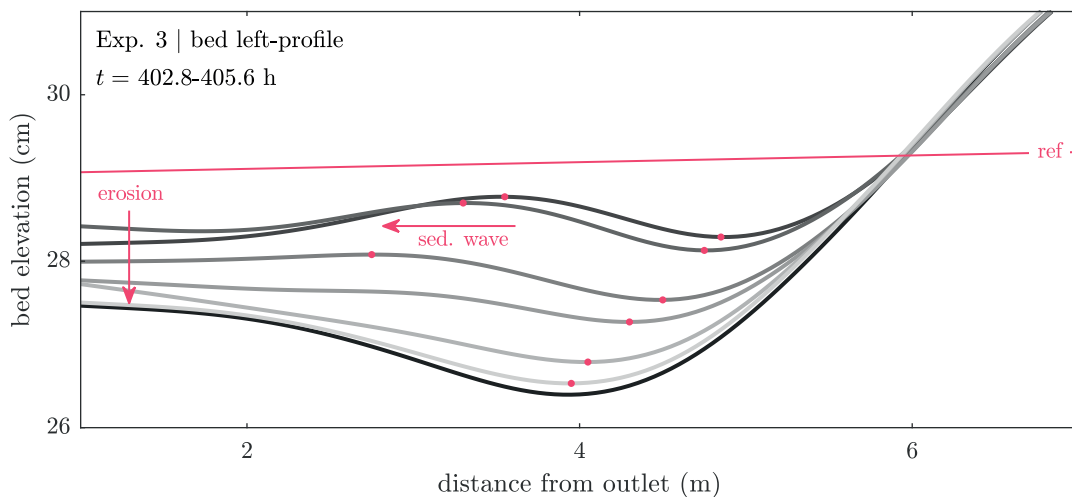
Figure 4.22: Illustration of the aggradation-degradation cycles in pools with an open downstream boundary using an example from experiment 3. The initial topography is plotted is black and the subsequent states are plotted in lighter shades of grey.

As shown in figure 4.22, the arrival of sediment into the pool induces the aggradation of the bed over the entire active length. Moreover, sediment is accumulated close to where they

entered the pool, forming a protrusion. When the pool is eroded, the protrusion migrates in the downstream direction, forming a sediment wave that flattens as it travels. At the end of the cycle, the pool has returned to its original shape.

4.6.3 Additional comments

The transfer of sediment in the pools, which are part of the system of alternate bars present in the bed, has been described above for the different configurations encountered using three characteristic examples. Since the observations made during the experiments are consistent with the processes discussed, the examples chosen are therefore considered as representative of the sediment transfer processes occurring in the pools when the bar configuration is stable.

The deposition and the erosion of sediment in the pools during the aggradation-degradation cycles is, in general, not uniform in space and time. As a consequence, the transfer of sediment has often a wave-like behavior, which is consistent with the observations made during the experiments. Indeed, we observed that sediment waves propagate in the pools and where they usually end up getting deposited. The change in geometry induced can trigger the erosion of the pools and the departure of other sediment waves. These observations lead us to consider that the different configurations the pools can take, with different depths and slopes, play a role in their transport capacity.

4.7 Discussion

4.7.1 Episodic bar migration

The bed topography in our experiments is characterized by single-row alternate bars that can episodically migrate in the downstream direction. This relative stationarity is due to stable bar heads, made of coarse material and in flush with the water surface, which resist to erosion and deflect the flow toward the adjacent pools as described in Lisle et al. (1993) and Lanzoni (2000b). When bars migrate avalanching on their downstream faces (Griffiths, 1979), they are submerged and bedload transport is observed across their surface in agreement with Lisle et al. (1991) and Ashmore (1991). Bar migration seems triggered by disturbances in the upstream boundary condition (e.g., sediment build-ups) and to occur as a chain reaction where each bar "pushes" in turn the next bar in the downstream direction. This concept of chain reaction contrasts with the regular trains of alternate bars sometimes reported (Lanzoni, 2000b) and supports the hypothesis of Crosato et al. (2012) that bar failure takes place as a domino effect.

Single-row alternate bars are often viewed as the beginning of the meandering process which was interrupted because of the width constraint (Jaeggi, 1984; Chang, 1985). The characteristics of their geometry have been largely documented (Ikeda, 1984), and the bar observed in this study verify the major scaling relations reported (e.g., in Ikeda, 1984; Yalin, 1992): their height and wavelength scale respectively with the flow depth and several flume widths (Lanzoni, 2000b). However, only two to three bars were observed in the flume which is not enough

(Ikeda, 1984) to compare in detail their geometry with theoretical predictions (the flume is too short and the bar development is certainly affected by the boundary conditions). Note that the issue of the formation and development such bedforms, which can be considered as fairly settled (Lanzoni, 2000a; Seminara, 2010), is beyond the scope of this study. In summary, the above considerations allow us to consider that the alternate bars observed are similar to the ones described in the comparable studies cited previously. In the following, we focus on the role they play in the transfer of sediment in the bed which is still an open issue in many regards (Church and Ferguson, 2015).

The migration of alternate bars necessarily induces bedload pulses, in the sense of large transport rate fluctuations, because of the important sediment volumes carried during this process (Gomez et al., 1989; Miwa and Daido, 1995). However, in this study, bar migration occurs infrequently and therefore only involves a limited portion of the total sediment volume transferred in the bed during the experiments. In other words, bar migration is not the primary means of sediment transport. Indeed, we observed that the latter takes place mainly in the pools which undergo successive aggradation-degradation cycles denoting an intense bedload transport activity. This observation raises the issue of bedload transport in stationary alternate bar systems which is still only partially understood although many studies investigated the effect of such bedforms on sediment transport capacity, for instance through their effect on form roughness (Francalanci et al., 2012). The approach employed here to address this problem is essentially qualitative and aims at identifying the physical processes involved.

4.7.2 Sediment waves

In the context of our experimental conditions, we identified sediment waves which travel from pool to pool in the downstream direction, inducing the aggradation-degradation cycles mentioned above. The term sediment wave is used here in a generic way in reference to a common process by which sediment is transported in alluvial rivers, i.e., as "sediment translation waves" producing variations in bed elevation and bed storage (Meade, 1985; Griffiths, 1993). However, note that many different phenomena, more or less related to each other, have been described as sediment waves (James, 2010), sometimes using a close terminology such as bedload sheets (Recking et al., 2009), bed waves (Hoey, 1992), and sediment slugs (Nicholas et al., 1995).

In braided channels, which is a morphology related to alternate bars, sediment waves have been reported (Griffiths, 1979; Ashmore, 1987; Hoey, 1992) as groups of migratory bars becoming increasingly diffuse as they move downstream and playing a predominant role in the morphodynamics of such systems (Ashmore, 1991). In the context of quasi-stationary alternate bars, the sediment waves we observed behave in a relatively different way because of the width constraint and the stable nature of bar heads. Although they possibly participate in destabilizing the bars, they appear to be essentially the primary means of sediment transfer in the downstream direction. This transfer occurs by discrete steps, a characteristic also reported by Ashmore (1991), as sediment volumes are transferred from one pool to the other. This

step-like motion of sediment waves reflects the bursty nature of bedload transport and its variability in space and time discussed in Chapter 3. Note that the migration process described above can be seen as a particular case of the bedload sheet dynamics (i.e., the migration of low relief bedforms) reported in Recking et al. (2009), in which sediment waves are successively "trapped" in the pools as they migrate downstream.

As a sediment wave travels through a pool, the geometry of latter (in terms of depth, length and local slope) changes which modifies the hydraulic conditions (these changes lead us to define a *filled* and an *empty* pool configuration in section 4.6.2). In return, the transport capacity of the pool also changes. This feed back loop is believed to drive the wave migration, resulting in a scour-and-fill process (Lanzoni, 2000b). As a consequence, it is not necessarily the "same" sediment that is transferred from pool to pool, as pointed in Ashmore (1991). Indeed, the arrival of sediment in a pool can mobilize "other" sediment (because of changes in hydraulic conditions) which is then transported further downstream as the primer remains "trapped" in the pool. However, in order to better describe and quantify these processes, further analyses are required.

4.7.3   Additional comments

Behind the idea of sediment waves moving from pool to pool, stands the concept of storage zones than can be filled and emptied, (Meade, 1985; Kelsey et al., 1987; Macklin and Lewin, 1989; Ashmore, 1991). In the context of this study, these sediment reservoirs are stationary which lead us to see the system of alternate bars as made of two distinct entities having different roles: the bars which are stabilizing elements and the pools which ensure the transfer of sediment in order to maintain a certain mass-balance equilibrium in the system.

In summary, the results commented above characterize the alternate bars observed in the bed and their relation with bedload transport. More specifically, we describe qualitatively how sediment is transferred in the bed through sediment waves migrating in pools which, to our knowledge, has not been done earlier. In the next chapter we quantify the effect of the bedform dynamics described above on the bedload pulses discussed in the previous chapter.

5 Alternate bars and bedload pulses

The alternate bars observed in the bed consist of a bar-and-pool system that evolves over time. As discussed in the previous chapter, the bars and the pools can be seen as two separate entities having different dynamics. Indeed, we have demonstrated that the bars are stable structures that migrate intermittently whereas the pools ensure the regular transfer of sediment in the bed through successive aggradation-degradation cycles.

In this chapter, we first discuss and quantify the effect of these two migrating bedforms on the bedload pulses measured at the flume outlet. We then investigate the sediment transport continuity in the flume in relation with the migration of sediment waves from pool to pool. Finally, we comment on the mechanisms which trigger bedload pulses in the system before discussing our results.

The analyses performed in the following are based on the comparison between the topographical measurements and the bedload transport rate (BTR) time series. For consistency purposes, the BTRs are averaged over the time intervals between the scans, which are about 10 min. They thus represent the average BTR between each topographical measurement, and are referred to as $Q_{s,10}$ hereafter.

5.1 Bar migration

When bars migrate, which occurs intermittently in the bed (see section 4.5), large amounts of sediment are transported in the downstream direction. Near the flume outlet, the sediment mobilized during this process is evacuated from the flume which induces peaks in the recorded BTR time series. In this section, we investigate these bedload pulses generated by bar migration (referred to as bar-generated pulses) in the downstream part of the flume and we quantify their overall contribution to the transfer of sediment in the bed.

5.1.1 Bar migration near the flume outlet

As discussed in section 4.4.2, the flume outlet is most of the time obstructed on one side by a bar. When the bar migrates, it is destructed and a new bar appears on the other side of the flume resulting in bar inversion. This process is illustrated for each experiment in figure 5.1

which shows the temporal evolution of the right and the left bed profiles near the flume outlet (i.e., 1–1.5 m away). In order to visualize the effect of bar inversion on bedload transport, the $Q_{s,10}$ time series are also plotted.

The truncated right and left profiles of the bed in figure 5.1 represent the elevation on both sides of the bed near the flume outlet. It appears clearly that when the bed elevation is high on one side, which reflects the presence of a bar, it is low on the other side (which inversely reflects the presence of a pool). When the bar changes side, it signals bar inversion near the flume outlet.

In some cases, for instance in experiment 1 (50–100 h), no bar appears in any of the bed profiles although we identified one in the complete topographical data (which are not presented here for conciseness purposes). In such situations, the bar is located on the side that shows low temporal variability in bed elevation compared to the other side.

The bar inversions during each experiment, as reported in figure 5.1, were identified based on the complete topographical data. They were respectively observed 5, 3 and 9 times in experiment 1, 2 and 3. The number of times bar inversion occurs is therefore low compared to the experiment durations, which confirms that bars are stable structures that migrate intermittently (see section 4.5). Moreover, bar inversions indicated in figure 5.1 are always associated with prominent bedload pulses in the $Q_{s,10}$ time series. Because of the nature of these two phenomena and of their proximity in space and time, we can conclude that bar destruction in the downstream part of the bed induces bedload pulses.

5.1.2 Bedload pulses originating from bar destruction

Bar destruction near the flume outlet, which results in bar inversion, generates bedload pulses as discussed in section 5.1.1. An example of this process during experiment 3 is given in figure 5.2 which shows the temporal evolution of the bed elevation on both sides of the flume along with the corresponding $Q_{s,10}$ time series.

At the beginning, a bar is located on the right side of the bed. It is about 10 cm higher than the pool located on the left side. Note that the bar elevation varies little over time compared to the pool elevation. At approximately 500 h, the bar on the right side is eroded which generates a bedload pulse. After the pulse, a new bar appears on the left side: the bar configuration at the flume outlet is inverted.

Examining the topographical data, we also observed that some major pulses are generated by partial bar erosion without bar inversion. Such bedload pulses were observed one time in experiment 2 and five times in experiment 3. We summarize the occurrence of bar-generated pulses in figure 5.3 which gives an overview of the BTR fluctuations due to bar dynamics.
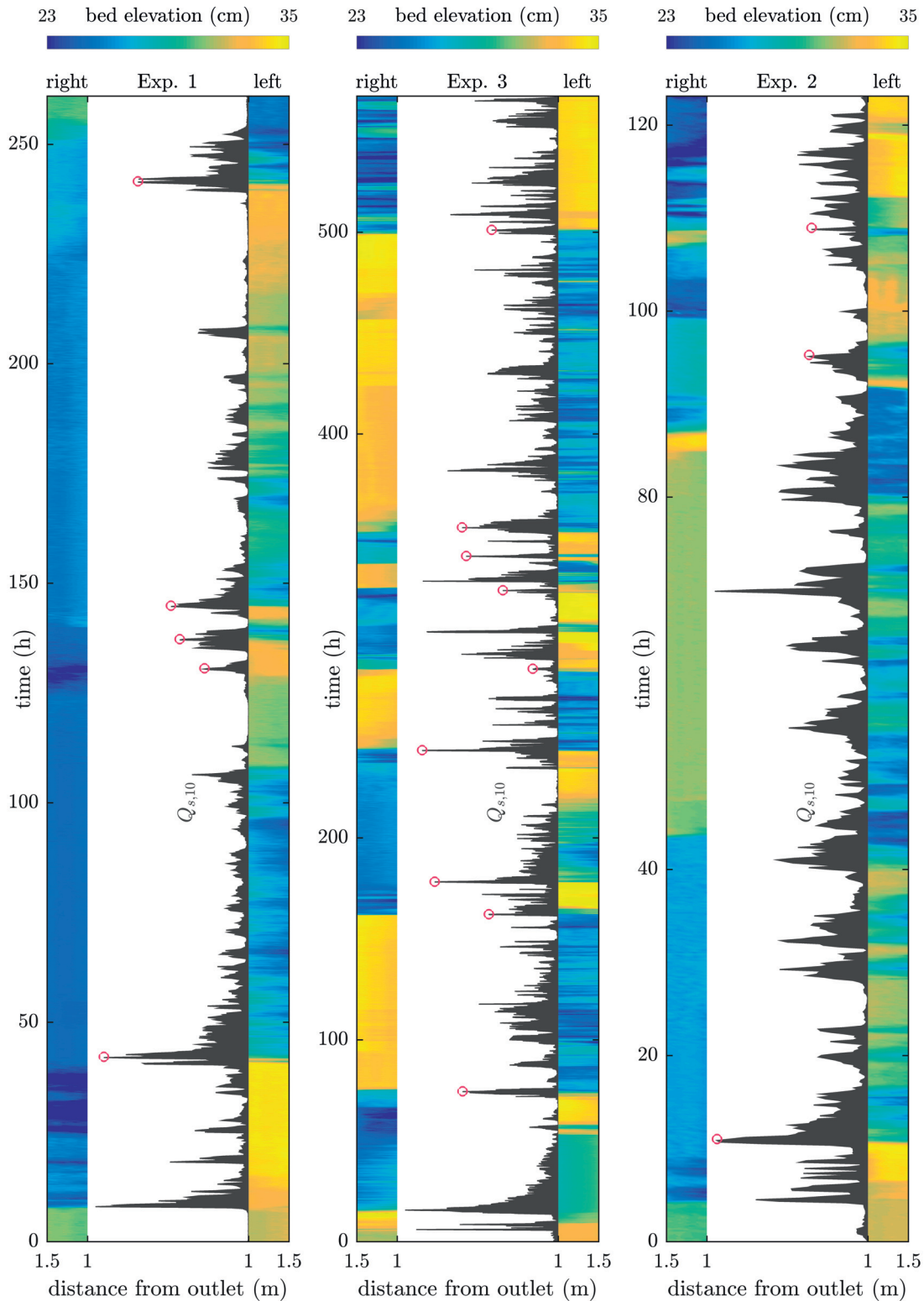
Figure 5.1: Temporal evolution of the right and left profiles of the bed near the flume outlet during experiment 1, 2 and 3. The bedload transport rates $Q_{s,10}$ are plotted in dark grey on an arbitrary scale, and empty circles indicate when bar inversions occur.
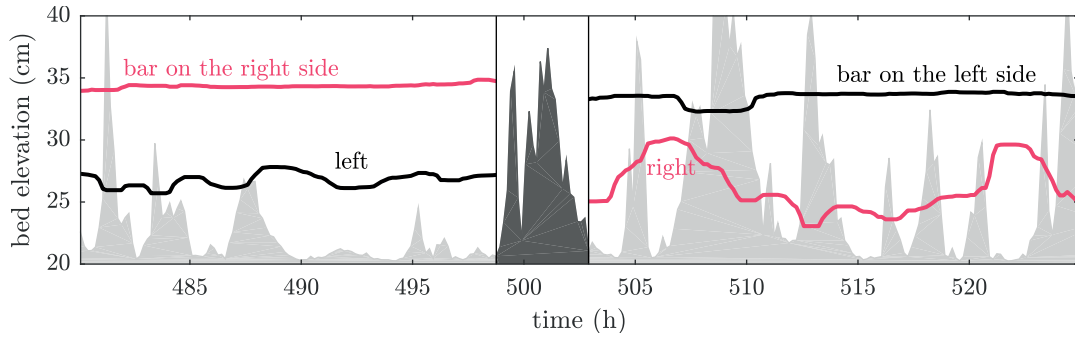
Figure 5.2: Example of bar inversion near the flume outlet generating a bedload pulse during experiment 3. The two curves represent the bed elevation on the right side ($x = 1$ m, $y = 5$ cm) and on the left side ($x = 1$ m, $y = 55$ cm) of the bed. The filled area plot represents the bedload transport rates on an arbitrary scale, and the bar-generated pulse is highlighted in dark grey.

The bar-generated pulses plotted in figure 5.3 seem randomly distributed over time: they can be spaced from few hours to about 100 hours (note that, in comparison, their duration is in the order of few hours). Therefore, bar migration near the flume outlet appears to be a non-periodic process.

It also appears in figure 5.3 that bar-generated pulses can be of different magnitudes. In the following, we define a bedload pulse as any consecutive set of $Q_{s,10}$ values above the average value $\bar{Q}_{s,10}$, and of which the maximum value is above a given threshold (the same approach was used in section 3.2). Three thresholds are here considered: $2 \times \bar{Q}_{s,10}$, $4 \times \bar{Q}_{s,10}$ and $6 \times \bar{Q}_{s,10}$.

In order to assess the significance of bar destruction in the generation of bedload pulses, two ratios are computed: the proportion of bedload pulses due to bar destruction (occurrence ratio) and the proportion of sediment mass transported during bedload pulses due to bar-generated pulses (transported mass ratio). The results are given in table 5.1 for the three threshold values mentioned above.

Table 5.1: Relative significance of bar destruction in the generation of bedload pulses larger than given threshold values during experiment 1, 2 and 3.

	threshold	Exp. 1	Exp. 3	Exp. 2
sediment feed rate		2.5 g/s	5.0 g/s	7.5 g/s
occurrence ratio	$2 \times \bar{Q}_{s,10}$	0.19	0.18	0.12
transported mass ratio	$2 \times \bar{Q}_{s,10}$	0.52	0.36	0.12
occurrence ratio	$4 \times \bar{Q}_{s,10}$	0.45	0.35	0.50
transported mass ratio	$4 \times \bar{Q}_{s,10}$	0.62	0.49	0.41
occurrence ratio	$6 \times \bar{Q}_{s,10}$	0.75	0.57	0.50
transported mass ratio	$6 \times \bar{Q}_{s,10}$	0.75	0.60	0.41
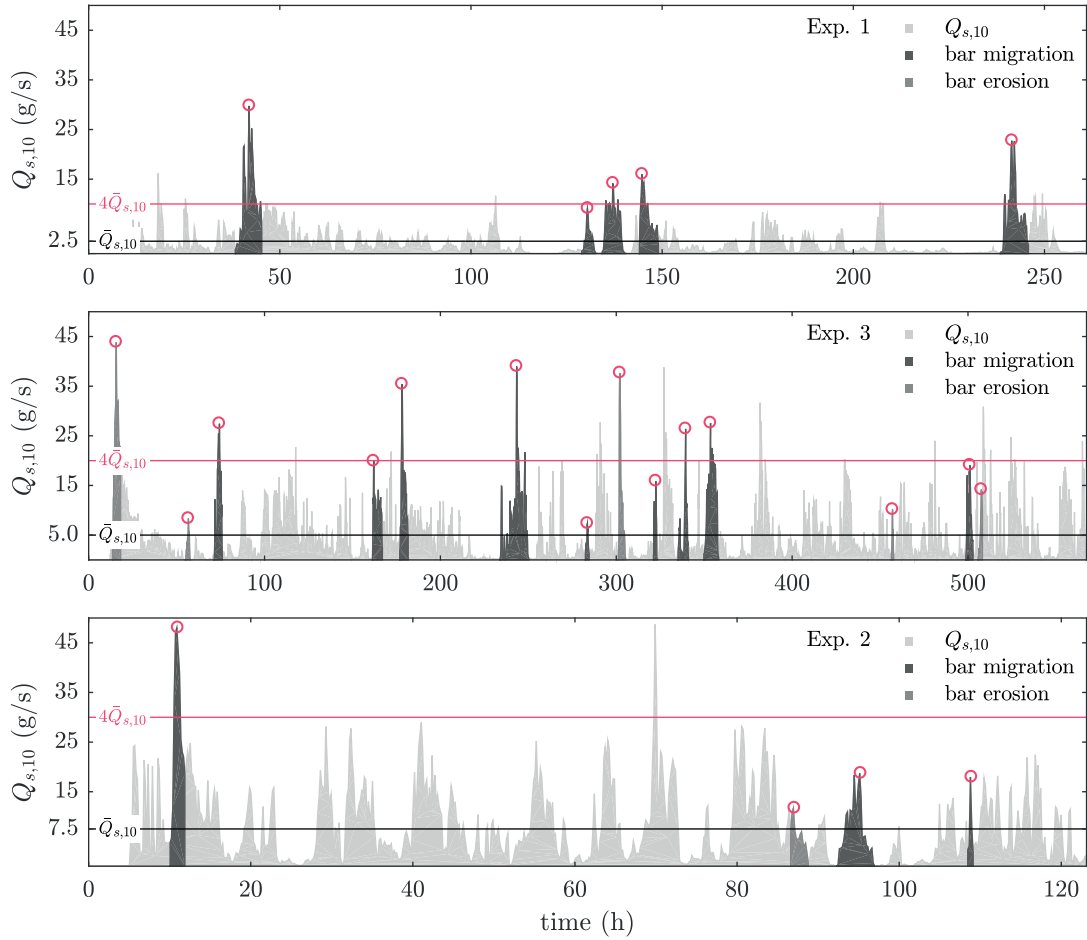
Figure 5.3: Bar-generated pulses during experiment 1, 2 and 3. The time series of the bedload transport rates are plotted in light grey, and the bar-generated pulses are highlighted in dark grey and marked with an empty circle. The pulses related to bar migration and bar erosion are differentiated using two different shades of dark grey.

The results given in table 5.1 indicate that bar-generated pulses are more frequent in experiments with lower sediment feed rates. For instance, in experiment 1 ($Q_{s,in} = 2.5$ g/s), 75% of the largest pulses and of the sediment mass they transport are due to bar destruction. Comparatively, these ratios are less than 50% in experiment 2 ($Q_{s,in} = 7.5$ g/s).

It also appears that bar-generated pulses become dominant when only the largest pulses are considered: the occurrence ratio is about three times larger when the threshold value is $6 \times \bar{Q}_{s,10}$ than when it is $2 \times \bar{Q}_{s,10}$. For instance, in experiment 3, it increases from 18% to 57%. More generally, the occurrence ratio for bedload pulses larger than $6 \times \bar{Q}_{s,10}$ is above 50% in all three experiments.

It is also interesting to note that the occurrence ratio tends to be lower than the mass ratio. This difference means that bar-generated pulses tend to transport more sediment than the other pulses.

5.1.3 Additional comments

The results presented in section 5.1.1 and section 5.1.2 point the importance of bar migration and partial erosion near the flume outlet in the generation of bedload pulses. Although they occur infrequently, they are responsible for at least 50% of the pulses larger than 6 times the mean BTR. If lower bedload pulses are considered, for instance the ones larger than 2 times the mean BTR, bar-generated pulses still represent 10–20% of them which is significant.

In addition it appears that bar migration/erosion, which generally involves large sediment volumes, contributes to a large extent to bedload transport during important bedload pulses (at least 40% of the total mass evacuated at the flume outlet for pulses larger than 4 times the mean BTR). However, if considering all significant transport events (pulses larger than 2 times the mean BTR), bar-generated pulses represent less than 50% of the mass evacuated. Bar migration is therefore not the primary means of bedload transport as commented in section 4.7.

Finally, the relative significance of bar-generated pulses increases with decreasing sediment feed rate. Indeed, bedload transport seems governed by bar dynamics in experiment 1 where it is responsible for most of the mass transported. In contrast, in experiment 2 (of which sediment feed rate is 3 times larger), this ratio remains under 40%.

5.2 Aggradation-degradation cycles in pools

The pools in the bed are characterized by continuous aggradation-degradation cycles, related to the migration of sediment waves, as discussed in section 4.6. In the pools near the flume outlet, these sediment waves generate fluctuations in the recorded BTRs. In this section, we investigate such pool-generated pulses in the downstream part of the flume.

5.2.1 Bedload pulses originating from sediment wave migration

Bar-generated pulses occur intermittently as discussed in section 5.1.2. In order to investigate pool-generated pulses, we therefore consider only the parts of the experiments during which no bar migration is observed. In the following, one representative long sample of each experiment, where the bedload pulses observed are independent from bar migration, is studied. We first focus on experiment 3 and then we extend our conclusions to experiment 1 and 2.

5.2.1.1 Pool-generated pulses in experiment 3

We consider hereafter the portion of experiment 3 between 370–490 h, which is the largest sample (120 h) during which no bar migration is observed (see figure 5.3). The temporal evolution of the bed elevation near the flume outlet, on both sides, is plotted for the whole sample in figure 5.4. The corresponding $Q_{s,10}$ time series is also represented for comparison purposes.
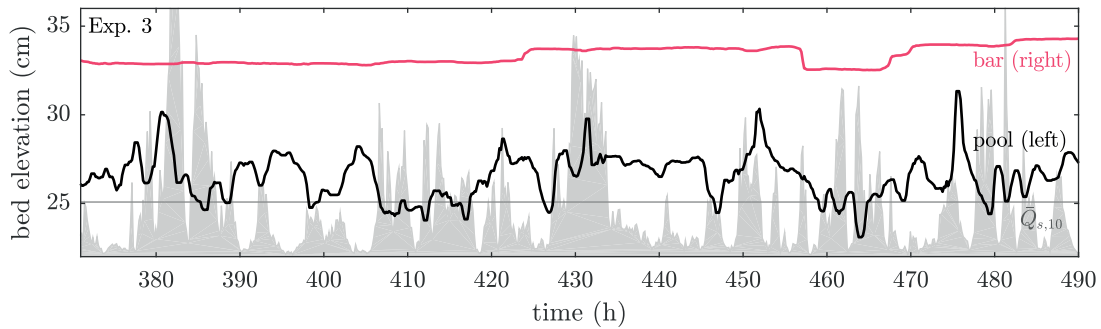
Figure 5.4: Temporal evolution of the bed elevation on the right side ($x = 1$ m, $y = 5$ cm) and the left side ($x = 1$ m, $y = 55$ cm) of the flume outlet during a sample of experiment 3 with no bar migration. The filled area plot represents the bedload transport rates $Q_{s,10}$ on an arbitrary scale.

The bed elevation on the right side is about 10 cm higher than on the other side and remains remarkably constant over time: it reflects the obstruction of the flume outlet on the right by a static bar. Inversely, a pool is located on the left side where the bed elevation fluctuates over time. These variations are related to aggradation-degradation cycles resulting from the migration of sediment waves in the pool (see section 4.6).

The bedload pulses observed in figure 5.4 are necessarily pool-generated since the bar is static. Moreover, the bed elevation fluctuations in the pool seems related to the BTR fluctuations: the pool tends to be degraded when pulses occur. In order to better examine this correlation, a 10 h sub-sample is presented in figure 5.5.
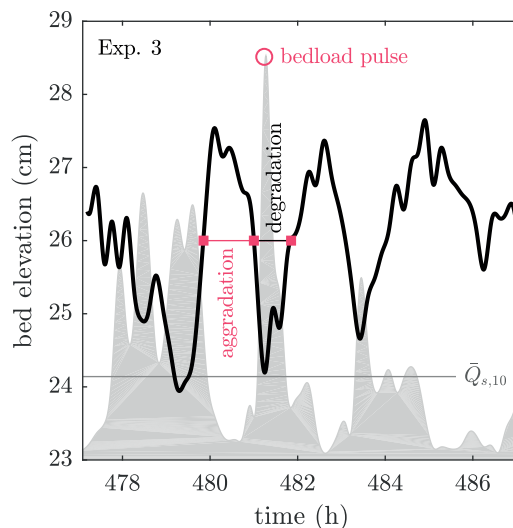
Figure 5.5: Example of bedload pulses originating from aggradation-degradation cycles in the pool near the flume outlet. The black curve represents the bed elevation in the pool and the bedload transport rates $Q_{s,10}$ are plotted in grey on an arbitrary scale.

97

The bedload pulses appearing in figure 5.5 are inversely correlated to the changes in bed elevation. When the pool is aggraded, because of sediment deposition, the BTRs are much lower than their mean value. Conversely, when the pool is degraded because of sediment erosion, a bedload pulse is observed. This example illustrates how aggradation-degradation cycles in pools, related to sediment wave migration, generate bedload pulses.

The cross-correlation coefficient between the bed elevation in the pool and $Q_{s,10}$ is 0.73 in the sub-sample (10 h) which indicates a strong dependency of the two time series on each other. Moreover, the cross-correlation is maximum for a zero time lag: the bedload pulses and the degradation phases are therefore not shifted by more than 10 min (which is the measurement resolution).

Considering the whole sample (120 h), the cross-correlation coefficient is 0.68 which is close from the one of the sub-sample. As a consequence, we conclude that bedload pulses occurring when bars are static are to a large extent due to sediment wave migration in the pools which confirms our conclusions in section 4.7.

5.2.1.2 Generalization to experiment 1 and 2

As for experiment 3, two large samples of experiment 2 and 1 during which no bar migration is observed were selected. They respectively last 75 h and 70 h and are presented in figure 5.6. These two samples have the same characteristics as discussed above: a static bar is located on the right side of the flume outlet, and a pool undergoing aggradation-degradation cycles is present on the left side. Note however that in the sample of experiment 1 the bedload pulses are of lower magnitude, and the bed elevation fluctuations are less marked, than in the samples of the other experiments. This observation is consistent with the result above that in this experiment bar-generated pulses represent most of the mass transported.

The cross-correlation coefficients between the bed elevation in the pool and $Q_{s,10}$ are respectively 0.72 and 0.64 for experiment 2 and experiment 1 which is close from the value in experiment 3 (0.68). Therefore, the conclusion in section 5.2.1.1 can be extended to these experiments: when bars are static, the sediment waves migrating in the pools generate most the BTR fluctuations observed.

5.2.2 Sediment wave migration

The results above provide evidences that sediment waves migrating in the downstream part of the bed are associated with bedload pulses. In the following, we extend the investigation to the entire flume length tracking the passage of the waves in the different pools. The analysis is performed using the same sample of experiment 3 (120 h) as in section 5.2.1.1 during which no bar migration is observed. Using this example, we demonstrate sediment transfer continuity along the bed, which is assumed by the migration of waves from pool to pool.
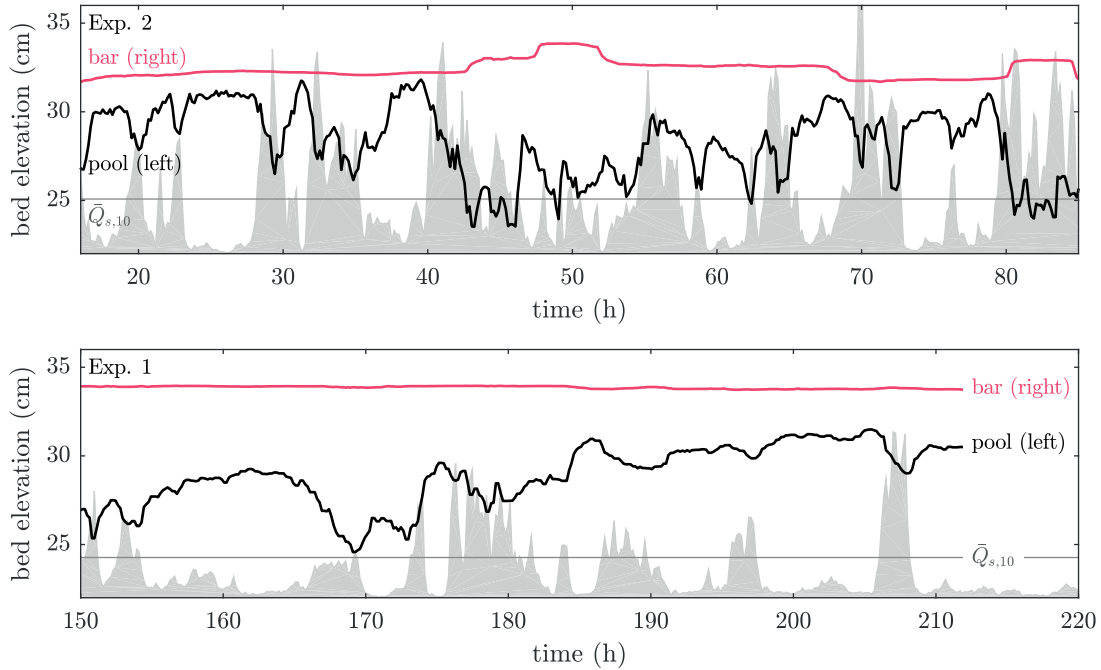
Figure 5.6: Temporal evolution of the bed elevation on the right side (bar location) and the left side (pool location) of the flume outlet during a sample of experiment 2 and 1 with no bar migration. The filled area plots represent the bedload transport rates $Q_{s,10}$ on an arbitrary scale.

In order to summarize the changes in the bed during the sample of experiment 3 considered, we compute the average erosion rate at each bed location (in the same way we did in section 4.4.1). The results in figure 5.7 indicate that, as commented in section 4.4.1.4, bed erosion occurs essentially in the three pools located on both sides of the bed. In the following, we are interested in the transfer of sediment in the form of sediment waves (see section 4.6.2) through these pools. As a consequence, we analyze the bed elevation changes in each pool at location P1, P2 and P3 as indicated in figure 5.7.

We first focus on the generation of sediment waves in the very upstream part of the bed comparing, in the upper plot in figure 5.8, the changes in bed elevation in the most upstream pool (P3, see figure 5.7) and the BTRs measured at the flume outlet. Analysing visually the time series it appears that most sudden decreases in P3 elevation, which indicate pool erosion, are followed by bedload pulses at the flume outlet. This link can be quantified computing the cross-correlation between the time series: the maximum cross-relation coefficient is 0.67 and obtained for a time lag of 70 min. In other words, the passage of bed waves in the most upstream pool is well correlated to the bedload pulses recorded at the flume end with a delay of about one hour. This result means that BTR fluctuations can result from the migration of sediment waves along the entire flume length, as illustrated in the lower plot in figure 5.8.
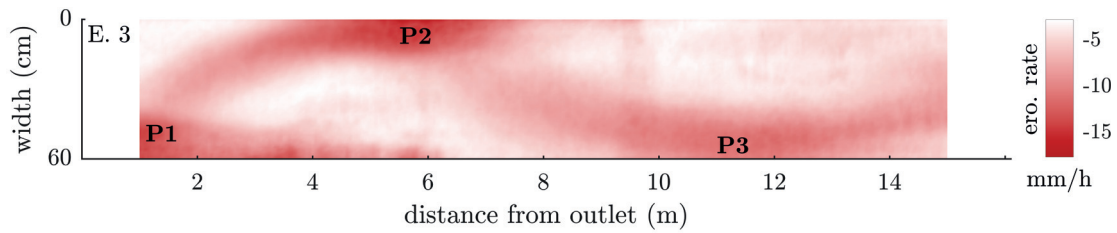
Figure 5.7: Average erosion rates in the bed during a sample of experiment 3 in which bars remain stationary. Zones of intense erosion, corresponding to the pool locations, are visible alternately on both sides of the bed. The bed elevation variations are extracted at location P1, P2 and P3, which correspond to the bottom of the pools.
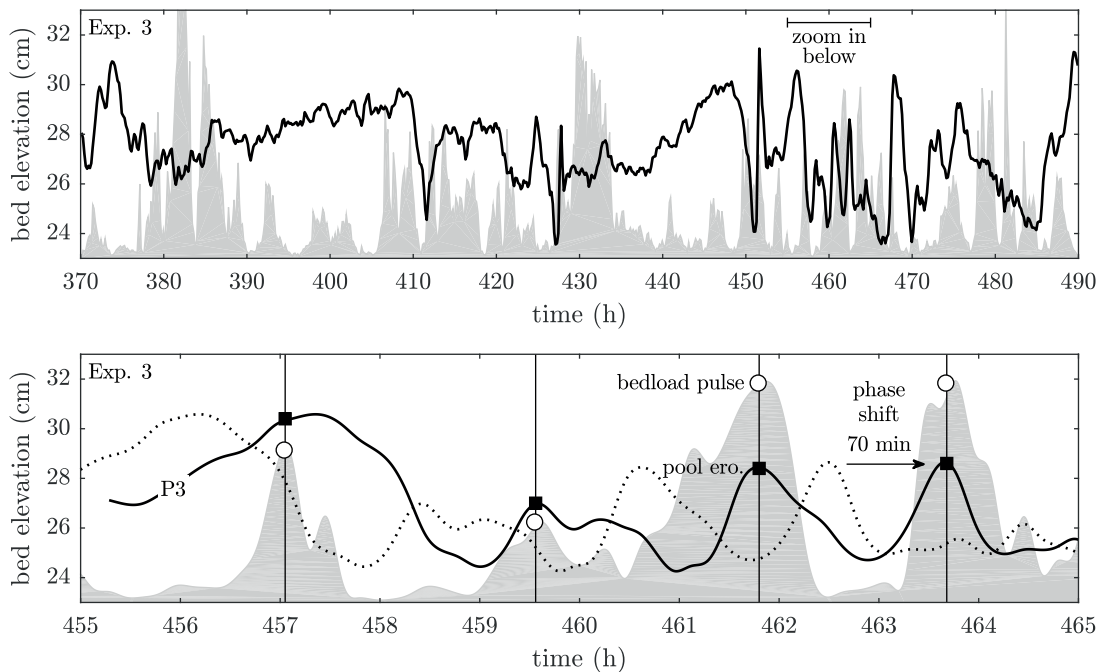
Figure 5.8: Temporal evolution of the bed elevation in the most upstream pool (P3) during a sample of experiment 3. The filled area plots represent the bedload transport rates $Q_{s,10}$ on an arbitrary scale.

As sediment waves migrate in the downstream direction, they travel through the different pools inducing changes in bed elevation (aggradation-degradation cycles) which can be tracked. An example is given in figure 5.9 where the bed elevation in P3, P1 and P2 (see figure 5.7) is plotted for the same 10-h sub-sample of experiment 3 as in figure 5.5.

During this sub-sample, the most upstream pool P3 is progressively eroded and the sediment mobilized is transferred in pool P2 where it is first stored and then released in the form of three sediment waves. These three waves appear clearly in the most downstream pool P1 from where they are ultimately evacuated generating bedload pulses. Note that this process, here
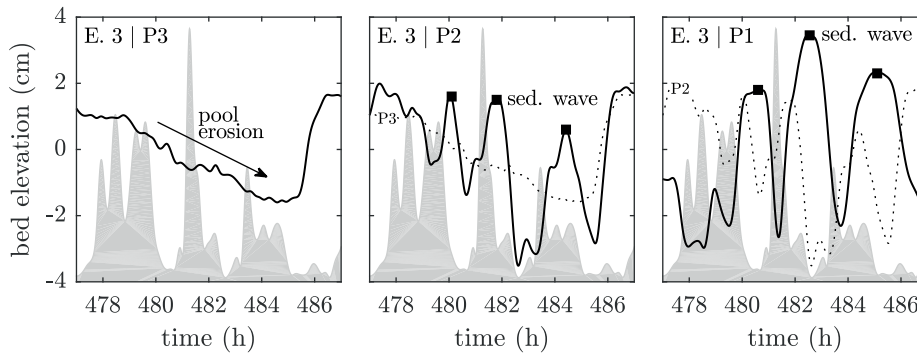
Figure 5.9: Example of sediment wave migrations from pool to pool (from P3 to P1) ultimately generating bedload pulses at the flume outlet. The black curves represent the bed elevation (with respect to its mean value in the sub-sample) in the pools, and the bedload transport rates $Q_{s,10}$ are plotted in grey on an arbitrary scale.

described using an example from experiment 3, is also observed in the other experiments and can be considered as common in the context of our experimental conditions.

The cross-correlation coefficient of the bed elevation in P1 and P2, considering the whole sample of experiment 3 (i.e., 370–490 h), is 0.99 and no phase shift is observed. This high dependency between the elevation time series means that sediment waves, of which height is in the order of few centimeters, transfer sediment along the flume length migrating from pool to pool. In addition, it seems that the upstream pool can act like a sediment reservoir which stores the sediment fed in the flume before it is transferred toward the downstream pools.

In summary, the observations made in this section support and complete our previous conclusions about sediment waves. The latter, which transfer sediment from pool to pool, are the primary means of sediment transport observed and are at the origin of the bedload pulses observed when no bar migration occur.

5.3   Bed storage capacity

5.3.1   Bed volume variations

As indicated by the results above, the bed can act like a sediment buffer storing bed material in the pools, which explains the burstiness in the BTR time series. In order to further investigate this effect, we focus hereafter on the evolution of the total bed volume during the experiments. More specifically, we are interested in the mechanisms triggering the release of large sediment amounts.

The temporal evolution of the bed volume computed from the topographical measurements is plotted for each experiment in figure 5.10, which is similar to figure 3.24 where the sediment stock was computed from the BTR measurements. For comparison purposes, the BTR time

series are also plotted highlighting the bar-generated bedload pulses as done in figure 5.3. Note that both the mass and transport rate time series were smoothed performing a moving average over 2 h in order to stress large-scale fluctuations.

As commented in section 3.6, the bed volume fluctuates over time with abrupt decreases (i.e., bed degradation phases), associated to large bedload pulses, and slower aggradation phases (see figure 5.10). This result was expected since large transport events necessarily imply an overall bed degradation. However, it appears that bed material is eroded much faster than sediment is deposited in the bed. This behavior explains why the BTRs can be larger than the sediment feed rate by several times during bedload pulses. Indeed, during bed aggradation, which is a relatively slow process controlled by the feed rate, large sediment volumes are stored. Then, at some critical point, these volumes are evacuated from the flume over relatively short time periods compared to the aggradations phases, inducing the so called bedload pulses.

The bed mass time series plotted in figure 5.10 show two fluctuation regimes: a large fluctuation regime (regime 1) observed during experiment 1 and at the beginning of experiment 3, and a limited fluctuation regime (regime 2) observed in the last part of experiment 3 and in experiment 2. Compared to regime 2, the bed aggradatation-degradation cycles in regime 1 are much slower (> 50 h) and of larger amplitudes. In addition, it appears that in regime 1 each degradation phases is associated with a large bar-generated pulse (see section 5.1.2) whereas in regime 2 pool-generated pulses (see section 5.2.1) can also mark the start of bed degradation phases.

The two fluctuation regimes commented above can also be differentiated by the bed configuration as illustrated in figure 5.11 using two examples from experiment 3: the bed is more sinuous (2 pools instead of 3) and the bars are more stretched in the longitudinal direction in regime 1 compared to regime 2. Since sediment is deposited in the pools (see section 4.4.1), these different bed configurations can explain why the aggradation phases in regime 1 are longer than in regime 2: less sediment can be "trapped" in the pools in the first case. This effect of the bed configuration is consistent with the BTR time series in figure 3.24 which indicate a significant bedload transport activity when the bed is highly degraded in regime 1.

As discussed in section 3.7, regime 1 is certainly a transitional regime resulting from the initial flat bed configuration which can be viewed as a strong external disturbance of the system. As the sediment feed rate increases, this regime is less persistent (and is apparently not even reached in experiment 2): the resilience time of the system seems to shorten when the feed rate is increased. An interesting outcome of these results is that they bring evidences the bed, under given steady feeding conditions, can take different configurations.
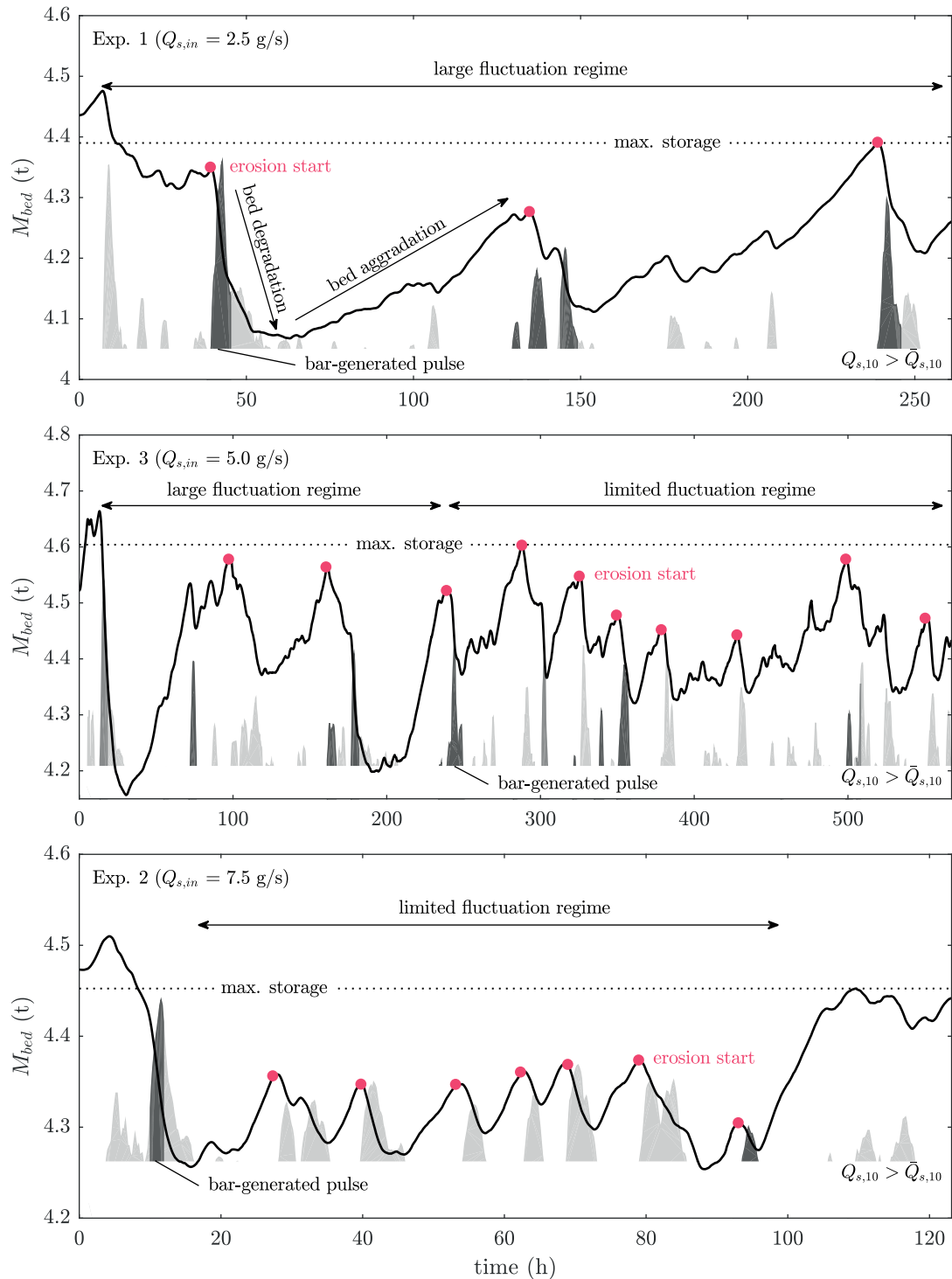
Figure 5.10: Temporal evolution of the sediment mass M_{bed} (in tonnes) stored in the bed during experiment 1, 2 and 3 (solid curve). The filled area plots represent the bedload transport rates $Q_{s,10}$ larger than their mean value $\bar{Q}_{s,10}$ on an arbitrary scale. The bedload pulses related to bar erosion and migration are differentiated using darker shades of grey, and both time series were smoothed performing a moving average over 2 h.
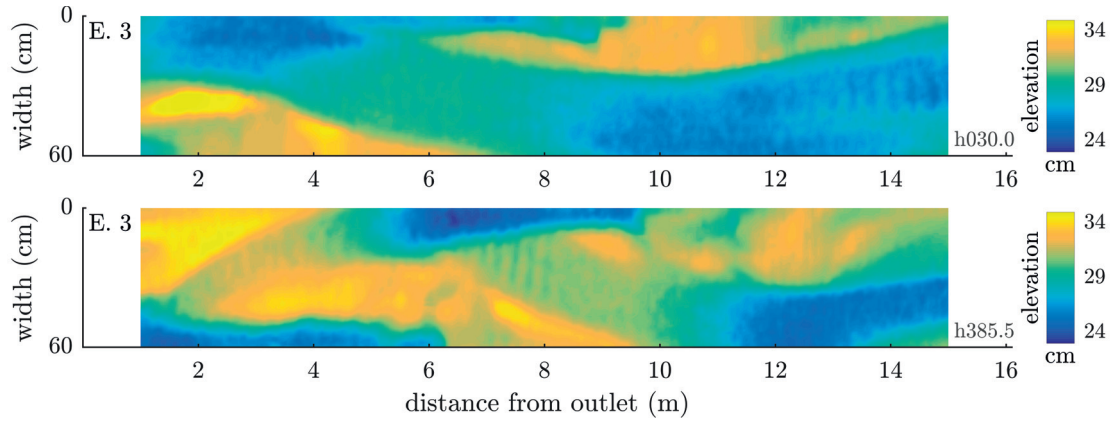
Figure 5.11: Typical bed topography in regime 1 (upper plot) characterized by long bed aggradatation-degradation cycles, and in regime 2 (lower plot) characterized by short bed aggradatation-degradation cycles.

5.3.2 Bedload pulses triggering

Considering the entire time series in figure 5.10, it appears that the bed volume fluctuations are bounded by a maximum storage capacity and that degradation phases are triggered when it is close to be reached. This observation supports the idea that the bed behaves like a sediment buffer which induces the bursty character of bedload transport (store-and-release process).

In an attempt to better describe the critical point for sediment release, we computed the dimensional shear stress for each bed scan as follow

$$\tau^\star = \frac{\rho\, h_w \sin(S_b)}{(\rho_s - \rho)\, d_{50}} \tag{5.1}$$

with h_w the water height, S_b the average bed slope, ρ_s the sediment density, ρ the water density and d_{50} the median grain diameter. However, the computation of the shear stress in alternate bar systems is not straightforward because of the high variability in space of the bed topography and hydraulic conditions (Lisle et al., 1993; Lanzoni, 2000a; Francalanci et al., 2012; Podolak and Wilcock, 2013). As a consequence, we estimated $\tau^\star$ computing its average value along the right and left bed profiles (see section 4.4.2 for definition) using the respective average slope and water height in the above equation in the same way as Venditti et al. (2012). The two values obtained were then averaged to obtain a rough estimation of $\tau^\star$ in the flume.

The time series of $\tau^\star$ plotted in figure 5.12 do not show any particular behavior when the bed degradation phases are triggered. However, they indicate that the shear stress is larger once the alternate bars are developed in the bed, and that it is larger in experiment 2 which has a larger sediment feed rate. Note that these tendencies and the $\tau^\star$ values computed are consistent the finding of several authors (Venditti et al., 2012; Podolak and Wilcock, 2013).

The shear stress computed as described above is largely affected by the changes in bed slope which explains why no specific behavior associated with bed aggradation-degradation phases arises from figure 5.12. Indeed, the bed can store sediment in different ways, for instance

– filling the dowstream pool first, which induces first a decrease in bed slope and then a raise when the uptream pools are filled;

– filling the upstream pools first, which induces first a raise in bed slope and then a decrease when the downstream pools are filled.

Similarly, the bed can be eroded first in its downstream or upstream part. An option to better estimate the bed shear stress in future complementary analyses is to implement the bed topography measurements in an hydrodynamic model as performed for instance by Nelson et al. (2010) and by Podolak and Wilcock (2013).
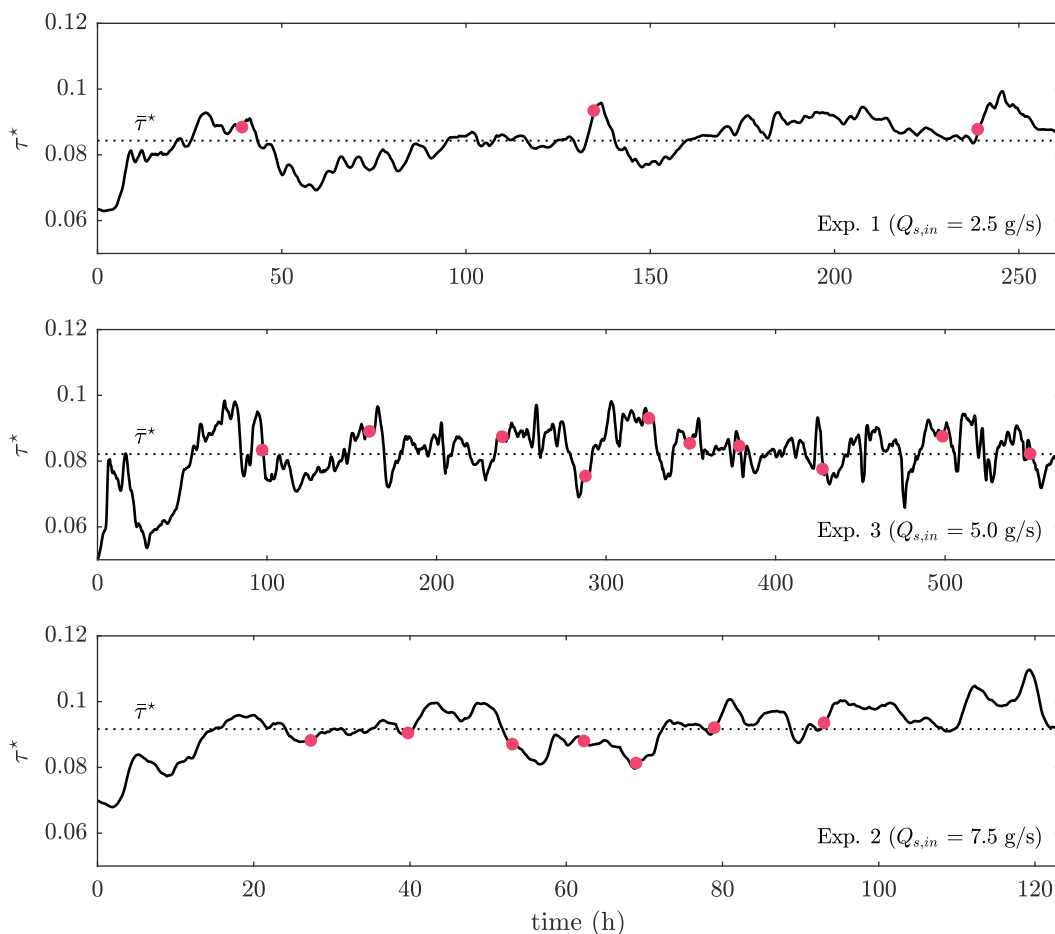
Figure 5.12: Temporal evolution of the dimensionless bed shear stress $\tau^\star$ during experiment 1, 2 and 3. The dashed lines indicate the mean values and the dots when bed aggradation phases are triggered. The time series were smoothed performing a moving average over 2 h.

5.4   Discussion

5.4.1   Bars and sediment waves

The transfer of sediment in the bed, of which topography is typical of bar-and-pool configurations, is ensured at the macro-scale by two main physical processes identified in Chapter 4: episodic bar migrations and sediment waves. We clarify that, despite their sporadic migration, the bars in our experiments are considered as stationary, or quasi-stationary if following the terminology used in Venditti et al. (2012). In addition we classify them as "free" bars since they arise spontaneously from the fundamental system instability (Colombini et al., 1987). Inversely, "forced" bars would result from persistent flow or topographic perturbations (Seminara and Tubino, 1992) which is not the case here given our experimental setup.

Free bars, which are common bedforms observed in straight alluvial channels, are often reported as migrating (Seminara, 1998). However, some authors observed a non-migrating behavior under certain width-to-depth ratio conditions (Blondeaux and Seminara, 1985) or when the experiment duration was long enough (Crosato et al., 2011). This latter condition is at the least fulfilled in this study.

The coexistence of bedforms at different spatial scales is common in gravel-bed experiments (Ikeda, 1983; Crosato et al., 2011, 2012; Podolak and Wilcock, 2013). In most of such studies the shortest bed structures observed, for instance small bars, are mobile. However, they are often attributed to a transient bed state and are reported to grow and ultimately stabilize forming stationary bars (Crosato et al., 2011, 2012; Podolak and Wilcock, 2013) which is not the process observed here. The sediment waves we describe, when bars are stationary, are indeed more similar to the migrating bedload sheets (Madej et al., 2009), the coarse particle patches (Lanzoni, 2000b), and the small bars (Podolak and Wilcock, 2013) reported in the cited studies. However, these authors focused on the large bar dynamics rather than on the smallest bedforms they observed. As a consequence, our study brings new insights about sediment transfer in quasi-stationary alternate bar configurations.

The considerations above motivated us to quantify the respective contribution of migrating bars and sediment waves to bedload transport. We found that episodic bar migration generates most of the largest bedload pulses which is consistent with the large sediment volumes they involve. However, in term of total mass transported during the experiments, sediment waves appear to be the primary means of bedload transport. This result supports substantially the conclusion of other studies that low-relief migrating bedforms play a predominant role in the transfer of sediment in gravel-bed systems (Ashmore, 1991; Griffiths, 1993), even in the presence of alternate bars.

Although migrating bars and sediment waves were analyzed as different mechanisms, they are not independent processes. Indeed, we observed that sediment waves modify momentarily the bar tails as they migrate through the pools. In addition, they can sometimes settle on the bars modifying their geometry, as observed by Podolak and Wilcock (2013). The observations made during the experiments suggest that this interaction participate in destabilizing the bars

and initiating their migration.

5.4.2 Sediment storage in the bed

The bursty character of the BTRs at the flume outlet was demonstrated to result from the episodic bar migration events and the step-like motion of sediment waves through the pools. Analysing jointly the bed volume and the BTR time series, we showed that these sudden releases of large sediment amounts occur when the bed is highly aggraded. In other words, bedload pulses are triggered when the bed reaches an apparent maximum storage capacity, which we believe is associated to a given bed configuration. In this view, the bed acts like a sediment buffer which alternatively stores and releases bed material, sediment storage being located in the pools and sediment release occurring in the form of either bar failures or sediment wave migration. In addition, this concept of maximum storage capacity is consistent with the periodic character of large-scale bedload pulses we reported. Indeed, in such a system the time for the bed storage capacity to be saturated is set by the constant feed rate (assuming similar initial storage states) which implies regular releases of large sediment amounts.

We wish to point here that the experiments were carried out in a flume with smooth glass walls. As a consequence, the flow velocity and the scour depth in the pools are likely to be larger than in similar experiments with rough side boundaries (e.g., in Lisle et al., 1997). We believe that these effects can influence the bedform dynamics described in this study. Therefore, any comparison with natural systems, which usually have rough (or erodible) banks, must be made with caution.

Sediment transfer in drainage networks has been modelled by some authors as the exchange of bed material between successive sediment reservoirs (Kelsey et al., 1987). For instance, Lisle and Church (2002) proposed a conceptual model in which the capacity to transfer or store sediment in each reservoir depends on the sediment feed rate and on the volume of sediment stored. Such an approach has several points in common with the description we made of the bar-and-pool system.

As a consequence, we believe that modelling stationary alternate bars as a series of connected sediment reservoirs (corresponding to the pools) may be appropriate to describe the transfer of sediment in the downstream direction. In particular, this approach may generate bedload pulses as a result of sediment buffering in the model, which would be a step forward in modelling bedload transport rate fluctuations.

5.4.3 Effect of sediment supply

The changes in bed topography between the experiments characterized by different sediment feed rates reflect the effect of increased sediment supply conditions on the alternate bar configuration, a topic that has drawn much attention (Lisle et al., 1997; Cui et al., 2003; Madej et al., 2009; Pryor et al., 2011; Podolak and Wilcock, 2013; Mueller and Pitlick, 2014; Zunka et al., 2015; Elgueta-Astaburuaga and Hassan, 2017). In each experiment, the evolution of

the bed from a flat configuration to an alternate bar configuration resulted in an increased transport capacity, which is in agreement with the conclusion of Francalanci et al. (2012) who investigated the effect of such bedforms on flow resistance.

We also observed that the general bed response to an increase in sediment supply was a raise in the average slope and a more braided configuration, as reported in other studies (Madej et al., 2009; Pryor et al., 2011; Mueller and Pitlick, 2014). These changes in the bed geometry both participate in increasing its transport capacity in order to adjust to the rate of sediment supply (Podolak and Wilcock, 2013).

However, the increase in average bed slope between experiment 1 and 3 was close to zero, whereas the sediment feed rate was doubled. The increase in transport capacity was therefore essentially due to the change in the alternate bar configuration (increased braiding), which illustrates the finding of several authors that adjustment in bar spatial configuration can increase locally the bed shear stress without necessarily changing its mean value (Paola, 1996; Nicholas, 2000; Ferguson, 2003; Francalanci et al., 2012; Podolak and Wilcock, 2013; Mueller and Pitlick, 2014).

Finally, we brought evidences of the dependency of the transport capacity on the sediment storage in the bed. Our observations thus confirm the conclusion of Lisle and Church (2002) and Madej et al. (2009) that a better knowledge of sediment transport-storage relationships in gravel-bed rivers can improve the understanding of their morphodynamics.

6 General discussion and conclusion

The results of this experimental investigation presented in the previous chapters are summarized and discussed in the following sections. The limitations of the study are then commented and we finally give a concise conclusion in regard to the objectives presented at the beginning of the document.

6.1 Experimental measurements

The main outcomes of this study rely essentially on the joint analysis of the bedload transport rate (BTR) and the bed topography measurements which were recorded with a fine resolution compared to the flume size (16 × 0.6 m) and the experiment durations (longer than 100 h). The BTR was measured continuously (and subsequently aggregated over 1-min time steps) at the flume outlet using vertical impact plates. These sensors are derived from passive acoustic techniques used in the field (Rickenmann, 2017) and were originaly developed in our laboratory by Mettra (2014) and Heyman (2014). However, we have brought a significant contribution regarding their calibration (Dhont et al., 2017).

The bed topography was scanned every ten minutes analysing the deformation of a laser sheet projected from a moving cart on the bed surface, through the water. Similar methods were used in smaller flumes and under "smoother" flow conditions (Soares-Frazão et al., 2007; Seizilles, 2013). However, the use of such a technique in a larger flume, with higher flow depths (~10 cm) and turbulent conditions (i.e., with a disturbed free surface), is a useful advancement for experimentalists. Indeed, the laser-sheet imaging technique has the major advantage to provide topography measurements without requiring the water flow to be stopped, a common procedure that can affect bed characteristics (Ockelford and Haynes, 2013; Vesipa et al., 2017). Note that complementary flow depth measurements were recorded using ultrasonic probes also mounted on the moving cart.

The data acquisition process was fully automated which allowed us to carry out long experimental runs (up to 24 h) without any intervention. The run durations were only limited by the capacity of the hopper feeding sediment in the flume, which could be overcome by a sediment recirculation system in future experiments. In summary, our experimental setup allowed the collection of a large dataset of joint BTR and bed topography measurements at

fine resolution and over long time periods. Such experimental records are scarce although they are crucial given the long durations of bed transient states in this type of experiments (Podolak and Wilcock, 2013), and the wide range of scales associated with BTR fluctuations and bed structure dynamics (Gomez et al., 1989). We thus believe that both our dataset and the technology used can be useful to future studies.

6.2 Bedload pulses

Bedload transport was characterized by a pulsating behavior in each of the three experiments conducted with different sediment feed rates (2.5, 5.0 and 7.5 g/s). However, it appeared that the BTR fluctuations tended to be shorter, of lower magnitude, and more frequent with increasing feed rate which is in agreement with the observations of other authors (e.g., Kuhnle and Southard, 1988; Singh et al., 2009; Ghilardi et al., 2014b). These "smoother" fluctuations at higher feed rates may result from an increased sediment availability in the bed, due to reduced grain sorting effects (Bathurst, 2007). However, this hypothesis is not based on any observation, and can be questioned given the moderately-sorted sediment mixture used.

The bed responded to the increase in sediment feed rate by a steeper average slope and a change in configuration from stretched alternate bars to a rougher topography (i.e., characterized by a higher spatial variability with more pools), which could be seen as the beginning of the braiding process (Mueller and Pitlick, 2014). Such a bed adjustment, corresponding to an increase in its transport capacity (Podolak and Wilcock, 2013), was expected and has been reported in other studies (Madej et al., 2009; Pryor et al., 2011). However, little is known about how these changes in bed morphology and hydraulic conditions affect the mode of bedload transport (Church, 2006). Indeed, available literature rather documents the effect of sediment supply on the bed morphology either following a change in feed rate (Venditti et al., 2012; Podolak and Wilcock, 2013) or the injection of sediment pulses (Lisle et al., 1997; Zunka et al., 2015; Elgueta-Astaburuaga and Hassan, 2017), than the effect of bed morphology on bedload transport mode which is more difficult to assess (Mueller and Pitlick, 2014).

Griffiths (1993) reported that bedload is transported in alluvial channels as *sediment translation waves*, which contains the idea that "sediment volumes" move in the bed. However, the pulsating nature of bedload transport refers also to the concept of "intermittency". We therefore argue that the mode of bedload transport in such channels is better described as the *step-like motion* of sediment waves, following Ashmore (1991). When such sediment waves are evacuated from the flume, they induce bedload pulses that can be described as intense *transport events* (Saletti et al., 2015).

Our results suggest that increased bed roughness (more bars and pools of shorter length) associated with steeper slopes mitigates the pulsating character of bedload transport. Given the considerations above, it would mean that sediment waves then involve smaller sediment volumes and that they are evacuated more frequently from the flume (resulting in lower and more frequent pulses). However, this hypothesis requires further experiments, covering a wider range of bed configurations, to be validated.

6.3 Sediment waves and migrating bars

The evolution of the bed topography during the experiments bears evidence of migrating sediment waves (see comments above) in alternate bar systems. We demonstrated that they migrate in the downstream direction from pool to pool, along the main flow path, which is consistent with the step-like motion (Ashmore, 1991) discussed above. In other words, bedload is transported in the bed discontinuously in spatially delimited zones (i.e., the pools with high flow depths) rather than continuously like in a sediment toboggan. Sediment wave migration thus induces aggradation-degradation cycles in the pools, which is consistent with the signature of low-relief bedform migration consisting in local changes in the bed elevation (Hoey, 1992). Note that the term *sediment wave* can be used in different contexts and we refer to the review in James (2010) for clarification.

We also observed episodic bar migration associated with large bedload pulses, as reported by Gomez et al. (1989). However, despite the large amounts of sediment carried by migrating bars (Church, 2010), we demonstrated that sediment waves are nonetheless the primary mode of bedload transport in the context of our experimental conditions (characterized by quasi-stationary alternate bars). Indeed, if considering only pulses larger than two times the average transport rate, sediment waves represent at least 50% of the total sediment mass transported during each experiment (this ratio increases to 85% in the experiment with the largest sediment feed rate).

We explain the overall non-migrating character of the bars by either a width-to-depth ratio at the value of resonance or a possible persistent forcing condition at the flume inlet (Seminara, 1998). This latter reason could result from the flow deflection toward one of the flume walls due to the accumulation of sediment in the center part of flume (non-uniform sediment feeding conditions). However, the stationary bars we report may also be an inherent feature of the system, as suggested by Crosato et al. (2011). The occasional bar failures observed seem due to local changes in hydraulic conditions (resulting from changes in bed geometry associated with sediment transport) that allow bar erosion and migration (Lanzoni, 2000b). In addition, our observations support the intuition of Crosato et al. (2012) that bar failure propagates from upstream to downstream as a domino effect, and therefore stress the need for further investigation on this phenomenon.

6.4 Fluctuations across time scales

The BTR fluctuations we measured were associated with a wide range of time scales, from one minute (the sampling time) to more than ten hours, which is in agreement with other authors (Gomez et al., 1989). Following the classification proposed by Hoey (1992), pulses in our experiments are at least associated with the passage of meso-forms (scaling with the flow depth) and macro-forms (scaling with the flume width). However, little attention was paid to the primer, although they were visually observed (e.g., antidune destruction and particle cluster failure). Indeed, given the scope of the study, we focused on sediment waves and bar migration which involve much larger sediment volumes. Nevertheless, it is interesting to

note that the fluctuations at different scales overlapped in the recorded BTR time series (as would have the noise due particle entrainment stochasticity if we had considered a temporal resolution finer than one minute).

An interesting property of BTR fluctuations within a limited range of time scales is the existence of scaling relations (due to scale-dependent statistics) generally following power laws (Ma et al., 2014). Evidences of such relationships have been brought both at the particle (Campagnol et al., 2012) and at slightly longer (Singh et al., 2009) time scales (in the order of minutes). Our results support the existence of scaling properties at larger time scales, from minutes to hours, which may have consequences for the appropriate design of BTR sampling strategies (Bunte and Abt, 2005; Recking et al., 2012). However, the link between the BTR fluctuations at the particle scale and at the bedform scale is still an open question (Singh et al., 2009; Heyman et al., 2013; Ma et al., 2014); and we believe our data can provide new insights into this relation in future work, aggregating the raw BTR measurements over temporal scales finer than one minute (e.g., sub-second scale).

6.5   Variations in bed volume

At the largest fluctuation time scale (i.e., in the order of ten hours), bedload pulses showed some periodicity and matched global variations in bed volume. The system is therefore also characterized by large-scale fluctuations, due to changes in sediment storage, in addition to the fluctuations associated with bedform migration. This underlying fluctuation pattern is characterized by sudden decreases in bed volume, corresponding to large bedload pulses, and long aggradation phases dependent on the sediment feed rate.

We therefore suggest that, under steady external conditions, the bed storage capacity governs the largest fluctuations in the system. For a given bed configuration, a maximum storage capacity may exist that bounds the magnitude and the time scale of the BTR fluctuations. This idea of bounded fluctuations supports and refines the statement by Jerolmack and Paola (2010) that the magnitude of the pulses has an upper limit set by the system size and the sediment feed rate. Moreover, it is in agreement with Cudden and Hoey (2003) who claim that bedload pulses are not only the expression of stochastic processes. In this view, the bed could act as an electric condenser storing incoming sediment up to its maximum capacity, and then releasing sediment over short time periods (generating thus pulses). These considerations could improve the modelling of bedload transport in regards to its pulsating nature.

Bed aggradation and degradation phases are necessarily associated with morphological changes. However, no systematic and univocal relation with the average bed slope was found (e.g., one could expect steeper slopes during aggradation phases). Further analyses are therefore needed to characterize the link between sediment storage and transport capacity in the bed. Our results point anyway, in agreement with Lisle and Church (2002), that a better knowledge of transport-storage relationships could improve the understanding of gravel-bed river morphodynamics.

6.6 Dynamic equilibrium

The pulsating nature of bedload transport makes the issue of equilibrium in gravel-bed rivers complex (Bracken and Wainwright, 2006; Nanson and Huang, 2016). In our experiments, the BTR and the average bed slope were found to fluctuate about their mean values when the observation time was long enough. Such a behavior in experiments with steady external conditions is usually considered as indicative of dynamic equilibrium (Recking et al., 2009), which is therefore conditional upon the time scale considered. However, an underlying assumption behind the concept of dynamic equilibrium is that fluctuations are bounded and that the observation time is long enough to capture all types of fluctuation. This assumption is supported by the comments above that BTR fluctuations have probably an upper limit, as well as by Recking (2006) who reported bounded bed slope fluctuations.

However, we observed that the average bed volume stabilizes after a much longer time than the average transport rate. As a consequence, we argue that dynamic equilibrium in flume experiments with an initial flat bed configuration is likely to be achieved after longer time periods than it is usually assumed. In addition, the bed had a different geometry during the transient states and the quasi-equilibrium states which suggests that it can respond to an external disturbance changing its configuration. However, further experiments are needed to assess if different persistent equilibrium states (e.g., regarding the morphology) can be observed under similar external conditions.

6.7 Limitations

The flume had glass walls, a common feature in such experimental setups, in order to visualize the processes occurring in the bed during the experiments. However, these smooth side boundaries affect the hydraulic conditions compared to straight natural streams with rough banks. We suspect they result in an increased scour depth (in the pools) that may amplify the pulsating behavior of bedload transport. Any quantitative comparison with natural river systems should therefore be made with caution.

Little attention was paid to grain sorting although we observed some of its effect in the bed. For instance, bar heads were made of coarse particles and the bottom of the pools featured special arrangements of fine grains. Moreover, the mechanisms of bedload transport and the changes in bed morphology we described are somehow related to grain sorting effects. Among the main reasons for not documenting this phenomenon we point: the moderately-sorted sediment mixture used, the difficulty to quantify its effects given the limited range of grain sizes (for instance compared to mixtures with sand and gravel), and the priority to carry out long experimental runs without stopping the water flow (which is generally needed to assess grain sorting in the bed).

This study relies on the extensive comparison between bedload transport and bed topography measurements. However, we provided limited information about the hydraulic conditions in the flume, although they are necessary to fully characterize the system dynamics. Indeed, the flow characteristics over such a complex topography are not readily computable because

of their three-dimensional nature and considerable variability at the local scale. A detailed investigation of the hydraulic conditions and the distribution of the bed shear stress (in time and space) would bring a valuable contribution to this study, and could be undertaken in a future research using a hydrodynamic model.

Our experiments covered a limited range of flow and sediment supply conditions, and therefore of bed configurations, because of the priority to carry out long experiments. Moreover, we tested only a single sediment mixture. Therefore, complementary experiments with different bed configurations and grain size distributions would be valuable to generalize our results and better describe bedload transport in straight alluvial channels.

Finally, we point that the experiments were run under steady external conditions given the scope of the study. However, natural streams are characterized by unsteady flow and sediment supply conditions which increases dramatically the complexity of bedload transport in gravel-bed rivers. We nevertheless believe that this study shed some light on the issue of bedload transport in alluvial channels documenting several of its mechanisms under controlled conditions.

6.8   Conclusion

In conclusion, this experimental study provides new insights into the origins of bedload pulses in gravel-bed flumes with quasi-stationary alternate bars. We demonstrated that sediment waves migrating in a step-like motion from pool to pool induce most of sediment pulses and are the primary mode of bedload transport in such systems. In addition, these migrating low-relief bedforms were found to cause occasional bar failures generating particularly large sediment pulses and associated with reworking of the bed.

The bedload pulses due to such migrating bedforms occur at the macro-scale. However, shorter fluctuations were also observed and our results suggest the existence of scaling relations across time scales ranging from minutes to hours. At the largest time scale, fluctuations seem associated with quasi-periodic variations in global bed volume which indicates that they may be governed by the bed storage capacity.

The particularly long durations of the experiments allowed us to investigate the issue of dynamic equilibrium in gravel-bed experiments which depends on the observation time period. It appears that the time period necessary to observe all types of fluctuations in the system may be much longer than it is usually assumed, which has important consequences for experimentalists.

Finally, we shown that the bed responds to an increase in sediment supply conditions by increasing its average slope and/or evolving toward a more braided configuration in order to adjust its transport capacity. In addition, we demonstrated that these morphological changes smooth the pulsating regime of bedload transport and result in shorter and more frequent sediment pulses of lower magnitude.

A Appendix

A.1 Supplementary online material

Movies available on the YouTube page of the Environmental Hydraulics Laboratory (LHE, EPFL, Switzerland).

Simple presentation of the experimental setup	https://youtu.be/XqMX151D8iI
Evolution of the bed topography during experiment 1	https://youtu.be/ObeSC_va6Gc
Evolution of the bed topography during experiment 2	https://youtu.be/V4H8_91Ho68
Evolution of the bed topography during experiment 3	https://youtu.be/uKv9GY76hOY
Side view of the flume during experiment 3	https://youtu.be/_1IwwYRGt4U

Uploaded on the 12/07/2017.

A.2 Accelerometer characteristics

Characteristics of the MMA7361LC accelerometers mounted on the impact plates as provided by the manufacturer Freescale Semiconductor Inc.

±1.5g, ±6g Three Axis Low-g Micromachined Accelerometer

The MMA7361LC is a low power, low profile capacitive micromachined accelerometer featuring signal conditioning, a 1-pole low pass filter, temperature compensation, self test, 0g-Detect which detects linear freefall, and g-Select which allows for the selection between two sensitivities. Zero-g offset and sensitivity are factory set and require no external devices. The MMA7361LC includes a Sleep Mode that makes it ideal for handheld battery powered electronics.

Features

- 3mm x 5mm x 1.0mm LGA-14 Package
- Low Current Consumption: 400 µA
- Sleep Mode: 3 µA
- Low Voltage Operation: 2.2 V – 3.6 V
- High Sensitivity (800 mV/g @ 1.5g)
- Selectable Sensitivity (±1.5g, ±6g)
- Fast Turn On Time (0.5 ms Enable Response Time)
- Self Test for Freefall Detect Diagnosis
- 0g-Detect for Freefall Protection
- Signal Conditioning with Low Pass Filter
- Robust Design, High Shocks Survivability
- RoHS Compliant
- Environmentally Preferred Product
- Low Cost

Typical Applications

- 3D Gaming: Tilt and Motion Sensing, Event Recorder
- HDD MP3 Player: Freefall Detection
- Laptop PC: Freefall Detection, Anti-Theft
- Cell Phone: Image Stability, Text Scroll, Motion Dialing, eCompass
- Pedometer: Motion Sensing
- PDA: Text Scroll
- Navigation and Dead Reckoning: eCompass Tilt Compensation
- Robotics: Motion Sensing

ORDERING INFORMATION				
Part Number	**Temperature Range**	**Package Drawing**	**Package**	**Shipping**
MMA7361LCT	–40 to +85°C	1977-01	LGA-14	Tray
MMA7361LCR1	–40 to +85°C	1977-01	LGA-14	7" Tape & Reel
MMA7361LCR2	–40 to +85°C	1977-01	LGA-14	13" Tape & Reel

MMA7361LC

MMA7361LC: XYZ AXIS ACCELEROMETER
±1.5g, ±6g

Bottom View
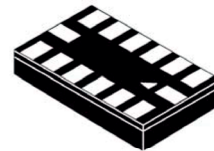
14 LEAD
LGA
CASE 1977-01

Top View

N/C

N/C — 1	14
X$_{OUT}$ — 2	13 — Self Test
Y$_{OUT}$ — 3	12 — N/C
Z$_{OUT}$ — 4	11 — N/C
V$_{SS}$ — 5	10 — g-Select
V$_{DD}$ — 6	9 — 0g-Detect
	8 — N/C
	7

Sleep
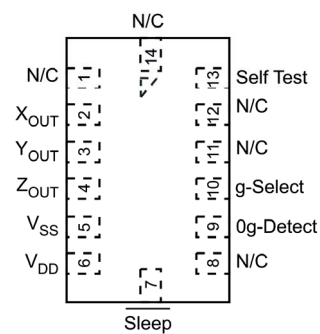
Figure 1. Pin Connections

© Freescale Semiconductor, Inc., 2010, 2011.

116

A.3 Calibration of the impact plates

Calibration coefficients of the impact plates to convert the number of impulses x measured by each accelerometer into grams using the relation $f(x) = 0.1ax$, with a a correction factor for the sensor sensitivity. The accelerometers are numbered from 1 to 6 from the right side to the left side of the flume with respect to the flow direction (see figure 2.3).

accelerometer	1	2	3	4	5	6
a	0.4000	1.0000	1.0667	0.5667	1.2000	1.0667

A.4 Calibration of the ultrasonic probes

Calibration coefficients of the ultrasonic probes to convert the signal x acquired in volt into millimeters using the linear relation $f(x) = ax + b$. The probes are numbered from 1 to 8 from the right side to the left side of the flume with respect to the flow direction (see figure 2.4).

probe	1	2	3	4
a	-80.3124	-72.9780	-74.2416	-74.1046
b	661.9529	652.0510	655.0985	651.1400

probe	5	6	7	8
a	-78.7012	-75.2746	-88.2138	-74.9597
b	664.5645	657.6237	676.1967	663.1177

A.5 Camera and laser characteristics

Characteristics of the Basler acA2000-165uc camera used for the laser-sheet imaging technique (see figure 2.6) as provided by the manufacturer Basler AG.

Sensor Vendor	CMOSIS
Sensor	CMV2000
Shutter	Global Shutter
Maximum Image Circle	2/3″
Sensor Type	CMOS
Sensor Size	11.3 mm×6 mm
Resolution (H×V)	2040 px×1086 px
Resolution	2 MP
Pixel Size (H×V)	5.5 μm×5.5 μm
Frame Rate	165 fps
Mono/Color	Color

Characteristics of the BES536-L green line laser module (< 50 mW) used for the laser-sheet imaging technique (see figure 2.6) as provided by the supplier Apinex.Com Inc.

Laser Class	2, 3R, 3B (II, IIIa, IIIb)
Wavelength	532 nm
Output Power	< 1, < 5, < 10, < 20, < 50 mW
Operation Voltage	3 V DC, (for 50 mW apply 3.5–5 V)
Operation Current	500 mA
Divergence	< 0.6 mrd
Optics	Glass with A/R coating
Beam	Line (60° fan angle)
Length	70 mm
Diameter	16 mm
Case Material	Metal
Operation Temp.	10–35 °C

A.6 Correction for refraction effects

Simplified representation of the refraction effects affecting the measurements of the laser-sheet imaging technique. In the figure below, h_a can be derived from the calculations detailed in section 2.3.2.2 (i.e., neglecting the refraction effects). In the following, we detail how the bed elevation can be corrected, through the calculation of h, in order to account for the laser refraction when entering the water.
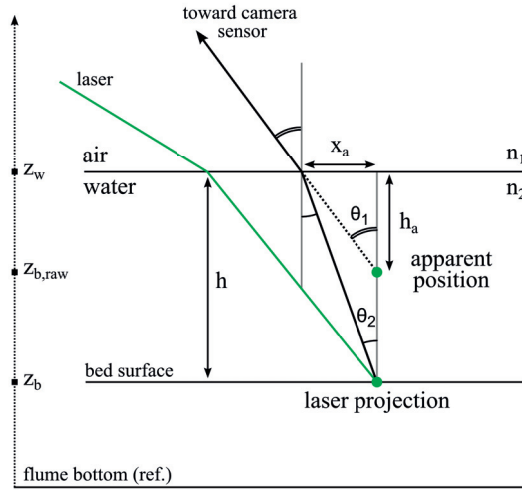
From the figure above, one can write

$$\frac{x_a}{h_a} = \frac{\sin\theta_1}{\cos\theta_1} \quad \text{and} \quad \frac{x_a}{h} = \frac{\sin\theta_2}{\cos\theta_2} \quad \text{which yields} \quad h = h_a \frac{\sin\theta_1}{\cos\theta_1}\frac{\sin\theta_2}{\cos\theta_2}.$$

Since

$$n_1 \sin\theta_1 = n_2 \sin\theta_2 \quad \text{with } n_i \text{ the refractive indexes,}$$

h can be computed as follow

$$h = h_a \frac{n_2}{n_1}\frac{\cos\theta_2}{\cos\theta_1} \approx h_a \frac{n_2}{n_1} \quad \text{for low angles,}$$

which implies that

$$z_b \approx z_w - \frac{n_2}{n_1}(z_w - z_{b,raw}).$$

A.7 Temporal evolution of the bed profiles

Temporal evolution of the right and left profiles of the bed during experiment 1.

Temporal evolution of the right and left profiles of the bed during experiment 2.

Bibliography

Almedeij, J. H. and Diplas, P. (2003). "Bedload transport in gravel-bed streams with unimodal sediment." *Journal of Hydraulic Engineering*, 129(11), 896–904.

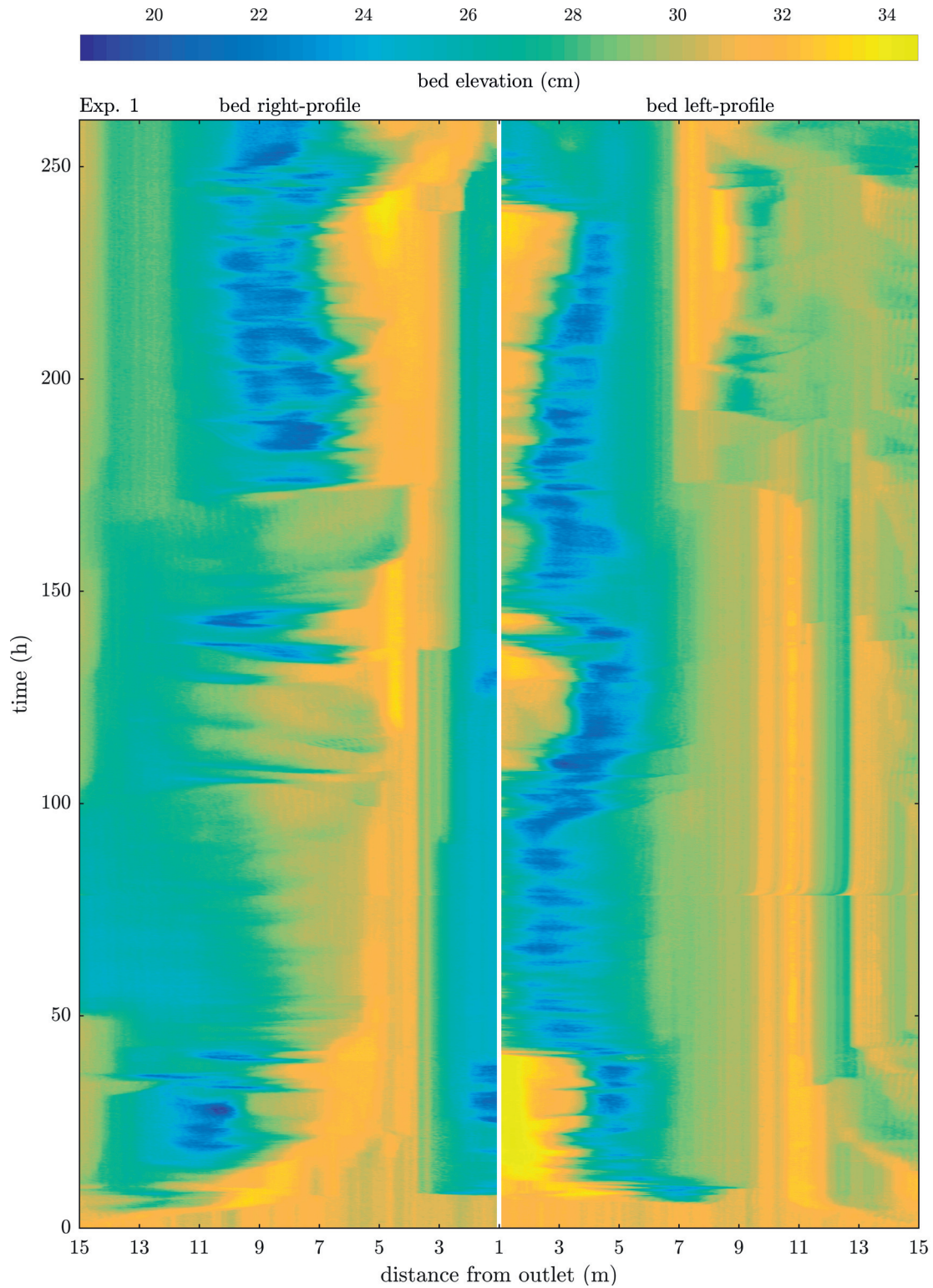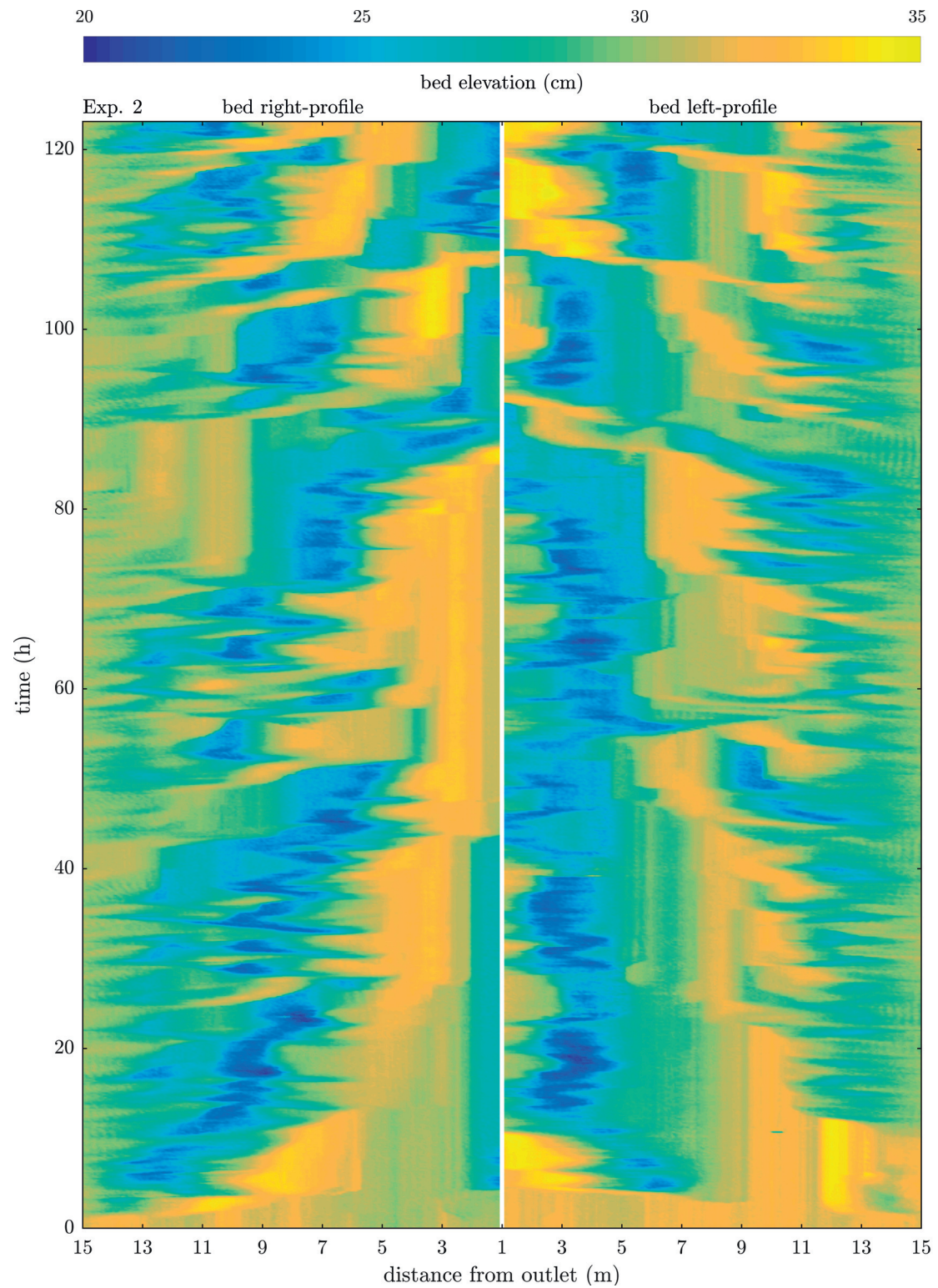Ancey, C., Boehm, T., Jodeau, M., and Frey, P. (2006). "Statistical description of sediment transport experiments." *Physical Review E*, 74(1).

Ancey, C., Bohorquez, P., and Bardou, E. (2014). "Sediment transport in mountain rivers." *ERCOFTAC Bulletin*, 100, 37–52.

Ancey, C., Bohorquez, P., and Heyman, J. (2015). "Stochastic interpretation of the advection-diffusion equation and its relevance to bed load transport." *Journal of Geophysical Research: Earth Surface*, 120(12), 2529–2551 2014JF003421.

Ancey, C., Davison, A. C., Boehm, T., Jodeau, M., and Frey, P. (2008). "Entrainment and motion of coarse particles in a shallow water stream down a steep slope." *Journal of Fluid Mechanics*, 595, 83–114.

Andrews, E. D. (1983). "Entrainment of gravel from naturally sorted riverbed material." *Geological Society of America Bulletin*, 94(10), 1225–1231.

Arnaud-Fassetta, G., Astrade, L., Bardou, E., Corbonnois, J., Delahaye, D.and Fort, M., Gautier, E., Jacob, N., Peiry, J.-L., Piégay, H., and Penven, M.-J. (2009). "Fluvial geomorphology and flood-risk management." *Geomorphology*, 15(2), 109–128.

Ashmore, P. (1987). "Bed load transfer and channel morphology in braided stream." *In: Erosion and Sedimentation in the Pacific Rim. Proceedings of the Symposium held Oregon State University, Corvallis, USA*, IAHS Publication 165, 333–341.

Ashmore, P. (1991). "Channel morphology and bed load pulses in braided, gravel-bed streams." *Geografiska Annaler*, 73A(1), 37–52.

Ashworth, P. J., Best, J. L., Leddy, J. O., and Geehan, G. W. (1994). *Process Models and Theoretical Geomorphology*. John Wiley & Sons Ltd, Chichester, UK, Chapter The physical modelling of braided rivers and deposition of fine-grained sediment, 115–139.

Bagnold, R. A. (1956). "The flow of cohesionless grains in fluids." *Proceedings of the Royal Society*, 249(964), 235–297.

Bibliography

Bagnold, R. A. (1966). "An approach to the sediment transport problem from general physics." *USGS Professional Paper*, 422-I.

Bagnold, R. A. (1980). "An empirical correlation of bedload transport rates in flumes and natural rivers." *Proceedings of the Royal Society*, 372(1751), 453–473.

Barry, J. J. (2004). "A general power equation for predicting bed load transport rates in gravel bed rivers." *Water Resources Research*, 40(10).

Bathurst, J. C. (2007). "Effect of coarse surface layer on bed-load transport." *Journal of Hydraulic Engineering*, 133(11), 1192–1205.

Blondeaux, P. and Seminara, G. (1985). "A unified bar-bend theory of river meanders." *Journal of Fluid Mechanics*, 157, 449–470.

Bracken, L. J. and Wainwright, J. (2006). "Geomorphological equilibrium: myth and metaphor?" *Transactions of the Institute of British Geographers*, 31(2), 167–178.

Bravo-Espinosa, M., Osterkamp, W. R., and Lopes, V. L. (2003). "Bedload transport in alluvial channels." *Journal of Hydraulic Engineering*, 129(10), 783–795.

Bunte, K. and Abt, S. R. (2005). "Effect of sampling time on measured gravel bed load transport rates in a coarse-bedded stream." *Water Resources Research*, 41(11) W11405.

Campagnol, J., Radice, A., and Ballio, F. (2012). "Scale-based statistical analysis of sediment fluxes." *Acta Geophysica*, 60(6), 1744–1777.

Carson, M. A. and Griffiths, G. A. (1987). "Bedload transport in gravel channels." *Journal of Hydrology (New Zealand)*, 26(1), 1–151.

Chang, H. H. (1985). "Formation of alternate bars." *Journal of Hydraulic Engineering*, 111(11), 1412–1420.

Chanson, H. (2004). *The Hydraulics of Open Channel Flow.* Butterworth-Heinemann, Oxford, UK, 2nd edition.

Church, M. (2006). "Bed material transport and the morphology of alluvial river channels." *Annual Review of Earth and Planetary Sciences*, 34(1), 325–354.

Church, M. (2010). *Sediment Cascades: An Integrated Approach.* John Wiley & Sons Ltd, Chichester, UK, Chapter Gravel-Bed Rivers, 241–269.

Church, M. and Ferguson, R. I. (2015). "Morphodynamics: Rivers beyond steady state." *Water Resources Research*, 51(4), 1883–1897.

Church, M. and Hassan, M. A. (2002). "Mobility of bed material in Harris Creek." *Water Resources Research*, 38(11) 1237.

124

Church, M., Hassan, M. A., and Wolcott, J. F. (1998). "Stabilizing self-organized structures in gravel-bed stream channels: Field and experimental observations." *Water Resources Research*, 34(11), 3169–3179.

Colombini, M., Seminara, G., and Tubino, M. (1987). "Finite-amplitude alternate bars." *Journal of Fluid Mechanics*, 181, 213–232.

Comiti, F. and Mao, L. (2012). *Recent Advances in the Dynamics of Steep Channels.* John Wiley & Sons Ltd, Chichester, UK, 351–377.

Crosato, A., Desta, F. B., Cornelisse, J., Schuurman, F., and Uijttewaal, W. S. J. (2012). "Experimental and numerical findings on the long-term evolution of migrating alternate bars in alluvial channels." *Water Resources Research*, 48(6) W06524.

Crosato, A., Mosselman, E., Beidmariam Desta, F., and Uijttewaal, W. S. J. (2011). "Experimental and numerical evidence for intrinsic nonmigrating bars in alluvial channels." *Water Resources Research*, 47(3) W03511.

Cudden, J. R. and Hoey, T. B. (2003). "The causes of bedload pulses in a gravel channel: the implications of bedload grain-size distributions." *Earth Surface Processes and Landforms*, 28(13), 1411–1428.

Cui, Y., Parker, G., Lisle, T. E., Gott, J., Hansler-Ball, M. E., Pizzuto, J. E., Allmendinger, N. E., and Reed, J. M. (2003). "Sediment pulses in mountain rivers: 1. Experiments." *Water Resources Research*, 39(9) 1239.

D'Agostino, V. and Lenzi, M. A. (1999). "Bedload transport in the instrumented catchment of the Rio Cordon part II: Analysis of the bedload rate." *CATENA*, 36(3), 191–204.

Dhont, B., Rousseau, G., and Ancey, C. (2017). "Continuous monitoring of bed-load transport in a laboratory flume using an impact sensor." *Journal of Hydraulic Engineering*, 143(6).

du Boys, M. P. (1879). *Le Rhône et les rivières à lit affouillable.* Annales des Ponts et Chaussées, Série 5, Tome 18, 141–195.

Ehrenberger, R. (1931). "Direct bedload mesurements on the Danube at Vienna and their results to date." *Die Wasserwirtschaft*, 34, 1–9.

Einstein, H. A. (1937). "The calibration of bedload trap used in the Rhine." *Schweuzerische Bauzeitung*, 110, 29–32.

Einstein, H. A. (1942). "Formulas for the transportation of bed load." *Transactions of the ASCE*, 107, 561–573.

Einstein, H. A. (1950). *The bed-load function for sediment transportation in open channel flows.* Tech. Bul. No. 1026. U.S. Dept. of Agriculture, Washington, D.C.

Bibliography

Elgueta-Astaburuaga, M. A. and Hassan, M. A. (2017). "Experiment on temporal variation of bed load transport in response to changes in sediment supply in streams." *Water Resources Research*, 53(1), 763–778.

Emmett, W. W. (1975). "The channels and waters of the upper Salmon River area, Idaho." *USGS Professional Paper*, 870A.

Ergenzinger, P. (1988). "The nature of coarse material bed load transport." *In: Sediment Budgets. Proceedings of the Symposium held at Porto Alegre, Brazil*, IAHS Publication 174, 207–216.

Fabre, J. A. (1797). *Essai sur la Théorie des Torrens et des Rivières.*

Ferguson, R. (2003). "The missing dimension: effects of lateral variation on 1-d calculations of fluvial bedload transport." *Geomorphology*, 56(1), 1–14.

Fienberg, K., Singh, A., Foufoula-Georgiou, E., Jerolmack, D. J., and Marr, J. D. G. (2010). *Bedload-Surrogate Monitoring Technologies.* USGS Scientific Investigations 2010-5091, Chapter A theoretical framework for interpreting and quantifying the sampling time dependence of gravel bedload transport rates, 171–184.

Folk, R. L. and Ward, W. C. (1957). "Brazos River bar: a study in the significance of grain size parameters." *Journal of Sedimentary Petrology*, 27, 3–26.

Francalanci, S., Solari, L., Toffolon, M., and Parker, G. (2012). "Do alternate bars affect sediment transport and flow resistance in gravel-bed rivers?" *Earth Surface Processes and Landforms*, 37(8), 866–875.

Frey, P., Ducottet, C., and Jay, J. (2003). "Fluctuations of bed load solid discharge and grain size distribution on steep slopes with image analysis." *Experiments in Fluids*, 35(6), 589–597.

Furbish, D. J., Haff, P. K., Roseberry, J. C., and Schmeeckle, M. W. (2012). "A probabilistic description of the bed load sediment flux: 1. Theory." *Journal of Geophysical Research: Earth Surface*, 117(F3) F03031.

Ghilardi, T., Franca, M. J., and Schleiss, A. J. (2014a). "Bed load fluctuations in a steep channel." *Water Resources Research*, 50(8), 6557–6576.

Ghilardi, T., Franca, M. J., and Schleiss, A. J. (2014b). "Period and amplitude of bedload pulses in a macro-rough channel." *Geomorphology*, 221, 95–103.

Gilbert, G. K. (1914). "Transportation of debris by running water." *USGS Professional Paper*, 86.

Gomez, B. (1991). "Bedload transport." *Earth-Science Reviews*, 31(2), 89–132.

Gomez, B. (1994). "Effects of particle shape and mobility on stable armor development." *Water Resources Research*, 30(7), 2229–2239.

Gomez, B. (2006). "The potential rate of bed-load transport." *Proceedings of the National Academy of Sciences of the United States of America*, 103(46), 17170–17173.

Gomez, B. and Church, M. (1989). "An assessment of bed load sediment transport formulae for gravel bed rivers." *Water Resources Research*, 25(6), 1161–1186.

Gomez, B., Naff, R. L., and Hubbell, D. W. (1989). "Temporal variations in bedload transport rates associated with the migration of bedforms." *Earth Surface Processes and Landforms*, 14(2), 135–156.

Graf, W. H. (1971). *Hydraulics of Sediment Transport.* Water Resources Publications, LLC.

Graf, W. H. and Altinakar, S. (2000). *Hydraulique fluviale: écoulement et phénomènes de transport dans les canaux à géométrie simple.* Traité de Génie Civil. Presses Polytechniques et Universitaires Romandes, Lausanne.

Griffiths, G. A. (1979). "Recent sedimentation history of the Waimakariri River, New Zealand." *Journal of Hydrology (New Zealand)*, 18(1), 6–28.

Griffiths, G. A. (1993). "Sediment translation waves in braided gravel-bed rivers." *Journal of Hydraulic Engineering*, 119(8), 924–937.

Harrison, A. S. (1950). *Report on special investigation of bed sediment segregation in a degrading bed.* University of California, Institute of Engineering Research.

Heyman, J. (2014). *A study of the spatio-temporal behaviour of bed load transport rate fluctuations.* Ph.D. thesis, EPFL, Lausanne, Switzerland.

Heyman, J., Mettra, F., Ma, H. B., and Ancey, C. (2013). "Statistics of bedload transport over steep slopes: Separation of time scales and collective motion." *Geophysical Research Letters*, 40(1), 128–133.

Hoey, T. B. (1992). "Temporal variations in bedload transport rates and sediment storage in gravel-bed rivers." *Progress in Physical Geography*, 16(3), 319–338.

Hoey, T. B. and Sutherland, A. J. (1991). "Channel morphology and bedload pulses in braided rivers: a laboratory study." *Earth Surface Processes and Landforms*, 16(5), 447–462.

Hubbell, D. W. (1987). *Sediment Transport in Gravel-Bed Rivers.* John Wiley & Sons Ltd, Chichester, UK, Chapter Bed load sampling and analysis, 89–118.

Ikeda, H. (1983). *Experiments on bedload transport, bed forms, and sedimentary structures using fine gravel in the 4-meter-wide flume.* Environmental Research Center Paper Ibaraki 2(1–78), University of Tskuba, Japan.

Ikeda, S. (1984). "Prediction of alternate bar wavelength and height." *Journal of Hydraulic Engineering*, 110(4), 371–386.

Bibliography

Iseya, F. and Ikeda, H. (1987). "Pulsations in bedload transport rates induced by a longitudinal sediment sorting: A flume study using sand and gravel mixtures." *Geografiska Annaler*, 69A(1), 15–27.

Jaeggi, M. (1984). "Formation and effects of alternate bars." *Journal of Hydraulic Engineering*, 110(2), 142–156.

James, L. A. (2010). "Secular sediment waves, channel bed waves, and legacy sediment." *Geography Compass*, 4(6), 576–598.

Jerolmack, D. J. and Paola, C. (2010). "Shredding of environmental signals by sediment transport." *Geophysical Research Letters*, 37(19) L19401.

Julien, P. Y. (1998). *Erosion and Sedimentation.* Cambridge University Press, UK.

Kelsey, H. M., Lamberson, R., and Madej, M. A. (1987). "Stochastic model for the long-term transport of stored sediment in a river channel." *Water Resources Research*, 23(9), 1738–1750.

Kleinhans, M. G. and van den Berg, J. H. (2011). "River channel and bar patterns explained and predicted by an empirical and a physics-based method." *Earth Surface Processes and Landforms*, 36(6), 721–738.

Kuhnle, R. A. (1996). *Advances in fluvial dynamics and stratigraphy.* John Wiley & Sons Ltd, Chichester, UK, Chapter Unsteady transport of sand and gravel mixtures, 183–201.

Kuhnle, R. A. and Southard, J. B. (1988). "Bed load transport fluctuations in a gravel bed laboratory channel." *Water Resources Research*, 24(2), 247–260.

Lane, E. W. (1955). "The importance of fluvial morphology in hydraulic engineering." *Proceedings of the American Society of Civil Engineers*, 81(745), 1–17.

Lanzoni, S. (2000a). "Experiments on bar formation in a straight flume: 1. Uniform sediment." *Water Resources Research*, 36(11), 3337–3349.

Lanzoni, S. (2000b). "Experiments on bar formation in a straight flume: 2. Graded sediment." *Water Resources Research*, 36(11), 3351–3363.

Laronne, J. B. and Duncan, M. J. (1992). *Dynamics of Gravel-Bed Rivers.* John Wiley & Sons Ltd, Chichester, UK, Chapter Bedload transport paths and gravel bar formation, 177–202.

Laronne, J. B., Garcia, C., and Reid, I. (2001). *Gravel-Bed Rivers V.* New Zealand Hydrological Society, Wellington, Chapter Mobility of patch sediment in gravel bed streams: patch character and its implications for bedload, 249–289.

Leopold, L. B. and Wolman, M. G. (1957). "River channel patterns: Braided, meandering, and straight." *USGS Professional Paper*, 282-B.

Lisle, T. E. and Church, M. (2002). "Sediment transport-storage relations for degrading, gravel bed channels." *Water Resources Research*, 38(11) 1219.

Lisle, T. E., Ikeda, H., and Iseya, F. (1991). "Formation of stationary alternate bars in a steep channel with mixed-size sediment: A flume experiment." *Earth Surface Processes and Landforms*, 16(5), 463–469.

Lisle, T. E., Iseya, F., and Ikeda, H. (1993). "Response of a channel with alternate bars to a decrease in supply of mixed-size bed load: A flume experiment." *Water Resources Research*, 29(11), 3623–3629.

Lisle, T. E., Pizzuto, J. E., Ikeda, H., Iseya, F., and Kodama, Y. (1997). "Evolution of a sediment wave in an experimental channel." *Water Resources Research*, 33(8), 1971–1981.

Ma, H., Heyman, J., Fu, X., Mettra, F., Ancey, C., and Parker, G. (2014). "Bed load transport over a broad range of timescales: Determination of three regimes of fluctuations." *Journal of Geophysical Research: Earth Surface*, 119(12), 2653–2673 2014JF003308.

Macklin, M. G. and Lewin, J. (1989). "Sediment transfer and transformation of an alluvial valley floor: The river South Tyne, Northumbria, U.K." *Earth Surface Processes and Landforms*, 14(3), 233–246.

Madej, M. A., Sutherland, D. G., Lisle, T. E., and Pryor, B. (2009). "Channel responses to varying sediment input: A flume experiment modeled after Redwood Creek, California." *Geomorphology*, 103(4), 507–519.

Marr, J. D. G., Gray, J. R., Davis, B. E., Ellis, C., and S., J. (2010). *Bedload-Surrogate Monitoring Technologies, SIR2010-5091*, Vol. 2010-5091. U.S. Geological Survey, Chapter Large-scale laboratory testing of bedload-monitoring technologies: overview of the StreamLab06 Experiments, 266–282.

Meade, R. H. (1985). "Wavelike movement of bedload sediment, East Fork River, Wyoming." *Environmental Geology and Water Sciences*, 7(4), 215–225.

Mettra, F. (2014). *Morphodynamic mechanisms in steep channels: from local processes to large-scale evolution*. Ph.D. thesis, EPFL, Lausanne, Switzerland.

Meyer-Peter, E. (1949). "Quelques problèmes concernant le charriage des matières solides." *La Houille Blanche*, B, 688–706.

Meyer-Peter, E. (1951). "Transport des matières solides en général et problèmes spéciaux." *Bull. Génie Civil d'Hydraulique Fluviale*, 5.

Meyer-Peter, E. and Müller, R. (1948). "Formulas for bed-load transport." *In: Proceedings of the 2nd meeting of the International Association for Hydraulic Research, Stockholm, Sweden*, 39–64.

Miwa, H. and Daido, A. (1995). "Fluctuations in bed-load transport rate in channel with alternate bars." *In: Management of Sediment: Philosophy, Aims, and Techniques. Proceedings of the Sixth International Symposium on River Sedimentation, New Delhi, India*, Oxford & IBH publishing, 641–648.

Bibliography

Montgomery, D. R. and Buffington, J. M. (1997). "Channel-reach morphology in mountain drainage basins." *Geological Society of America Bulletin*, 109(5), 596–611.

Mueller, E. R. and Pitlick, J. (2014). "Sediment supply and channel morphology in mountain river systems: 2. Single thread to braided transitions." *Journal of Geophysical Research: Earth Surface*, 119(7), 1516–1541 2013JF003045.

Mueller, E. R., Pitlick, J., and Nelson, J. M. (2005). "Variation in the reference shields stress for bed load transport in gravel-bed streams and rivers." *Water Resources Research*, 41(4) W04006.

Mühlofer, L. (1933). "Investigation into suspended load and bedload of the river Inn, near Kirchbichl, Tirol." *Die Wasserwirtschaft*, 26(1–6).

Nanson, G. C. and Huang, H. Q. (2016). "A philosophy of rivers: Equilibrium states, channel evolution, teleomatic change and least action principle." *Geomorphology*, In Press.

Nelson, J. M. (1990). "The initial instability and finite-amplitude stability of alternate bars in straight channels." *Earth-Science Reviews*, 29(1-4), 97–115.

Nelson, P. A., Dietrich, W. E., and Venditti, J. G. (2010). "Bed topography and the development of forced bed surface patches." *Journal of Geophysical Research: Earth Surface*, 115(F4) F04024.

Nesper, F. (1937). "Results of bedload and silt movement observations on the Rhine at the Brugg Bridge." *Schweuzerische Bauzeitung*, 110(143–148 and 161–164).

Nicholas, A. (2000). "Modelling bedload yield in braided gravel bed rivers." *Geomorphology*, 36(1), 89–106.

Nicholas, A., Ashworth, P., Kirkby, M., Macklin, M., and Murray, T. (1995). "Sediment slugs: large-scale fluctuations in fluvial sediment transport rates and storage volumes." *Progress in Physical Geography*, 19(4), 500–519.

Ockelford, A.-M. and Haynes, H. (2013). "The impact of stress history on bed structure." *Earth Surface Processes and Landforms*, 38(7), 717–727.

Paintal, A. S. (1971). "A stochastic model of bed load transport." *Journal of Hydraulic Research*, 9(4), 527–554.

Paola, C. (1996). *Coherent Flow structures in Open Channels.* John Wiley & Sons Ltd, Chichester, UK, Chapter Incoherent structure: Turbulence as a metaphor for stream braiding, 705–723.

Paola, C. (2001). *Gravel-Bed Rivers V.* New Zealand Hydrological Society, Wellington, Chapter Modelling stream braiding over a range of scales, 11–46.

Paola, C. and Seal, R. (1995). "Grain size patchiness as a cause of selective deposition and downstream fining." *Water Resources Research*, 31(5), 1395–1407.

Papanicolaou, A., Diplas, P., Evaggelopoulos, N., and Fotopoulos, S. (2002). "Stochastic incipient motion criterion for spheres under various bed packing conditions." *Journal of Hydraulic Engineering*, 128(4), 369–380.

Parker, G. (1976). "On the cause and characteristic scales of meandering and braiding in rivers." *Journal of Fluid Mechanics*, 76(3), 457–480.

Parker, G., Klingeman, P. C., and McLean, D. G. (1982). "Bedload and size distribution in paved gravel-bed streams." *Journal of the Hydraulics Division*, 108(4), 544–571.

Parker, G. and Sutherland, A. J. (1990). "Fluvial armor." *Journal of Hydraulic Research*, 28(5), 529–544.

Parker, G., Wilcock, P. R., Paola, C., Dietrich, W. E., and Pitlick, J. (2007). "Physical basis for quasi-universal relations describing bankfull hydraulic geometry of single-thread gravel bed rivers." *Journal of Geophysical Research: Earth Surface*, 112(F4).

Pitlick, J., Mueller, E. R., Segura, C., and Cress, R.and Torizzo, M. (2008). "Relation between flow, surface-layer armoring and sediment transport in gravel-bed rivers." *Earth Surface Processes and Landforms*, 33(8), 1192–1209.

Podolak, C. J. P. and Wilcock, P. R. (2013). "Experimental study of the response of a gravel streambed to increased sediment supply." *Earth Surface Processes and Landforms*, 38(14), 1748–1764.

Pryor, B. S., Lisle, T. E., Montoya, D. S., and Hilton, S. (2011). "Transport and storage of bed material in a gravel-bed channel during episodes of aggradation and degradation: A field and flume study." *Earth Surface Processes and Landforms*, 36(15), 2028–2041.

Radecki-Pawlik, A., Pagliara, S., and Hradecky, J. (2017). *Open Channel Hydraulics, River Hydraulic Structures and Fluvial Geomorphology*. Taylor & Francis.

Recking, A. (2006). *Etude expérimentale de l'influence du tri granulométrique sur le transport solide par charriage*. Ph.D. thesis, INSA Lyon, France.

Recking, A. (2010). "A comparison between flume and field bed load transport data and consequences for surface-based bed load transport prediction." *Water Resources Research*, 46(3) W03518.

Recking, A., Frey, P., Paquier, A., and Belleudy, P. (2009). "An experimental investigation of mechanisms involved in bed load sheet production and migration." *Journal of Geophysical Research: Earth Surface*, 114 F03010.

Recking, A., Frey, P., Paquier, A., Belleudy, P., and Champagne, J. Y. (2008). "Feedback between bed load transport and flow resistance in gravel and cobble bed rivers." *Water Resources Research*, 44(5).

Bibliography

Recking, A., Liébault, F., Peteuil, C., and Jolimet, T. (2012). "Testing bedload transport equations with consideration of time scales." *Earth Surface Processes and Landforms*, 37(7), 774–789.

Recking, A., Piton, G., Vazquez-Tarrio, D., and Parker, G. (2016). "Quantifying the morphological print of bedload transport." *Earth Surface Processes and Landforms*, 41(6), 809–822.

Recking, A., Richard, D., and Degoutte, G. (2013). *Torrents et rivières de montagne: Dynamique et aménagement.* Savoir faire. Quae éditions, Versaille.

Reid, I., Frostick, L. E., and Brayshaw, A. C. (1992). *Dynamic of gravel bed rivers.* John Wiley & Sons Ltd, Chichester, UK, Chapter Microform roughnesss elements and the selective entrainment and entrapment of particles in gravel bed rivers, 253–275.

Reid, I., Frostick, L. E., and Layman, J. T. (1985). "The incidence and nature of bedload transport during flood flows in coarse-grained alluvial channels." *Earth Surface Processes and Landforms*, 10(1), 33–44.

Richard, D. (1997). *Des grands écoulements naturels à la dynamique du tas de sable.* CEMAGREF Editions, Chapter Transport solide par charriage torrentiel.

Rickenmann, D. (1990). *Bedload Transport Capacity of Slurry Flows at Steep Slopes.* Ph.D. thesis, ETH, Zürich, Switzerland.

Rickenmann, D. (2001). "Comparison of bed load transport in torrents and gravel bed streams." *Water Resources Research*, 37(12), 3295–3305.

Rickenmann, D. (2017). "Bed-load transport measurements with geophones and other passive acoustic methods." *Journal of Hydraulic Engineering*, 143(6).

Rickenmann, D. and Koschni, A. (2010). "Sediment loads due to fluvial transport and debris flows during the 2005 flood events in switzerland." *Hydrological Processes*, 24(8), 993–1007.

Rickenmann, D., Turowski, J. M., Fritschi, B., Wyss, C., Laronne, J. B., Barzilai, R., Reid, I., Kreisler, A., Aigner, J., Seitz, H., and Habersack, H. (2014). "Bedload transport measurements with impact plate geophones: comparison of sensor calibration in different gravel-bed streams." *Earth Surface Processes and Landforms*, 39(7), 928–942.

Ryan, S. E., Porth, L. S., and Troendle, C. A. (2002). "Defining phases of bedload transport using piecewise regression." *Earth Surface Processes and Landforms*, 27(9), 971–990.

Saletti, M., Molnar, P., Zimmermann, A., Hassan, M. A., and Church, M. (2015). "Temporal variability and memory in sediment transport in an experimental step-pool channel." *Water Resources Research*, 51(11), 9325–9337.

Schielen, R., Doelman, A., and de Swart, H. E. (1993). "On the nonlinear dynamics of free bars in straight channels." *Journal of Fluid Mechanics*, 252, 325–356.

Schoklitsch, A. (1934). "Der geschiebebetrib une die geschiebefracht." *Wasserkraft Wasser-wirtschaft*, 4, 1–7.

Schoklitsch, A. (1950). *Handbuch des Wasserbaues.* Springer, Vienna, 2nd edition.

Schumm, S. A. (1985). "Patterns of alluvial rivers." *Annual Review of Earth and Planetary Sciences*, 13(1), 5–27.

Seizilles, G. (2013). *Forme d'équilibre d'une rivière.* Ph.D. thesis, Université Paris-Diderot, Paris VII, France.

Seminara, G. (1998). "Stability and morphodynamics." *Meccanica*, 33(1), 59–99.

Seminara, G. (2010). "Fluvial sedimentary patterns." *Annual Review of Fluid Mechanics*, 42, 43–66.

Seminara, G. and Tubino, M. (1992). "Weakly nonlinear theory of regular meanders." *Journal of Fluid Mechanics*, 244, 257–288.

Shields, A. (1936). "Anwendung der ähnlichkeitsmechanik und der turbulenzforschung auf die geschiebebewegung." *Mitteilungen der Preussischen Versuchsanstalt für Wasser-, Erd-und Schiffbau*, 26.

Singh, A., Fienberg, K., Jerolmack, D. J., Marr, J. D. G., and Foufoula-Georgiou, E. (2009). "Experimental evidence for statistical scaling and intermittency in sediment transport rates." *Journal of Geophysical Research: Earth Surface*, 114(F1) F01025.

Smart, G. M. and Jaeggi, M. (1983). "Sediment transport on steep slopes." *Mitteilungen der Versuchsanstalt für Wasserbau, Hydrologie und Glaziologie, Eidgenossischen Technischen Hochschule, Zurich*, (64).

Soares-Frazão, S., Le Grelle, N., Spinewine, B., and Zech, Y. (2007). "Dam-break induced morphological changes in a channel with uniform sediments: measurements by a laser-sheet imaging technique." *Journal of Hydraulic Research*, 45, Iss. sup1, 87–95.

Strom, K., Papanicolaou, A. N., Evangelopoulos, N., and Odeh, M. (2004). "Microforms in gravel bed rivers: Formation, disintegration, and effects on bedload transport." *Journal of Hydraulic Engineering*, 130(6), 554–567.

Thorn, C. E. and Welford, M. R. (1994). "The equilibrium concept in geomorphology." *Annals of the Association of American Geographers*, 84(4), 666–696.

Tubino, M., Repetto, R., and Zolezzi, G. (1999). "Free bars in rivers." *Journal of Hydraulic Research*, 37(6), 759–775.

Turowski, J. M. (2010). "Probability distributions of bed load transport rates: A new derivation and comparison with field data." *Water Resources Research*, 46.

Bibliography

Venditti, J. G., Nelson, P. A., Bradley, R. W., Haught, D., and Gitto, A. B. (2017). *Gravel-Bed Rivers, Processes and Disasters*. John Wiley & Sons Ltd, Chichester, UK, Chapter Bedforms, Structures, Patches, and Sediment Supply in Gravel-Bed Rivers, 439–466.

Venditti, J. G., Nelson, P. A., Minear, J. T., Wooster, J., and Dietrich, W. E. (2012). "Alternate bar response to sediment supply termination." *Journal of Geophysical Research: Earth Surface*, 117(F2) F02039.

Vericat, D., Batalla, R. J., and Gibbins, C. N. (2008). "Sediment entrainment and depletion from patches of fine material in a gravel-bed river." *Water Resources Research*, 44(11).

Vesipa, R., Camporeale, C., and Ridolfi, L. (2017). "Effect of sampling time in the laboratory investigation of braided rivers." *Water Resources Research*, 53(6), 5184–5197.

Wainwright, J., Parsons, A. J., Cooper, J. R., Gao, P., Gillies, J. A., Mao, L., Orford, J. D., and Knight, P. G. (2015). "The concept of transport capacity in geomorphology." *Reviews of Geophysics*, 53(4), 1155–1202.

Whiting, P. J., Dietrich, W. E., Leopold, L. B., Drake, T. G., and Shreve, R. L. (1988). "Bedload sheets in heterogeneous sediment." *Geology*, 16(2), 105.

Wilcock, P. R. and Jaeggi, M. (1993). "Surface-based fractional transport rates: Mobilization thresholds and partial transport of a sand-gravel sediment." *Water Resources Research*, 29(4), 1297–1312.

Wohl, E. (2006). "Human impacts to mountain streams." *Geomorphology*, 79(3–4), 217–248.

Wohl, E. (2010). *Mountain Rivers Revisited*. American Geophysical Union Press, Washington, D.C.

Wohl, E. (2014). "Time and the rivers flowing: Fluvial geomorphology since 1960." *Geomorphology*, 216, 263–282.

Yalin, M. S. (1972). *Mechanics of Sediment Transport*. Pergamon Press Ltd, Oxford, UK.

Yalin, M. S. (1992). *River Mechanics*. Pergamon Press Ltd, Oxford, UK.

Young, W. J. (1989). *Bedload transport in braided gravel-bed rivers : a hydraulic model study*. Ph.D. thesis, University of Canterbury, Christchurch, New Zealand.

Zunka, J. P. P., Tullos, D. D., and Lancaster, S. T. (2015). "Effects of sediment pulses on bed relief in bar-pool channels." *Earth Surface Processes and Landforms*, 40(8), 1017–1028.

Curriculum Vitae

Blaise Dhont

EPFL ENAC IIC LHE
Station 18
CH-1015 Lausanne
blaise.dhont@gmail.com

Education

Ph.D. in Fluvial Geomorphology   2013-2017
École Polytechnique Fédérale de Lausanne (EPFL), Switzerland
    Supervisor: Prof. Christophe Ancey
    Thesis title: Sediment Pulses in a Gravel-Bed Flume with Alternate Bars

M.Sc. in Water, Soil and Ecosystems Engineering   2009-2011
École Polytechnique Fédérale de Lausanne (EPFL), Switzerland
    Award for excellence
    Master thesis at the University of Queensland, Australia (SVAF award)

B.Sc. in Environmental Engineering   2006-2009
École Polytechnique Fédérale de Lausanne (EPFL), Switzerland
    3rd year at the Indian Institute of Technology Madras, India

Professional Experience

Hydrique Ingénieurs   2012
Hydraulic Engineer (Switzerland)
    Flood hazard mapping and numerical wave modelling

Publications

Dhont, B., Rousseau, G., and Ancey, C. (2017). Continuous monitoring of bed-load transport in a laboratory flume using an impact sensor. *Journal of Hydraulic Engineering*, 143(6).

Amini, A., **Dhont, B.**, and Heller, P. (2017). Wave atlas for Swiss lakes: Modeling design waves in mountainous lakes. *Journal of Applied Water Engineering and Research*, 5(2), 103–113.

Conferences and Workshops

Transport Solide et Morphodynamique des Rivières (**TSMR**, Lyon, 2017). *Rôle des bancs alternés dans le transfert de sédiment par charriage*, **oral presentation**.

10th symposium on River, Coastal and Estuarine Morphodynamics (**RCEM**, Padova, 2017). *Bedload transport rate fluctuations in a flume with alternate bars under steady state conditions*, poster presentation.

Bibliography

Summer School on Fluvial Geomorphology (June 2016), Losone, Switzerland.

European Geosciences Union (**EGU General Assembly**, Vienna, 2016). *High-resolution monitoring of bedload transport rates: a benchmark of two approaches (accelerometers and image processing)*, poster presentation.

American Geophysical Union (**AGU Fall Meeting**, San Francisco, 2015). *Time scales, bedforms and bedload transport*, poster presentation.

My Thesis in 180 Seconds (**MT180 EPFL**, Lausanne, 2015). *Transport solide et rivières de montagne*, **finalist**.

École Thématique d'Automne: Technique Laser pour la Mécanique des Fluides (September 2015), Oléron, France.

Complexity in Geomorphology Workshop (June 2015), ETH Zürich, Switzerland.

European Geosciences Union (**EGU General Assembly**, Vienna, 2014). *Effects of successive floods on bed load transport in a steep flume*, poster presentation.

Teaching

Teaching assistant: "Probabilités et statistique", "Mécanique des fluides", "Ondes de crue et de rupture de barrage", and "Risques hydrologiques et aménagements".

Supervision of student projects:
- Sommer, D. and Subrin, A. (2016). Étude de la morphologie d'une rivière.
- Szüle, F. (2016). Mesure de la topographie du lit du canal Armfield par projection de nappes lasers II.
- Martinez Y Royo, M. (2015). Calibration des accéléromètres du canal Armfield.
- Darcourt, A. and Sarrasin, O. (2014). Mesure de la topographie du lit du canal Armfield par photogrammétrie.
- Jüstrich, S. and Vandevelde, K. (2014). Mesure de la topographie du lit du canal Armfield par projection de nappes lasers I.
- Jüstrich, S., Ruetsch, V., and Vandevelde, K. (2014). Étude hydraulique de la Borgne (VS).
- Jacot-Guillarmod, P. (2013). Étude du bilan de masse dans le canal Armfield après des cycles de crues-décrues.